STUDIES ON LOW AND HIGH ENERGY PARTICLES IN COSMIC RAY EXTENSIVE AIR SHOWERS OBSERVED IN THE EARTH'S ATMOSPHERE

THESIS SUBMITTED FOR THE DEGREE OF
DOCTOR OF PHILOSOPHY (SCIENCE)
OF THE
UNIVERSITY OF NORTH BENGAL
1997

By
Gopal Saha, M. Sc.

DEPARTMENT OF PHYSICS
University of North Bengal
Darjeeling – 734430
INDIA

****

To
my mother

****

ACKNOWLEDGEMENTS

I express my deep gratitude to Prof. N.Chaudhuri for his supervision and helpful suggestions throughout the present investigation .His valuable guidance , constant inspiration and constructive criticism have been of immense help at every stage of this work.

The financial assistance in the form of a research fellowship from the University of North Bengal is thankfully acknowledged.

I am indebted to my colleagues , Dr. Biswanath Ghosh , Dr. Samir Kumar Sarkar , Dr. Subrata Sanyal , Dr. Arunava Bhadra and Mr. Arindam Mukherjee for their help and co-operation . I also thank Mr. Ambarish Chettri for his assistance at all stages of the work.Help and co-operation given by Mr. Chandibrata Chakrabarti , Mr. Dipesh Chanda and Mr.Rajat Dey of High Energy and Cosmic Ray Research Centre are sincerely acknowledged .

I sincerely thank Mr. P.Tamang , Senior Technical Assistant , Physics Department , NBU for his valuable assistance in the present experiment.

The inspiration and encouragement that I always received from my parents and other members of the family would be remembered . Specially , I remember the inspiration and affection of my mother who has passed away before I could complete the thesis work . The thesis is dedicated to her memory.

Department of Physics
University of North Bengal
Darjeeling 734 430
INDIA

Gopal Saha
(Gopal Saha)

PREFACE

The Primary Cosmic Ray energy spectrum extending over the range from 10^9 to 10^{20} eV and the primary composition at various energy bands in this spectral range have been the subject of investigation for more than 30 years now. The status of our knowledge concerning the primary composition is more unsatisfactory even from 10^{12} eV onwards . The integral primary flux steepens at around 10^{15} eV and flattens at around 10^{19} eV and these features are called the "knee" and the "ankle" of the primary spectrum . No "toe" of the primary spectrum indicating the end of the spectrum has been found in the experiments so far . At the "ankle" not more than 10 air shower events have been detected to date in the Extensive Air Shower observatories . The proposed Pierre Auger Observatory aims to detect statistically significant Primary Cosmic Ray events at the "ankle" and above.

The direct observations of the primary nuclei with nuclear emulsion stacks have provided evidence that the nuclei heavier than the proton are present in the Primary Cosmic Rays up to energy 10^{14} eV , but the proportion of such nuclei heavier than He^4 remains unconfirmed as yet and is less than that expected from lower energy data .

The aim of the present work is to extract information about the primary composition at the "knee" energy region from the detailed study of both low and high energy muons in smaller air showers detected near sea-level . In this thesis we present all the results on the electron and muon components in air showers in the size range 10^4 - 10^6 particles and examine these results critically together with the results of previous air shower studies to derive conclusion on the primary composition in the knee energy region.

The candidate , a Senior Research Fellow at the High Energy and Cosmic Ray Research Centre holding a University fellowship for a tenure of 5 years from December 1993 has worked with other workers of the group . His contribution to the work during this period is stated below :

(1) Calibration of the detectors

(2) Rearrangement of the array and resetting the detectors
(3) Operation and day-to-day maintenance of the set-up
(4) Data taking
(5) Development of computer programs and analysis

As an additional support to the candidature the reprints of papers published as listed below are submitted with the thesis .

Published papers

(1) Study of electrons simultaneously with muons in Extensive Air Showers (EAS) initiated by Primary Cosmic Rays of energy 10^{14} - 10^{16} eV.
C.Chakrabarti , D. Chanda , G.Saha , A.Mukherjee , A.Bhadra , S.Sanyal , S.Sarkar, B.Ghosh , N.Chaudhuri .
24th International Conference on Cosmic Rays , Rome , 1(1995)387
(2) Low and high energy muons in Extensive Air Showers of size 10^4 to 10^6 particles.
C.Chakrabarti , D. Chanda , G.Saha , A.Mukherjee , A.Bhadra , S.Sanyal , S.Sarkar, B.Ghosh , N.Chaudhuri .
24th International Conference on Cosmic Rays , Rome , 1(1995)569
(3) A search for anisotropy in the arrival direction of EAS by cosmic rays from discrete sources.
C.Chakrabarti , D. Chanda , G.Saha , A.Mukherjee , A.Bhadra , S.Sanyal , S.Sarkar, B.Ghosh , N.Chaudhuri .
24th International Conference on Cosmic Rays , Rome , 1(1995)462
(4) A new lateral distribution function for electrons in Extensive Air Showers (EAS) detected near sea level.
B.Bhattacharyya , A. Bhadra , A.Mukherjee , G.Saha , S.Sanyal , S.Sarkar , B.Ghosh and N.Chaudhuri.
IL Nuovo Cimento , 18C(1995)325

Submitted paper

(1) An experimental study of Primary Cosmic Rays at the knee energy region by observation of Extensive Air Showers(EAS)

CONTENTS

CHAPTER 1

INTRODUCTION

There are two main reasons for investigating the primary cosmic radiation . The first is to obtain information about the astrophysical aspect and second is to obtain information about the nuclear interactions at extremely high energies. Accelerators can accelerate particles only upto energy $\sim 10^{13}$ eV. Above this energy cosmic radiation is the only source of obtaining high energy particles and properties of their interactions. For both aspects of study we need to know the primary composition , flux and energy spectra of the particles.

A branch of cosmic ray physics which is important both from the point of view of nuclear physics and astrophysics is the study of the Extensive Air Showers (EAS) discovered by Auger in 1938. Primary Cosmic Ray particles interact in the earth's atmosphere and give rise to a cascade of secondary particles known as Extensive Air Showers. Let's now discuss the formation of air showers in the atmosphere.

1.1. The phenomena of EAS :

A high energy cosmic ray particle arriving at the top of the atmosphere collides with a nucleon of an air nucleus , loses a fraction of its energy and passes through the atmosphere . The energy that is lost by the primary particle leads to the production of a large number of secondaries . The secondary particles are mostly charged and neutral pions ($\Pi^{\pm}$, Π^{0}) and a small fraction of kaons and nucleon-antinucleon pair . The neutral pions decay immediately into two gamma ray photons which create the electron-positron pair by the pair production process . The new electrons radiate more photons by bremsstrahlung process which again forms electron - positron pair and create the electromagnetic cascade . Some of the charged pions and kaons decay into muons and give rise to the muon component of air showers . The remaining pions , kaons and all other hadrons suffer further collisions and generate more secondaries . At each new step the number of secondary particles increases and their average energy decreases . However a stage is reached when the energy of the particles become so low that secondary particle production stops and thereafter the number of particles decreases due to ionization

loss and decay. Due to multiple coulomb scattering the secondary particles arrive at the ground level spreading over large area .

Since most of the electrons are ultra-relativistic and pass through the atmosphere with a velocity greater than the velocity of light , they give rise to a considerable amount of Cerenkov radiation . The electrons also emit radio waves in the frequency range of 1 MHz to several hundred MHz. Thus ultimately at the sea-level the various components of EAS particles are the

(1) soft component (electrons , positrons and gamma rays)
(2) muon component
(3) hadron component (pions , kaons and nucleon-antinucleons) mainly
(4) Cerenkov radiation
(5) radio waves

Considering the scope of the present experiment only the electron-photon component and the muon component of EAS are discussed briefly in the following section.

1.2. Electron-photon component :

The electron photon component is the most abundant component of the shower and constitutes almost 90% of the shower particles. Because of multiple coulomb scattering the shower particles spread laterally to hundred of metres. The density of shower particles is maximum at the core of the shower and it falls off rapidly with the distance from the shower core. A photon electron cascade in EAS with radial symmetry is described laterally at a distance r from the EAS axis by expressing the shower particle density $\Delta(r)$ by

$$\Delta(r) = N_e/r_o^2.f(r/r_0,s) \quad \text{----------} \quad (1.1)$$

Where N_e is the total number of particles in EAS, s is a parameter called the shower age which determines the steepness of the lateral distribution function and r_o is the Moliere unit of displacement . The value of r_o in air is 9.5 g cm^{-2} and its geometrical length λ (m) depends on the level of observation .

The most extensively used electron lateral distribution function given by Greisen [1] is a modification of the form given by Nishimura -Kamata [2] which is referred to as NKG function . The form of the function is

$$\Delta(N_e,s,r) = N_e/r_0^2.c(s).(r/r_0)^{s-2}.(1+r/r_0)^{s-4.5} \quad \text{-------(1.2)}$$

where c(s) is the normalisation constant , r_0= 79m (Moliere unit of displacement at sea-level).

The age parameter s is closely linked to the longitudinal development of the shower . For photon originated showers of primary energy E_0 observed at a depth of t (radiation lengths) from the point of origin,s is given by

$$s= 3t / [\ t+2\ln(E_0/\varepsilon_0)\ ] \quad \text{----------(1.3)}$$

ε_0 being the critical energy for electrons in air and is equal to 84 MeV. More accurately s is a function of the lateral distance from the axis also.

Recently it has been shown that the NKG function does not give a good fit to the lateral distribution of electrons and the observed distribution is steeper than the NKG distribution. Several forms of the distribution function have been given by different authors (Hara et al [3] , Dedenko et al [4] , Linsley [5] , Kaneko et al [6] , Capdevielle et al [7] , Lagutin et al [8] , Hillas and lapikens [9]) to fit the observed distribution of electrons.

The electron density distribution as a function of core distance calculated by Hillas and Lapikens [9] is represented by the following formula

$$\Delta(r) = N_e/r_0^2.c(s).[(r/r_0)^{a1+a2(s-1)}.(1+r/r_0)^{b1+b2(s-1)}] \quad \text{----------(1.4)}$$

where the parameters chosen for the best fit of the experimental results are

r_0=24m, a1= -0.53, a2=1.54, b1= -3.39, b2=0

Capdevielle et al [7] assumed that the shower age parameter in the fitting function should be the <effective age> for radial development of shower and defined it as

$$s(r) = \alpha.\log\beta(r/r_0) + s_l \text{ , for } r \leqslant 150m \quad \text{----------(1.5)}$$

where s_l is the longitudinal age parameter at the level of observation and α,β,s_l are constants at sea-level for a given shower size. With this modification the radial density distribution of electrons according to Capdevielle et al can be expressed as

$$\Delta(r) = N_e/r_0^2.[\ c(s).(\ r/r_0\ )^{s(r)-2}.\ (\ 1+r/r_0\ )^{s(r)-4.5}\ ] \quad \text{----------(1.6)}$$

The shower size (N_e), age parameter (s) and the shower core (X_0,Y_0) are determined by fitting a chosen function to the density of shower particles at various points. The shower size is a measure of the total energy of the primary particle. The relation between the average shower size and primary energy (E_0) can be expressed as

$$E_0 \sim N_e^{\beta} \quad \text{----------(1.7)}$$

where β is a constant .
The value of β is 0.86 (Trzupek et al [10]) for showers in the size range $3x10^3$-10^5 particles initiated by primary proton .Thus the shower size spectrum represents the energy spectrum.

1.3. Muon component :

Muons, having no strong interaction, reach the observation level from the point of their production. Hence they loose energy only by ionisation and disappear only by decay. The ionisation loss in the atmosphere is comparetively small and the mean life of muons is comparetively long. Therefore, neither process is very effective in eliminating muons before they reach sea-level. This accounts for the fact that the number of muons after reaching a maximum in the upper atmosphere decreases slowly with increasing atmospheric depth. As a consequence muons become the dominant component of the cosmic radiation near the sea-level. Muons constitute about 10% of the total number of particles in EAS and spread out to much wider area than the electromagnetic component.

The muons of different energies in EAS have been studied using magnetic spectrographs associated with air shower array by different cosmic ray groups such as Durhum Group, Kiel Group, Moscow Group. The lateral distribution of low and high energy muons can be represented by the equation of the form

$$\rho_\mu(r) \sim r^{-\alpha}.e^{-r/ro} \qquad \text{----------(1.8)}$$

where α is a fitting parameter. The values of α obtained from the present experiment lie in between 0.3 to 0.9 for muon energies 2.5 to 100 GeV and shower size 3.15×10^4 to 1.79×10^6 particles.The total number of muons N_μ in a shower can be obtained by integrating the lateral distribution function (eqn. 1.8).The average number of muons N_μ per shower can be represented by the relation

$$N_\mu \sim N_e^{\alpha} \qquad \text{---------- (1.9)}$$

The present experimental data show that the value of α is about 0.6

The detection of muon component is sensitive to both cosmic ray primary composition and high energy nuclear interaction processes. At near sea-level atmospheric depths , an average shower size of 10^4 particles correspond to a primary energy of $\sim 10^{14}$ eV if the primary is a proton, and to an energy of $\sim 3 \times 10^{14}$ eV if the primary is an iron nucleus . The air showers , of average energy $\sim 10^{14}$ eV, when analysed in terms of lateral distribution and total size of muons of all energies would reveal differences with respect to these characteristics depending on the mass of the particle initiating the shower . For example , in an EAS of size $\sim 10^4$ particles , initiated by an iron nucleus primary of energy $\sim 3 \times 10^{14}$ eV , the total size of muons and the lateral structure of both low and high energy muons will be different from those in the shower produced by a proton primary of energy $\sim 10^{14}$ eV . These differences in characteristics are largely independent of the high-energy nuclear model characteristics and that have been used to simulate, under necessary experimental conditions , the EAS data on various EAS components.

It should be mentioned here that the information available so far on primary composition in the energy range 10^{13}-10^{15} eV has been inadequate and it has been suggested by Cowsik et al [11] and Yodh [12] that the relative abundance with respect to iron group nuclei becomes very high at ~10^{14} eV.

Let's now see how the total number of muons (N_μ) and the lateral distribution of muons in EAS are affected by the presence of heavy nucleus in the Primary Cosmic Ray .

A shower initiated by a heavy nucleus of mass number A with energy E_0 is equivalent to the superposition of A number of showers initiated by a proton of energy E_0/A . The total number of muons N_μ in a shower initiated by primary proton is experimentally known to be

$$N_\mu = K.N_e^{\alpha} \quad , \alpha<1 \qquad \text{---------- (1.10)}$$

Now if the effect of fluctuation is not taken into account the shower size is roughly proportional to the primary energy. Then the total number of muons (N_μ') in a shower initiated by a heavy nucleus of mass number A is roughly given by

$$N_\mu' = K.A.(N_e/A)^{\alpha}$$
$$= K.A^{1-\alpha}.N_e^{\alpha}$$
$$\text{so, } N_\mu' > N_\mu$$

Hence the total number of muons in a shower initiated by a heavy primary is larger than the corresponding one of the proton primary.As a result the N_μ-N_e curve for heavy primary will be shifted upward compared to the N_μ-N_e curve for proton primary.

Because of lower energy per nucleon , the showers of a given size initiated by heavy primaries at a given altitude are older than showers initiated by primary protons . Also the production height of muons is always higher for heavy primary induced showers than that of proton showers . Since the total number of muons and muon production height are higher , the lateral distribution of

muons for showers initiated by heavy primaries will be flatter compared to proton initiated showers.

Therefore, the total number of muons and muon lateral distribution in an EAS at sea-level , if the primary is heavy nucleus will be different from those in a proton initiated shower. An Extensive Air Shower experiment in which the lateral distribution of muons and variation of total number of muons with shower size can be measured accurately can indicate the nature of the primary particle.

The lateral distribution of muons and the variation of total number of muons with shower size have been studied by the air shower experiment at the NBU campus to interpret the nature of the primary in the energy range 10^{14}-10^{16} eV.

1.4. Results on composition of Primary Cosmic Rays:

The study of EAS is highly complicated since most of the observed parameters are highly dependent on high energy interaction characteristics as well as primary mass composition both of which are unknown. Thus conclusions from one depends on the assumptions regarding the other.

From EAS measurements it is seen that the Primary Cosmic Ray energy spectrum steepens in the energy range 10^{14}-10^{16} eV, known as the knee energy region. At the 1959 Conference in Moscow the MSU group reported a steepening of the sea-level size spectrum for $N_e > 8x10^5$. A group working at Norikura (2770m. a.s.l.) reported a steepening from integral exponent 1.55 to 2.04 occuring for N_e between $3x10^5$ and $5x10^5$ (Kameda et al 1960). The steepening of the energy spectrum has been most widely interpreted as probably reflecting an increased rate of leakage of high rigidity particles from the galaxy. Peters [13] suggested in 1961 that due to magnetic field in the galaxy the galactic cosmic rays will be cut off at constant rigidity.Alternatively it is suggested that the knee is produced in the source region due to either a threshold for break up of preferentially accelerated heavy nuclei (Zatsepin et al [14] .) or to the threshold for photodisintegration (Hillas [15]). It has also been suggested that the knee is formed

due to cosmic rays from a different class of sources perhaps pulsars (Karakula et al [16]). In all these models a change of primary mass composition is expected at around the knee.

There is a lot of controversy regarding the primary mass composition . The primary mass composition below 10^{14}eV has been measured by balloon borne detectors , like emulsion stacks, scintillation detectors, cerenkov counters flown to the top of the atmosphere (Balasubrahmanyan and Ormes [17] ; Juliusson [18] ; Ormes et al [19] ; Lezniak and Webber [20]). Chemical composition of Primary Cosmic Rays have been estimated from the fractal analysis of the charged particle distribution near the core of individual EAS by Kempa et al [21] .From the fractal analysis they concluded that (1) Neither before the knee ($10^5<N_e\leqslant 5x10^5$) nor after the knee ($5x10^5<N_e\leqslant 5x10^6$) heavy primaries dominate in the primary spectrum . (2) After the knee the fraction of heavy primaries decreases to a value of 14%±4% while the fraction of protons increases to 67%±13%.

At energies above 10^{14} eV an indirect estimation of the primary mass composition has been made from EAS measurements. Composition of Primary Cosmic Rays has been derived indirectly by various groups from the study of various parameters in Extensive Air Showers : i.e. from the study of delayed hadrons, fluctuation of muons, high energy muons and their correlations with other parameters of EAS and the depth of shower maximum from atmospheric cerenkov radiation observations.Unfortunately the various experiments indicate compositions which are at variance with each other. Delayed hadron and shower maximum measurements favour an iron rich composition at ~10^{15} eV. Whereas the observations based on muons are consistent with the normal mixed composition. Some of the results are summarised below:

From the variation of central density of EAS electrons with size and its fluctuation Sydney group (Mc.Cusker et al [22]) concluded that around 10^{15} eV the primary mass composition is mixed which becomes progressively richer in heavy nuclei upto 10^{17} eV.

By measuring the same parameters the Kiel group (Samorski et al [23]) suggested that the primaries are either proton or mixed but not all heavy primaries in the energy interval 10^{15}-10^{16} eV.

From the variation in the number of very high energy muons ($E_\mu \geqslant 220$ GeV) with the shower size together with the expected behaviour of showers generated by pure proton and heavy primaries by Monte Carlo simulation, KGF(Kolar Gold Field, India) group favoured for a mixed composition with a gradual enrichment of heavy primaries in the energy range $10^{14.7}$-$10^{15.7}$ eV (Sivaprasad [24]). Afterwards the same group (Acharya [25]) concluded that the mixed composition is consistent up to $10^{15.7}$ eV.In the primary energy interval $10^{15.7}$-10^{16} eV the primary composition changes from mixed to proton dominant. At energies greater than 10^{16} eV the primaries are dominant in protons.

Some of the recent and main observations other than those as discussed above are given in table 1.

Table 1. Composition of Primary Cosmic Rays from EAS observations

Authors	EAS-particles studied	Conclusion
Andam et al. [26]	Depth of maximum development of shower from atmospheric cerenkov light	Rate of change of primary mass with energy in the range 10^{15}-10^{18}eV is constant
Linsley and Watson [27]	Depth of maximum development of shower from atmospheric cerenkov light	Predominantly heavy at 10^{15} eV and changes to lighter at $3x10^{16}$ eV
Walker and Watson [28]	Rise time of pulses from water cerenkov detectors	Mass composition is nearly constant between 10^{17}-10^{19} eV

Yodh et al. [29]	Delayed hadrons	Heavier nuclei is dominant in the primary energy range 10^{14}-10^{16} eV
Stamenov et al [30]	Muon and electron flux fluctuation distribution in EAS	The mass composition of the primary cosmic radiation in the energy interval 10^{15}-10^{16} eV is mixed and does not substantially change with energy.The relative contributions of primary protons is not smaller than (39±4)% and for iron nuclei group (15±5)%
Nikolsky et al. [31]	Fluctuations of muons	The primary composition is constant and mixed (40% proton, 15% Fe)
Muraki [32]	Variation of muon size with shower size	In the primary energy range $2x10^{16}$- $2x10^{17}$eV the iron component does not become dominant
Dawson [33]	Lateral distribution of cerenkov light in EAS	Cosmic ray primary composition is rich in iron over the energy range $3x10^{15}$-$5x10^{16}$ eV
Cho et al [34]	High energy muons in EAS above 200 GeV	Primary composition of cosmic rays in the energy range till $10^{14.5}$ eV is proton dominant

Blake et al. [35]	Muon component in EAS	Primary mass changes from heavier to lighter in the primary energy range $0.6x10^{15}$-$5x10^{15}$ eV

1.5. Present investigation:

The present experiment has been carried out to study the low and high energy particles (electrons and muons) in EAS at the knee energy region (10^{14}-10^{16} eV) by using the NBU air shower array. The air shower array consisting of 19 electron density detectors , 8 fast timing detectors , two shielded magnet spectrographs (with a spacing of 4m, maximum detectable momentum 500 GeV/c , each of area 1m x 1m and cut off at an energy 2.5 GeV) and a neon flash tube chamber is designed to detect electrons and muons of various energies simultaneously.

All the particle detectors in the array working simultaneously under the four fold coincidence measure particle density and particle momentum in individual EAS and the data are processed by a 486-DX2 computer to provide the shower parameters i.e. the EAS axis co-ordinates, EAS age, EAS size (measured in number of particles). From these estimations we obtain the radial distribution of particle density as well as the energy distributions of particles in EAS.

There is a great deal of controversy regarding primary composition obtained by various groups. A number of observations indicate the presence of heavy nuclei in the primary energy range 10^{14}-10^{16} eV while some other observations show the lighter composition of the primary cosmic rays in the same energy range. In the present work , the characteristics of the radial density distribution of muons in terms of measured shower parameters and the variation of total number of muons with shower size have been studied and compared with different

Monte Carlo simulation results to draw conclusion about the average nuclear mass of the primaries of EAS.

CHAPTER 2

EXPERIMENTAL SET-UP AND DATA ANALYSIS

2.1. Experimental set-up:

In the present investigation the air shower array operating at the North Bengal University (NBU) (atmospheric depth ~1000g cm^{-2} , latitude $26^0 45'N$, longitude $88^0 21'$) is designed to detect electrons and muons of various energies simultaneously. The array is sensitive to air showers initiated by cosmic ray primaries of energy in the range 10^{14}-10^{16} eV.

2.1.1. NBU air shower array:

The NBU EAS array for observation of air showers has been developed in stages since 1980 (Basak et al [1]). At present the air shower array has nineteen plastic scintillation detectors for the measurement of electron density , eight fast timing detectors to determine the arrival directions of the detected EAS and two magnet spectrographs (maximum detectable momentum 500 GeV/c , each of area 1m x 1m and cut off at an energy 2.5 GeV) with a spacing of 4m to measure the momentum of muons in EAS. The lay-out of the detectors shown in fig.2.1 covers an area of about 1200 m^2 with detector spacing of about 8m.

2.1.2 Electron density detectors:

Scintillation detectors are used in the NBU air shower experiment to detect the EAS particles. Plastic scintillators each of size 50cm x 50cm and width 5 cm are kept within a pyramidical light tight aluminium enclosure. The inner surfaces of the enclosure are coated with a highly reflecting material composed of titanium dioxide (Tio_2). A Dumont 6364 photomultiplier tube separated by a distance of about 39 cm from the plastic scintillator is placed to view the scintillations produced in the scintillator . Performance of each detector was studied by measuring the single particle pulse height. To measure the single particle pulse height, each scintillation counter is placed along a line of alignment of G.M counter telescope as shown in fig.2.2.Out of three G.M. counters one is crossed and the scintillation counter is placed in such a way that if a charged particle passes through the four counters it

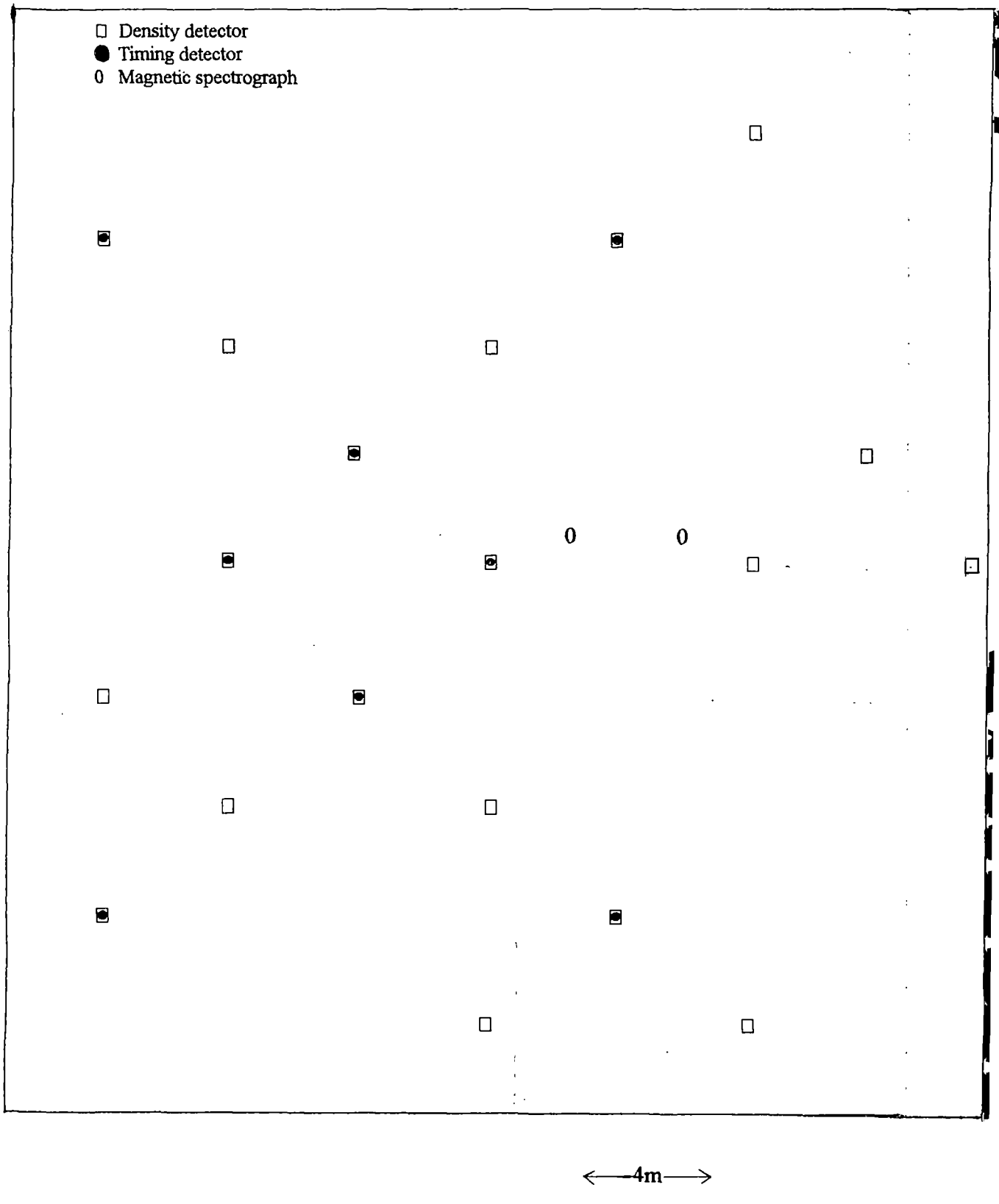

Fig. 2.1. The NBU EAS array

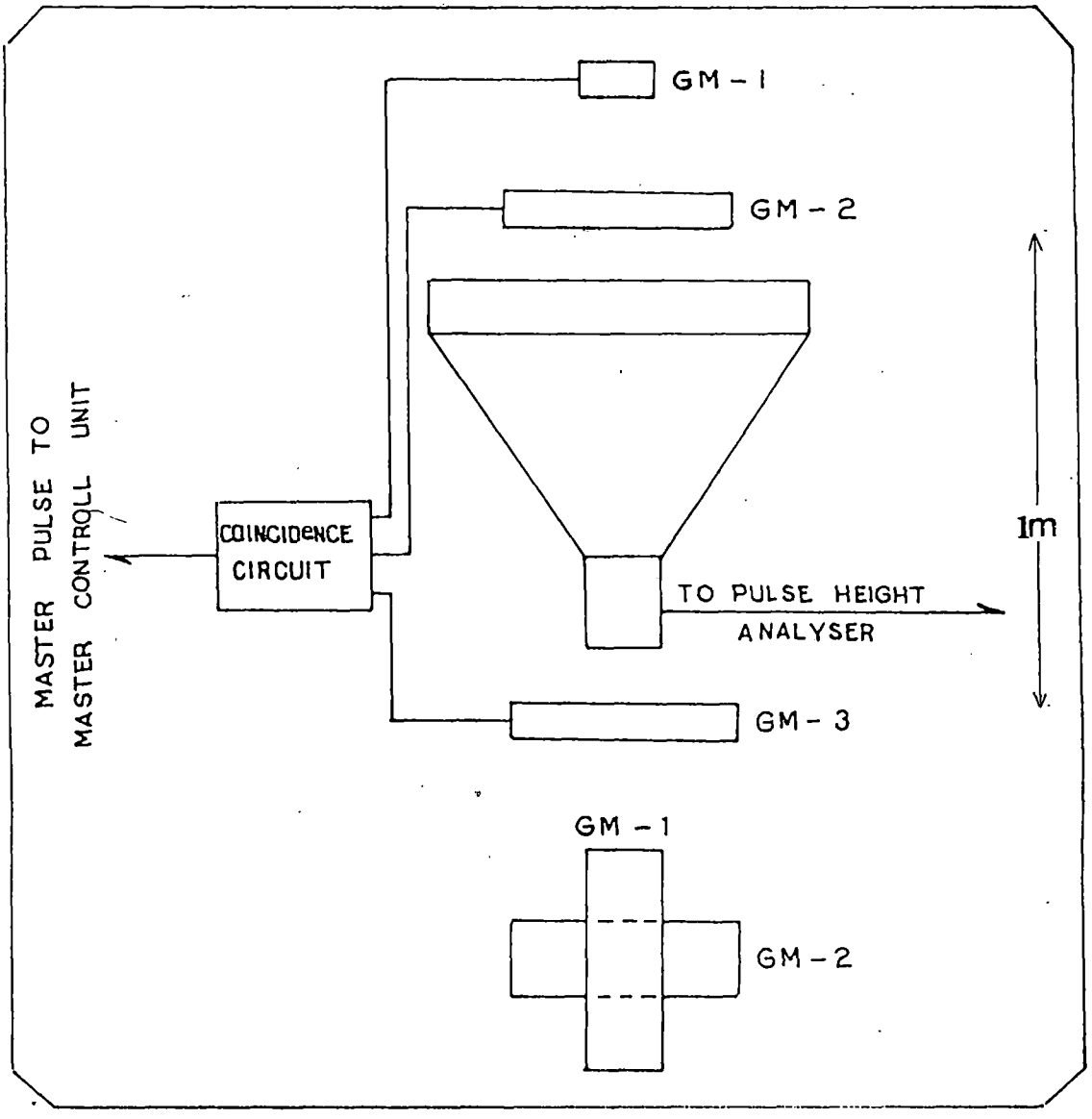

Fig. 2·2. Arrangement for measuring single particle pulse height .

produces four negative pulses at the output of the four counters. The three G.M. pulses are used for the coincidence. For the measurement of pulse height the coincidence pulse from the three G.M. counters is used to trigger the Master Control Unit and the output from the plastic scintillator is connected to the first channel of the pulse height measuring circuit . The digitised output represents the scintillation counter pulse height. The experiment is repeated for all the detectors and different voltages in the range 850-1200 Volts are applied to different photomultiplier tubes to ensure that the single particle pulse height in different detectors are nearly same . The relative efficiency in terms of single particle pulse height is nearly uniform from centre to edge of each plastic scintillation detector.

2.1.3. Fast timing detectors:

Eight fast timing detectors are employed in the NBU air shower experiment to measure relative time delays between their output pulses to determine the arrival direction of a detected EAS. The shape and size of the scintillator and enclosure of these detectors are the same as the electron density detectors but Philips fast photomultiplier tubes (XP 2020 , rise time 1.5 ns) are used in stead of relatively slow photomultipliers (rise time ~ 20-30 ns) used in the electron density detectors.

2.1.4. Magnetic spectrograph unit:

Two identical magnet spectrograph units separated by a distance of 4m are operated under an EAS trigger to detect the muons of EAS particles. The arrangement of the magnetic spectrograph unit is shown in fig.2.3. Each magnet spectrograph consists of a solid iron magnet in between four neon flash tube trays. The solid iron magnet is composed of 80 low carbon content steel plates (180 cm x 125 cm x 1.25 cm) having a rectangular hole (35 cm x 19 cm) at the centre. Both the longer arms of the magnets are wound with 600 turns of double cotton covered copper wire.The power requirement for each magnet when operated at 15 amp. current is 2.3 kilowatts. There are four neon flash tube trays (T_1, T_2, T_3, T_4) , two of which are placed above the magnet and other two are placed below the magnet for the accurate location of muon trajectory as shown in fig.2.3 . Each neon flash tube tray consists of 120 neon flash tubes arranged in 8 layers and each layer contains 15 tubes. The tubes in each tray are staggered in such a way that a single particle

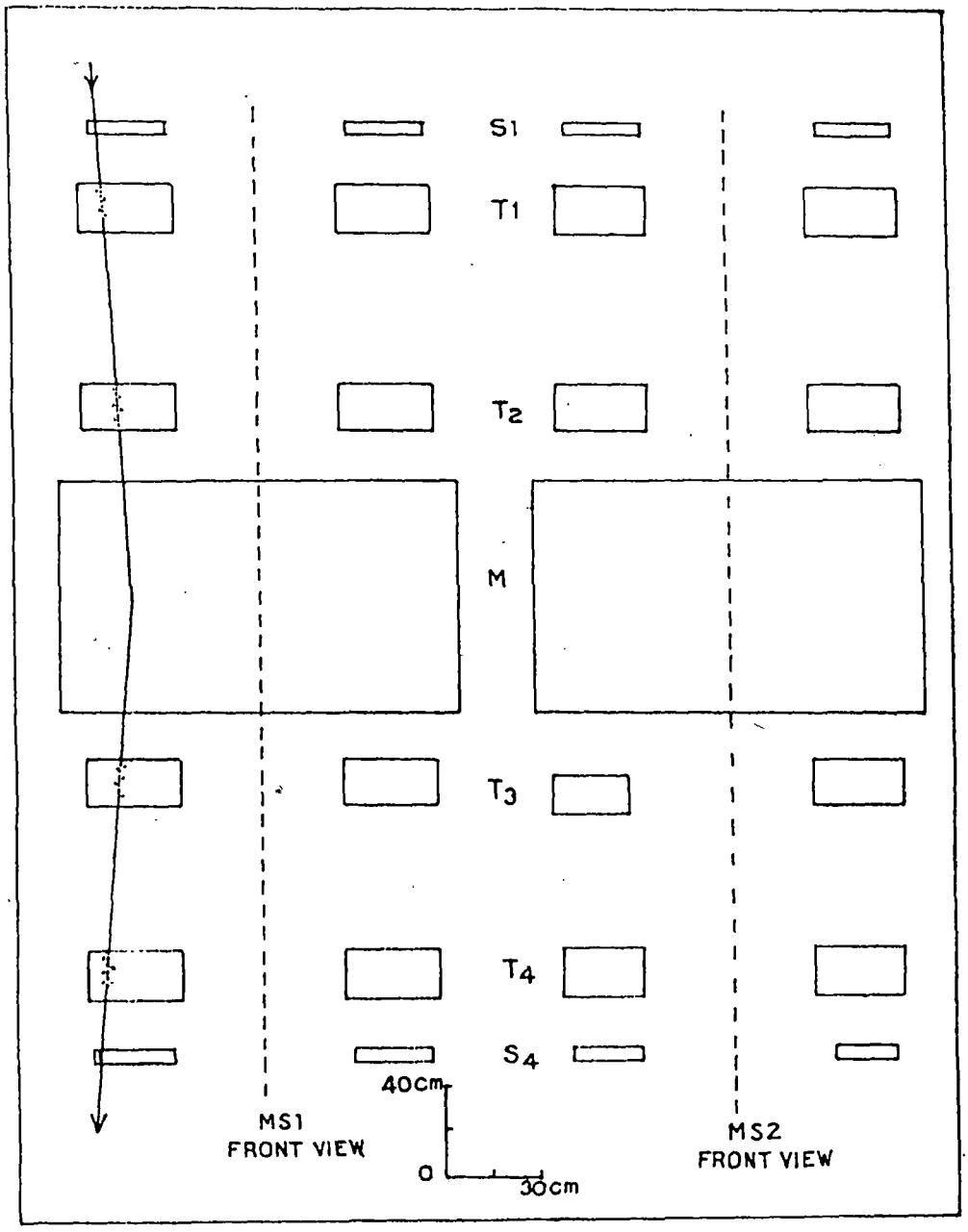

Fig. 2·3. Schematic diagram of magnetic spectrograph unit .

passing through a tray must traverse at least four tubes . The arrangement of the flash tubes in a tray is shown in fig.2.4. The tubes in each tray are supported by duraluminium bars by means of milling machine at Central Mechanical Research Institute , Durgapur,India. Thin aluminium electrodes are placed in between two layers of neon flash tubes. The horigontal separation between two tubes is 1.999 ± 0.002 cm which is referred to as one tube separation (t.s) unit. The vertical separation between two tubes of adjacent layers is 2.8 cm . Four cameras are used to record the flashes of the neon flash tubes photographically. To remove the electronic components an absorber of concrete of about 1m thick is used at a distance of about 1m above the spectrograph unit on the roof of the laboratory building . Moreover, lead absorber of about 5cm thick is also placed above the top tray of the spectrograph to absorb any electron component .

2.1.5. Principle of operation of the NBU EAS array:

The data acquisition system in the NBU EAS set-up can be divided into four parts - shower selection system (coincidence circuit) , timing data handling system , density data handling system and muon data handling system . The actual circuit diagram and detailed discussion of the control electronics of the whole data acquisition system are given in [2]. Here only the operation of different parts of the data acquisition system are discussed briefly in the following section. The block diagram of the data acquisition system is shown in fig.2.5.

2.1.6. Shower selection system:

Shower is recorded by the shower selection system if the registered electron density in any four adjacent detectors of the eight central triggering detectors is greater than 4 particles/m^2.

2.1.7. Timing data handling system:

The output pulses from eight fast timing plastic scintillation detectors are fed to the discriminator (Lecroy 623B) and level adopter (Lecroy 688 AL) unit with equal time delay by means of equal length RG 58 cables. The shower event is selected by means of a four fold fast coincidence within 50 ns time delay. This four

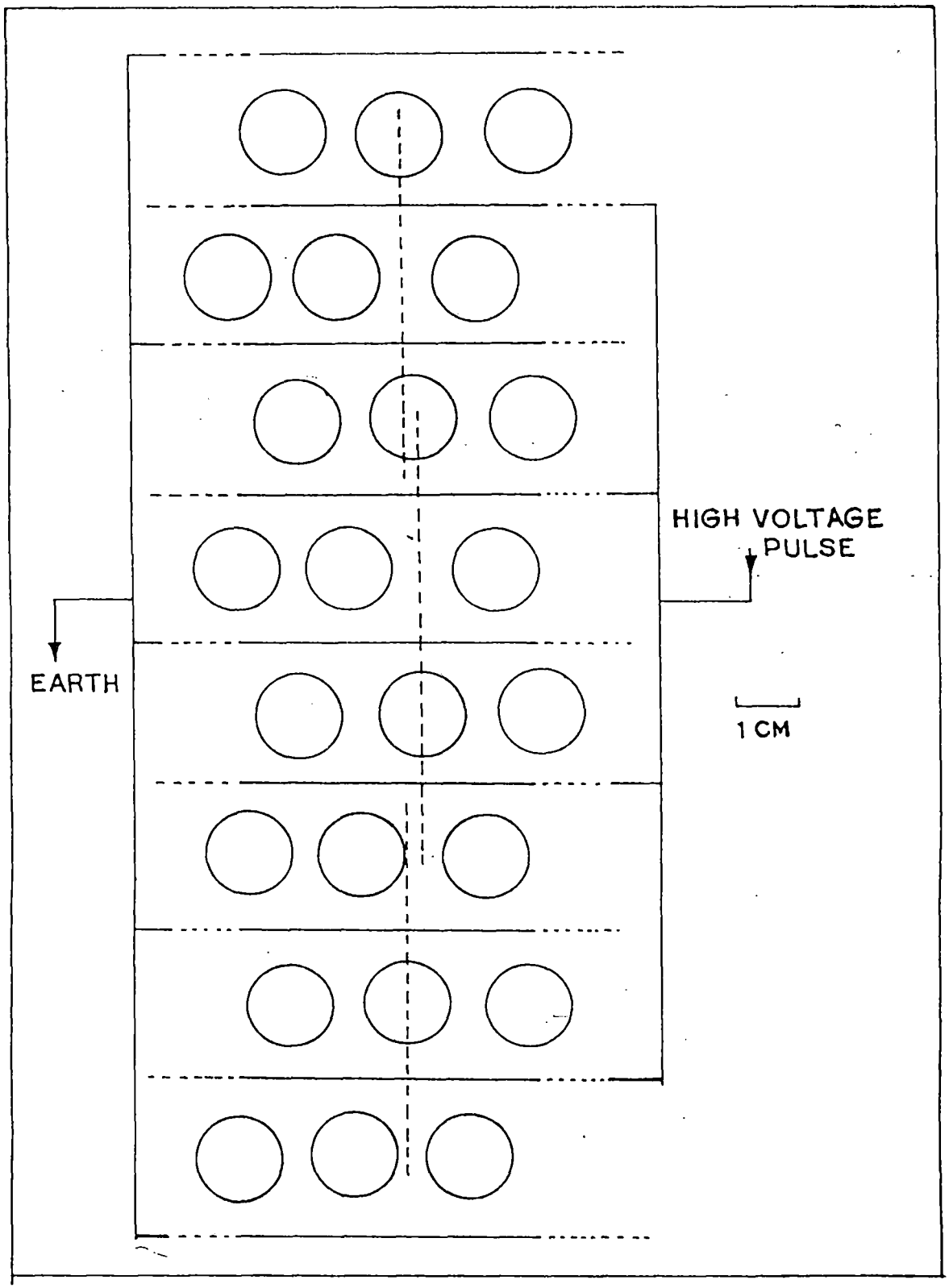

Fig. 2·4. The staggering arrangement of the flash-tubes in a tray of magnetic spectrograph units.

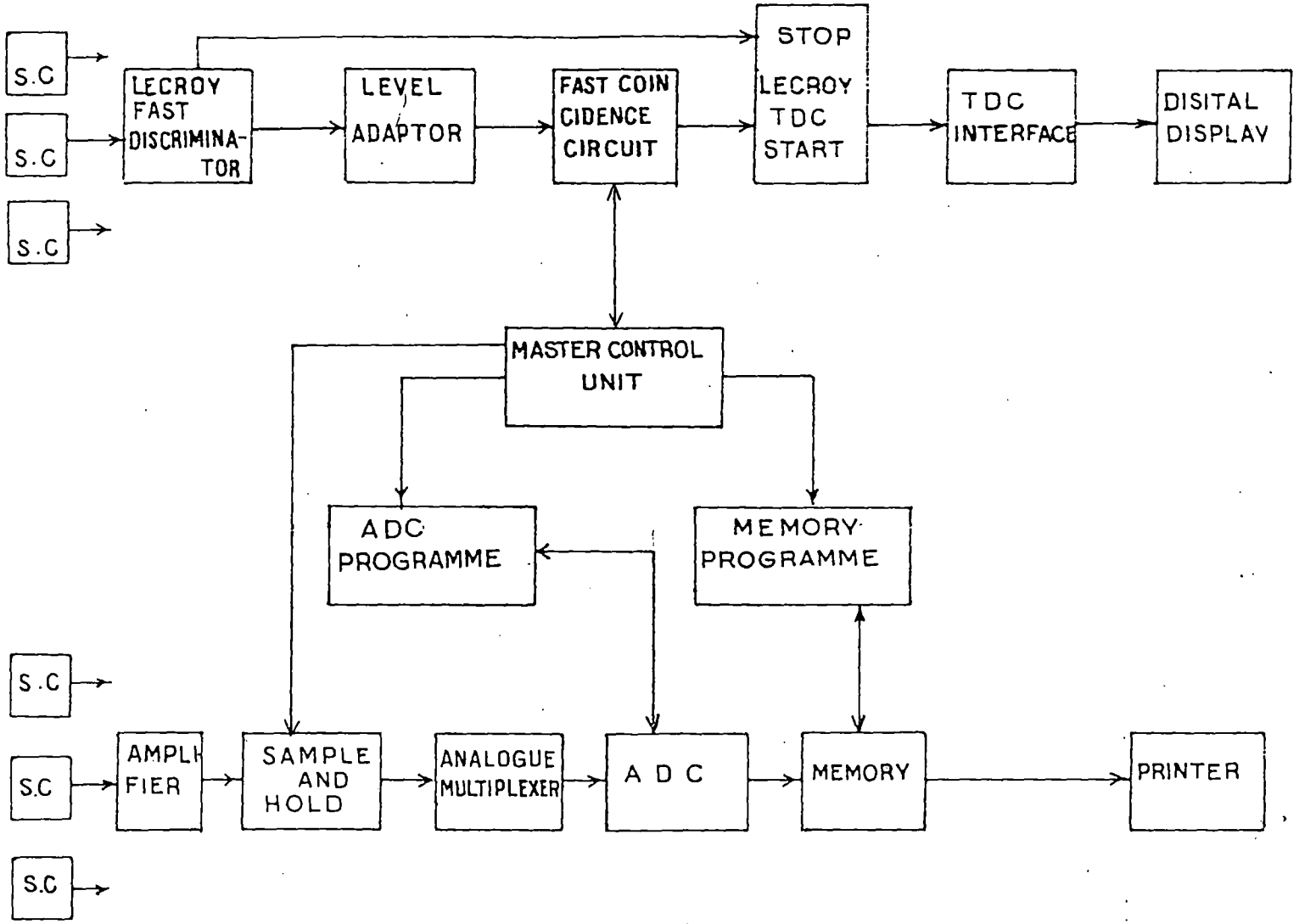

Fig. 2·5. Block diagram of the data handling system.

fold coincidence pulse (start pulse) is used to start the TDC system (Lecroy 2228A) and the Master Control unit (MCU) of the density recording system . At the same time this four fold coincidence pulse is used for the input Veto of the four fold coincidence circuit. The common start pulse of the input of TDC unit starts charging the capacitors of eight channels and are stopped by the relative arrival of eight pulses (stop pulse) from fast timing detectors through 172ft RG 174 cables for equal amount of delay.The different amount of charge stored in eight channels correspond to the relative arrival times of eight pulses from fast timing scintillation detectors. These charges are converted directly to times by the method of discharge and their corresponding digitized forms are stored in the memory of TDC unit. At the end of storing the data into the memory a manual switch is used by which the digitized data are displayed. Then the Veto is withdrawn for the next event.

2.1.8. Density data handling system:

The analogue outputs from nineteen scintillation detectors of the array after amplification first by preamplifiers and then by main amplifiers are fed to the Sample and Hold circuit by charging capacitors for about 3μs after the triggering of the MCU unit by a master pulse generated from a four fold coincidence . At the end of 3μs , these capacitors will discharge and will be ready to accept the next input pulses. As soon as the MCU unit is triggered , it gives a hold command to the Sample and Hold circuit , switches off the input lines by an analogue switch and disconnects the coincidence circuit from MCU unit and sends a start pulse to the ADC (analogue to digital converter[3]) programme unit. Once ADC programme unit is triggered , it connects all the pulses at the output of the Sample and Hold [4] circuit by the analogue multiplexer one after the other to the ADC . The total time to scan the nineteen channels is about 8 msec. After scanning the first channel the ADC gives a write pulse to the memory for writing the digital information in the memory . As soon as the counting in the first channel is over , the ADC programme unit initiates the multiplexer to connect the second channel and write the digital information to the memory in the similar way . After completion of scanning for all the channels , a read pulse is generated from the memory programme unit which in turn operates on the memory unit for recording the digital information on a paper tape by a line printer. After this operation (33 sec) the analogue switch is opened and it switches on the input lines for the next event .

2.1.9. Muon data handling system:

Each spectrograph unit is placed in between two scintillation detectors to select the vertical muons passing through it.When muon passes through the spectrograph, a two fold coincidence pulse is generated and if this pulse occurs in coincidence with the air shower then it is fed to the base of a power transistor. The output pulse from the power transistor fires a thyratron (5C22/XH-16-200) which in turn discharges a condenser (0.05 μf) charged to 12kV through a 100 ohm non-inductive resistance . The resulting high voltage pulse is then applied to the electrode plates between the flash tube layers. The rise time and the time delay between the passage of the particle through the spectrograph and the application of the pulse to the flash tube trays are 0.75μs and 5μs respectively . In the presence of the high voltage , the gas in the neon flash tubes ionize and glow when muon passes through the tubes . Four cameras are used to record the muon trajectories from the flashes of the neon tubes.

2.2. Data analysis:

The present experiment has been continued from January 1994 to September 1995 and in the mean time 16,000 shower data associated with 2927 muon data have been collected . The shower data have analysed by Fortran language in a 486-DX2 computer and the momentum of muons have measured by means of projector method . Artificial shower analysis has been carried out to obtain the errors in the measurement of shower parameters.

2.2.1. Shower data analysis:

The output (P) printed on the paper tape for a particular detector is related to the electron density Δ as given by

$$\Delta = P / (A \cdot H)$$

where A is the area of the detector and H is a constant representing the mean of the single charged particle pulse height distribution.

The measured charged particle densities in individual EAS are fitted to a fitting function to determine the parameters (N_e, X_0, Y_0, s) of the detected shower .The fitting function by Hillas et al [5] as given below is chosen in the present analysis.

$$\Delta(r) = (N_e/r_o^2).c(s).[\ (r/r_o)^{a1+a2(s-1)}\ (1+r/r_o)^{b1+b2(s-1)}\ ] \text{ ---------- } (2.1)$$

where c(s) is the normalisation constant and the parameters are chosen for best fit of the experimental results as r_o=24m , a1= -0.53 , a2= 1.54 , b1= -3.39 , b2= 0.

2.2.2. Determination of shower parameters:

The estimation of the shower parameters namely the shower size (N_e), shower core (X_0, Y_0) and shower age (s) are necessary for the complete description of a shower . The shower size gives the total number of shower particles present in the shower at the level of observation . The shower core is a point in the shower plane having maximum shower particle density and the shower age parameter describes the longitudinal development of the shower . Even though the density of particles measured is due to all charged particles yet the measured densities can be approximated to electron densities without appreciable error since the density of the non-electronic components present in a shower is almost a few percent of that of the electrons.

The shower parameters are determined by fitting Hillas function to the observed electron densities at different points by minimising the quantity

$$\chi^2 = \sum_i W_i\ (\Delta_i^o - \Delta_i^e)^2 \qquad \text{---------- } (2.2)$$

with respect to all the shower parameters simultaneously . Here Δ_i^o is the observed particle density in the ith detector , Δ_i^e is the expected particle density in the same detector which is calculated by substituting the estimated shower parameters in the Hillas function . The weight factor W_i is taken as

$$W_i = 1/\ \Delta_i^{e2}$$

The summation is over all the detectors which record the densities . The condition of minimisation of χ^2 with respect to the shower parameters is given by

$$\delta\chi^2/\delta Q_i = 0 \quad ;\ i = 1 \text{ to } 4 \qquad \text{---------- } (2.3)$$

where Q_i are the four shower parameters (N_e, s, X_o, Y_o). The above equations are highly non-linear and difficult to solve analytically . So independent estimation of the shower parameters are not possible from the above equations . Hence an iterative procedure is necessary to estimate the shower parameters . In the present analysis the steepest descent iterative process by using the gradient search method of minimizing χ^2 is taken .

Initially χ^2 is set at a large value and s is taken as 1.2 .The initial estimation of the core location (X_o , Y_o) is made by using the following two equations

$$X_0 = \sum_i \Delta_i^0 . X_i \,/\, \sum_i \Delta_i^0$$
$$Y_0 = \sum_i \Delta_i^0 . Y_i \,/\, \sum_i \Delta_i^0$$

where X_i , Y_i are the co-ordinates of the ith detector . With these values of X_0,Y_0 the initial estimation of the shower size (N_e) is made by solving the equation

$$\delta\chi^2 / \delta N_e = 0 \qquad \text{---------- (2.4)}$$

which yields a cubic equation of the form

$$N_e^3 + a.N_e + b = 0 \qquad \text{---------- (2.5)}$$

where a and b are functions of the core location and age .

From these values of X_0 ,Y_0 , s and N_e,the quantity χ^2 and its gradient $\nabla\chi^2$ for various components are evaluated . If the new value of χ^2 is less than its initial value , the parameters are then changed in accordance to the respective components of $\nabla\chi^2$ and a new set of parameters are obtained . The process is continued until the difference between the two successive values of χ^2 per degree of freedom is less than 0.001. When this condition is reached the present value of the shower parameters are taken as the best fitted values . If it is found that within 500 iterations the above condition is not reached , then the current values of

the parameters are taken because in such cases it has been found that the value of χ^2 oscillate very close to the minimum value . A flow chart to measure the shower parameters is shown in fig.2.6.

Three forms of fitting function $f(r/r_0,s)$ have been taken and tested the goodness of fit to the observed density distribution of particles in EAS in a previous experiment of different EAS array lay-out by Bhattacharyya et al [6] . These are : NKG function $f_{NKG}(r/r_0,s)$ [7] , Hillas function $f_H(r/r_0,s)$ [5] and Capdevielle function $f_C(r/r_0,s)$ [8] . The forms of these three functions (f_{NKG} , f_H ,f_C) are given in chapter 1. The observed probability distribution P_χ corresponding to ν degrees of freedom for the reduced χ_ν^2 ($= \chi^2/\nu$) for a given shower size over the whole radial range 0-120m using NKG , Hillas and Capdevielle functions are shown in figs.2.7,2.8 and 2.9 . The mean values of the reduced χ_ν^2 for the three distribution functions are given in table 2.1 and it is seen that $f_H(r/r_0,s)$ among the three distributions is the best fit to the observed distribution in the radial range 0-120m.

Table 2.1. Mean values of the reduced χ_ν^2 from figs.2.7,2.8 and 2.9 for the distribution functions (for EAS radial range 0-120m)

$f_{NKG}(r/r_0,s)$	$f_H(r/r_0,s)$	$f_C(r/r_0,s)$
1.81	1.77	1.80

An examples of observed shower data and reconstructed shower parameters from the observed data for an EAS events is shown in fig.2.10. Chi-square distribution for experimentally observed shower data and artificial shower data are shown in fig.2.11 .

2.2.3. Muon data analysis :

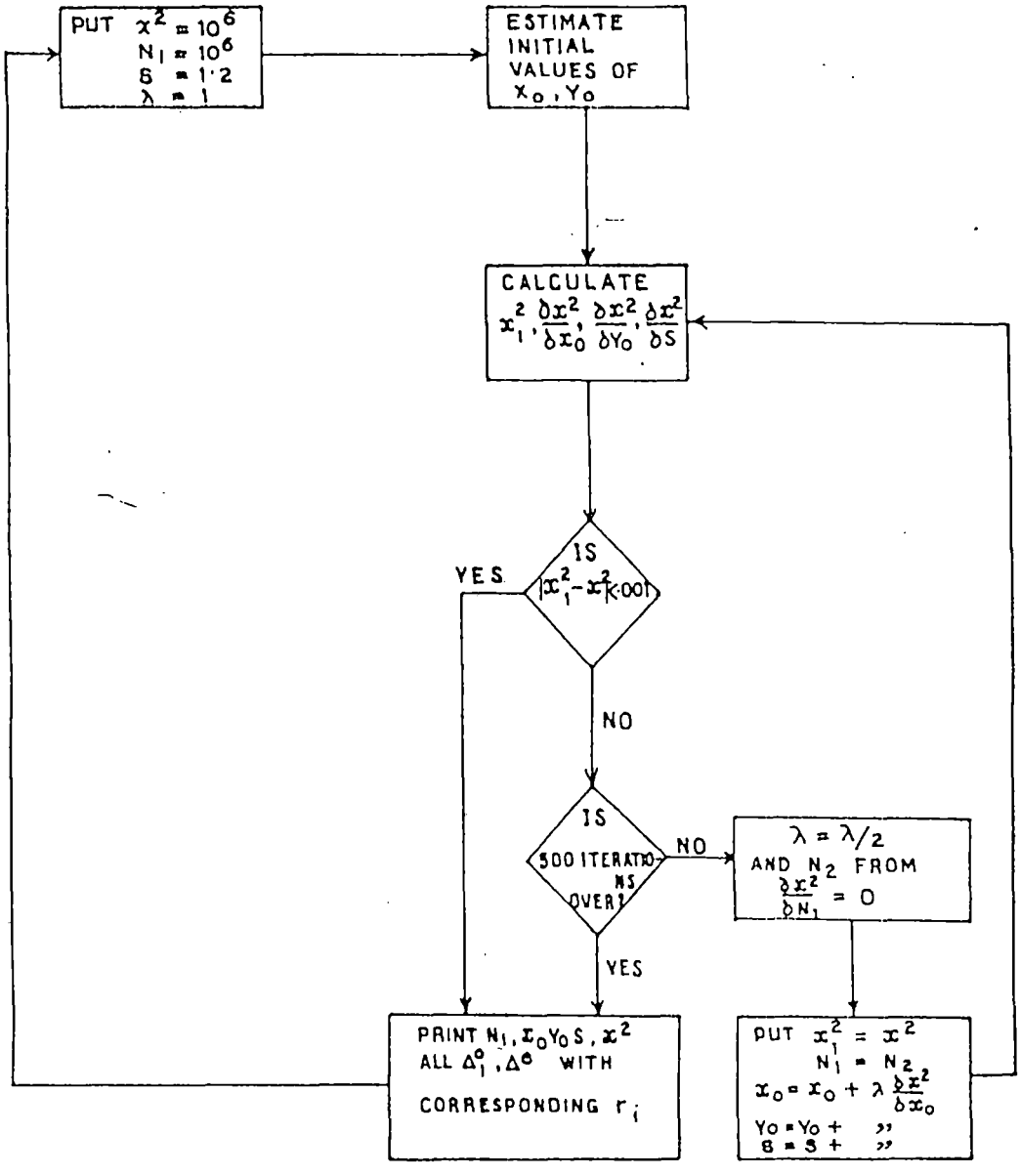

Fig. 2.6. Flow chart for x^2 - minimisation.

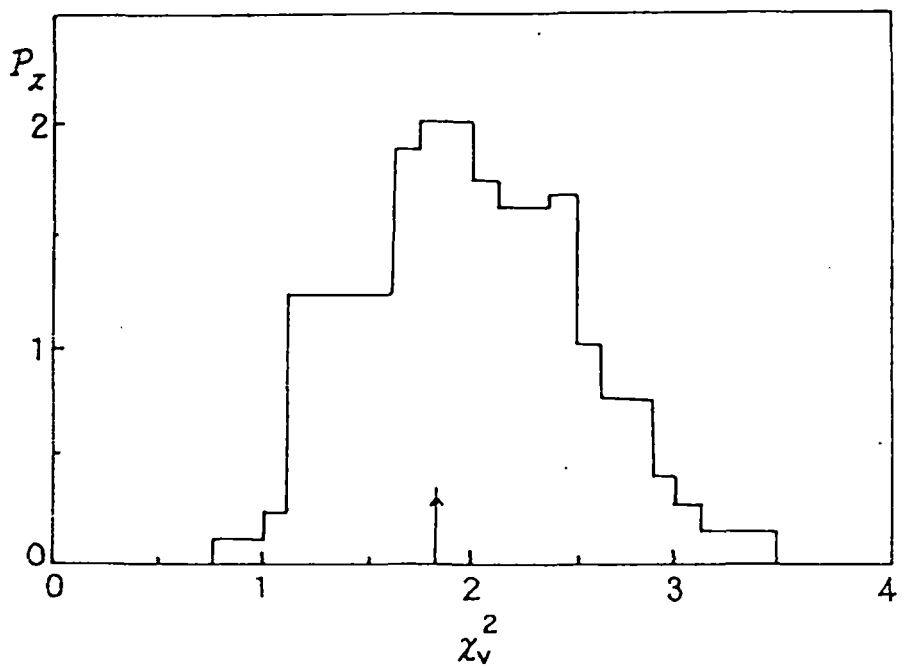

Fig. 2·7. The observed probability distribution P_χ for the reduced chi square χ_ν^2 using the NKG function in the radial range 0–120m.

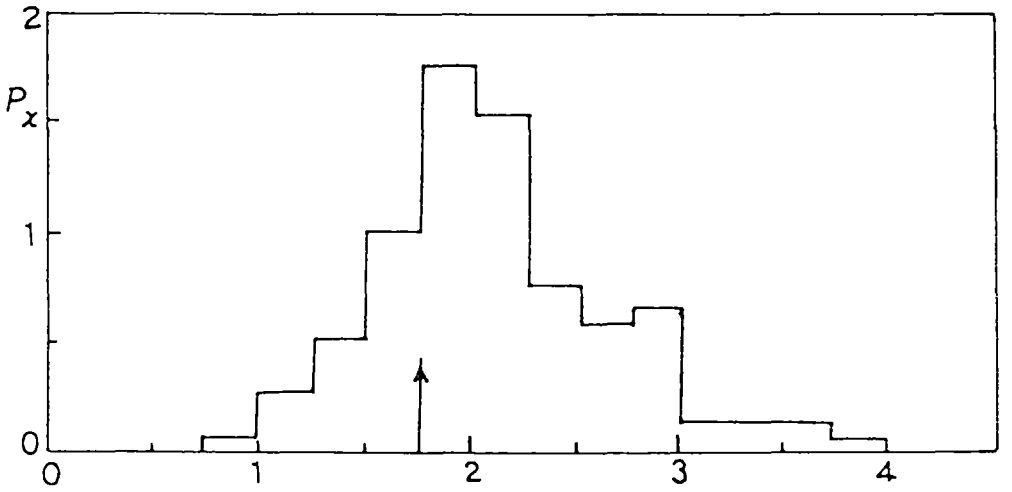

Fig. 2·8. The observed probability distribution P_χ for the reduced chi square χ^2_ν using the Hillas function in radial range 0–120 m.

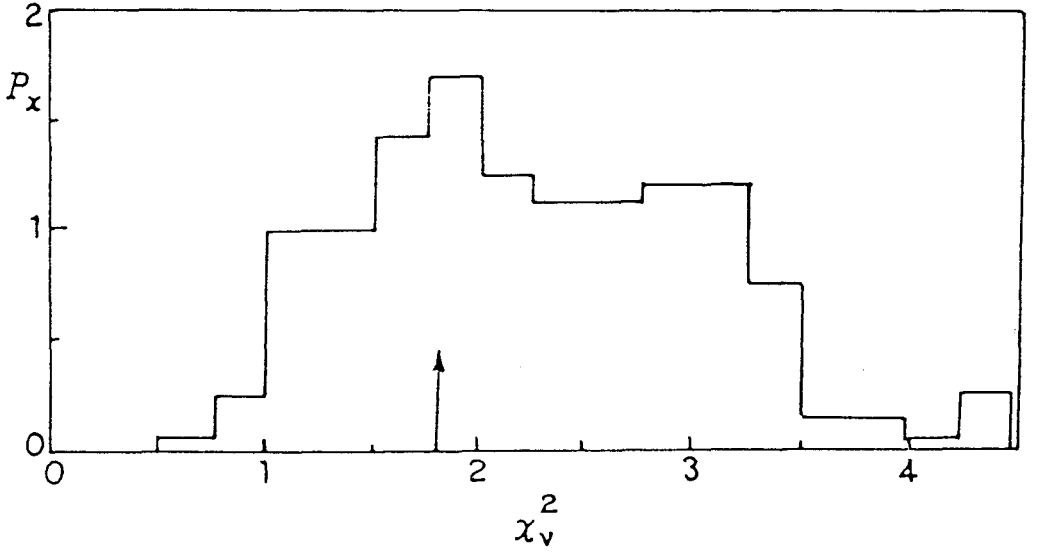

Fig. 2·9. The observed probability distribution P_χ for the reduced chi square χ^2_ν using the Capdevielle function in the radial range 0 – 120 m.

Event number : 2669

Date:12.2.94

Chi-square (per degree of freedom) : 0.582

Shower core : X_0 = 29.19m Shower size (N_e) = 6.2x 10^4

Y_0 = 20.99m Shower age (s) = 1.13

Distance (r) in m.	Fitted density in particles/m^2	Observed density in particles/m^2
7.65	26.12	22.93
22.40	5.00	6.04
22.75	4.85	2.67
15.35	9.93	10.52
9.59	19.75	17.42
17.65	7.79	7.47
15.23	10.03	8.71
12.84	13.16	17.60
8.73	22.25	18.67
21.27	5.54	4.44
14.60	10.77	10.24

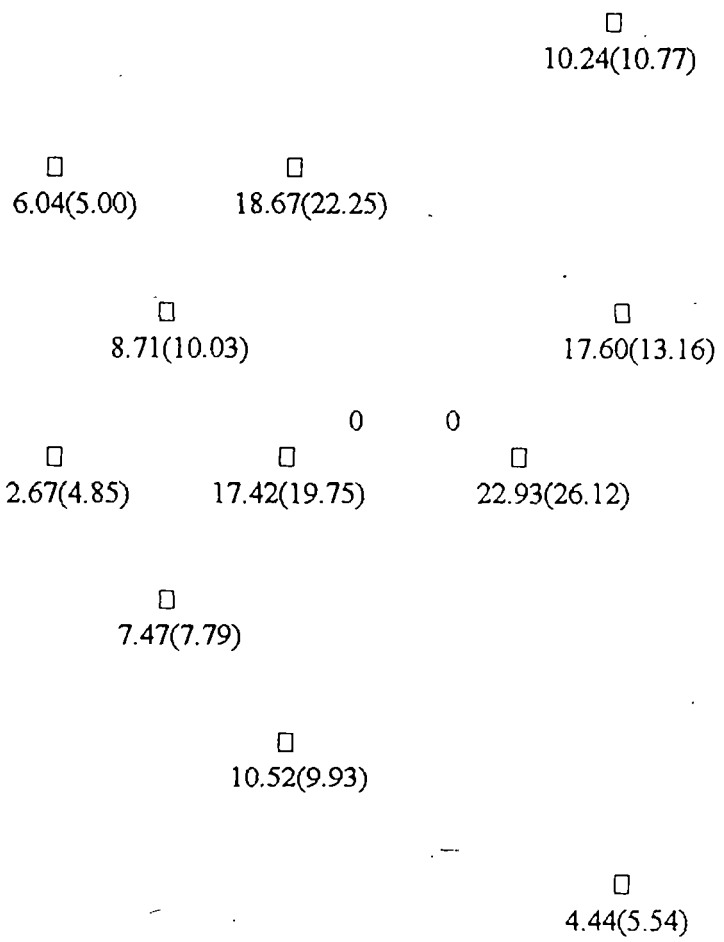

Fig.2.10. Observed shower data and reconstructed shower parameters from the observed data

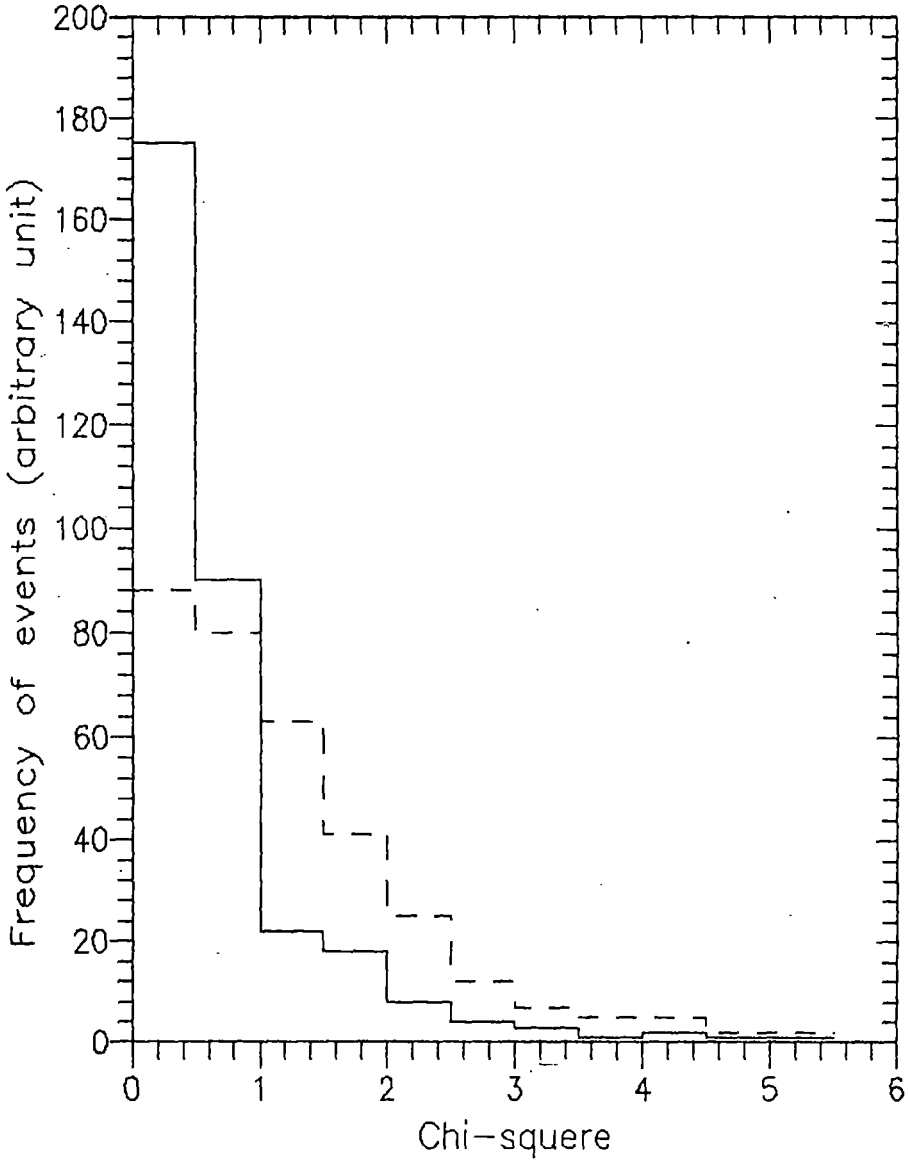

Fig.2.11. Chi-square distributions for experimentally observed shower data(dashed line)and for artificial shower data (solid line)

The momentum of a muon is measured from the deflection of its path in the magnetic field . A particle of momentum P and charge e moving transversely through a magnetic field of induction B is related to the radius of curvature R of its path given by

$$P = 300.B.R \ (eV/c) \qquad \text{---------- (2.6)}$$

where B is in Gauss , R is in cm.
If dl be the length of the element of path traversed by the particle normal to the field and $d\phi$ be the deflection of the particle due to magnetic field , then

$$R = dl/d\phi \qquad \text{———————— (2.7)}$$

Neglecting energy loss in the material of the magnet , the momentum of the particle can be written as

$$P = (300 \ Bdl) / \phi \qquad \text{---------- (2.8)}$$

where l is in cm. , ϕ is in radian and P is in eV/c.
A schematic diagram of the magnetic spectrograph along with the particle trajectory is shown in fig.2.12. The deflection in the magnetic field is calculated from the four measured co-ordinates along the length of the trajectory . FT_1, FT_2, FT_3, FT_4 are four neon flash tube trays which determine the particle trajectory. The reference line ACEG is at a distance a_0, b_0, c_0, d_0 from the four flash tube trays respectively. CL is the central line of the spectrograph and the effective length of the magnet is 2L where 2L = 106.3 cm. X_1, X_2 are the distances of the trays as shown in fig.2.12 where X_1=31.85 cm., X_2 = 85 cm., $L+X_1=X_2=85$ cm.
Since ϕ is the deflection at the central place of the magnet M ,

$$FT_1.FT_2 = FT_3.FT_4$$

If a perpendicular line is drawn from H' on EF' , we get from the geometry of the particle trajectory ,

$$GH' - EF' = CD - AB \qquad \text{.....(2.8a)}$$

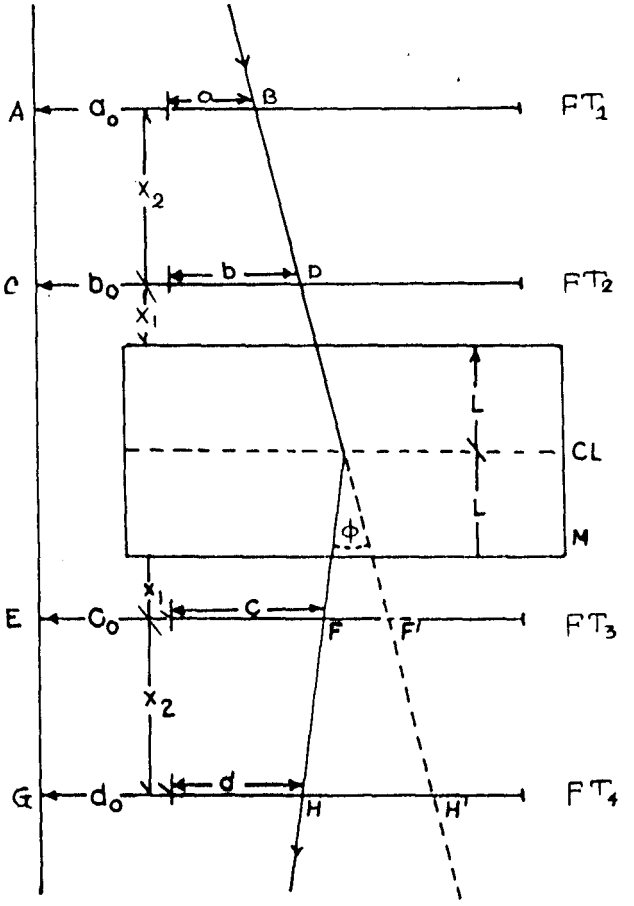

Fig. 2.12 A schematic diagram of the magnetic spectrograph along with the particle trajectory.

$$\text{or,} \quad (GH + HH') - (EF + FF') = CD - AB$$

$$\text{Now,} \quad HH' = \phi(L + X_1 + X_2) \;, \; FF' = \phi(L + X_1)$$

$$\text{Hence,} \; GH' = GH + HH' = (d_0 + d) + \phi(L + X_1 + X_2)$$

$$EF' = (c_0 + c) + \phi(L + X_1)$$

Using equation 2.8a, we get,

$$(d_0+d) + \phi(L+X_1+X_2) - (c_0+c) - \phi(L+X_1) = (b_0+b) - (a_0+a)$$

$$\text{or,} \quad \phi X_2 + (d+d_0) - (c+c_0) = (b+b_0) - (a+a_0)$$

$$\text{or,} \quad \phi = [\{(b+b_0)-(a+a_0)\} + \{(c+c_0)-(d+d_0)\}] / X_2$$

Now we can write

$$\phi = (\Delta_0 + \Delta_m) / X_2$$

$$= \Delta / X_2 \qquad \text{----------(2.9)}$$

where $\Delta_0 = (b_0-a_0) + (c_0-d_0)$

and $\Delta_m = (b-a) + (c-d)$

The quantity Δ_0 is the geometrical constant of the magnetic spectrograph and Δ_m is the geometrical constant due to magnetic deflection .

From equations 2.8 and 2.9 , we have

$$P = 300 \; Bdl/\phi$$

$$= 300.B.2L.X_2/\Delta$$

$$= C/\Delta \quad (eV/c)$$

where $C=300.B.2L.X_2$

For the NBU magnetic spectrograph , $B=1.62\text{x}10^4$ Gauss, $2L=106.3$ cm. , $X_2=85$ cm.

Hence $C= 300\text{x}1.62\text{x}10^4\text{x}106.3\text{x}85/1.999$ (eV/c)(t.s)

and $P = 21.96/\Delta$ (GeV/c) ---------- (2.10)

where Δ is in t .s unit (1 t .s =1.999 cm.)

The momentum can be calculated from equation 2.10 by measuring the quantity Δ. The values of a_0, b_0, c_0, d_0 are measured from the alignment of the spectrograph and a, b, c, d are measured by using the projector method as discussed below.

To obtain the exact position of the tubes flashed in the trays ,first, the films are projected on the vertical board by a 35 mm film projector . All the boards contain the serial number of the tubes with respect to the fiducial marks. With the aid of the fiducial marks, images of the flashed tubes are positioned on this reference board and the row number and the column number for each tray are recorded on a data sheet . Hence after determination of a, b, c, d for each muon event equation 2.10 is used for the calculation of momentum of a muon passing through the magnetic spectrograph .

2.2.4. Error estimation in the measured shower parameters:

To have any confidence in the experimental results , it is essential to have an idea of the errors in the value of the shower parameters determined by the minimisation procedure discussed in sec.2.2.2 since all the properties of EAS are defined in terms of the shower parameters. The errors arise owing to fitting a fluctuated set of densities to an average lateral distribution function and also owing to the arbitrary criteria for locating the minimum of the χ^2 -surface . If the χ^2-surface is flat , we may be far away from the minimum even though the criteria for the minimum is satisfied . An artificial shower analysis is done for this purpose.

The errors in the determination of shower parameters have been evaluated by using the standard procedure of artificial shower analysis . A shower of known parameters is allowed to be incident at any point within the array selected at random and the particle density in each detector is calculated according to the Hillas function [5] .To reproduce the experimental conditions, the statistical fluctuations in the number of particles in each detector and the systemetic error in the conversion of pulse height into particle density are superposed on each detector .For a set of densities for each shower , χ^2 - minimisation procedure is applied to estimate the shower parameters . The estimated shower parameters deviate from the corresponding shower parameters used for an artificial shower and the deviations are given below

(1) $\Delta X = \pm 2.4$ m
(2) $\Delta Y = \pm 2.7$ m
(3) $\Delta N_e/N_e = \pm 9.6\%$
(4) $\Delta s = \pm 0.13$

Some histogramsfor the deviations of the parameters are shown in figs.2.13, 2.14, 2.15 and 2.16.

2.2.5. Sensitivity of the EAS array:

Showers of all sizes with their cores at all points are recorded so long as they satisfy the triggering condition as discussed in sec.2.1.6 but the detection efficiency and triggering probability for a particular shower size are dependent on the distance from the centre of the array . Therefore to observe the sensitivity of the EAS array , the detection efficiency and triggering probability at different N_e and s have to be determined.

Detection efficiency of the EAS array:

The efficiency of detection is nothing but the fraction of showers that were selected .To find the detection efficiency ε (N_e, s, X, Y) at any point (X,Y) of the array for detecting showers of size N_e and age s , the circular symmetry of the array was used because of reduced numerical computation . The array was divided into a number of annular rings . Showers with fixed size N_e and s were uniformly selected in an annular ring and the expected density at each detector was calculated by using Hillas function .To these densities ,the Poissonian and systemetic errors were superposed .Then the selection criteria was applied and checked whether the particular shower was selected or not .A total of 1000 showers were generated in each annular ring .The computation was repeated by varying the shower size N_e and distance bin. The variation of detection efficiency with radial distance for different N_e and s are shown in figs. 2.17, 2.18, 2.19 and 2.20. If R_0 is the distance from the centre of the array at which the detection efficiency is 90% , the 90% efficient area of the array is πR_0^2 .

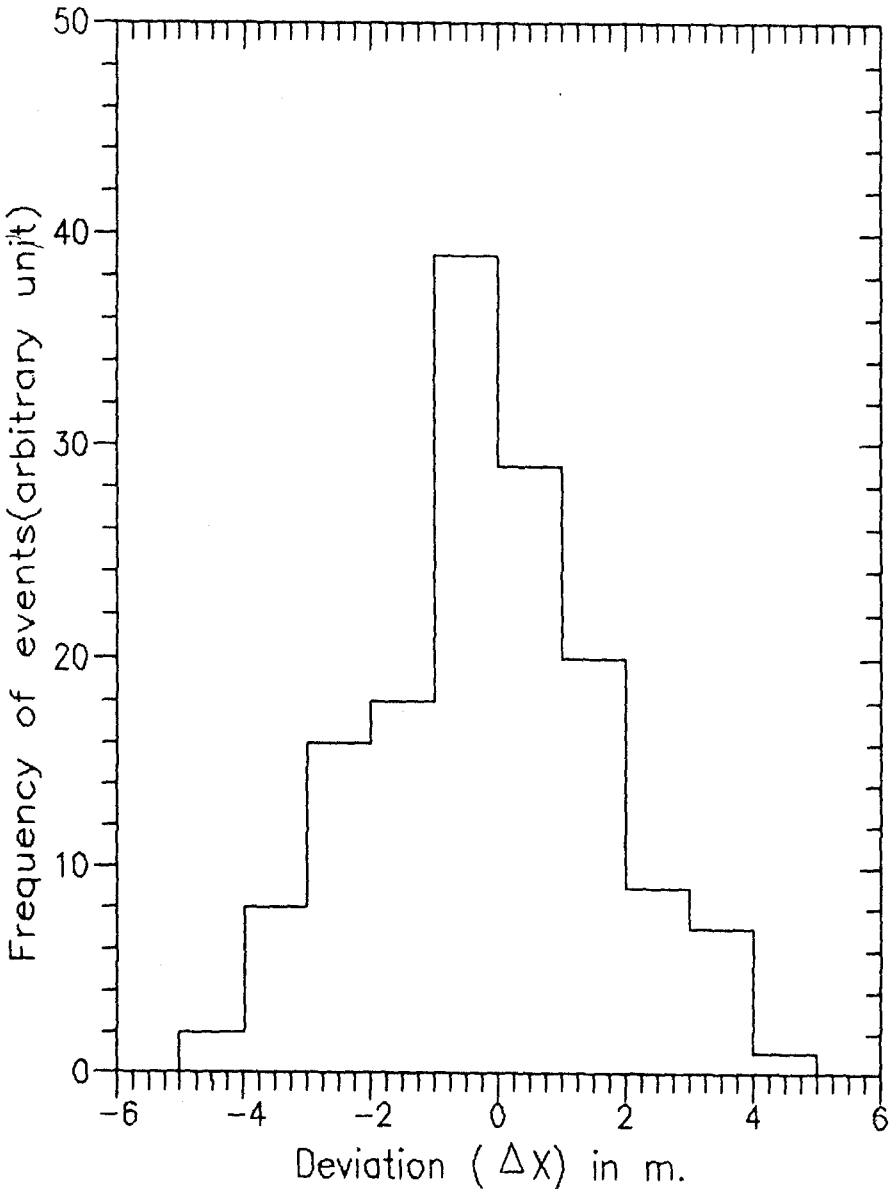

Fig.2.13. Frequency distribution of deviations in core location along the X-axis

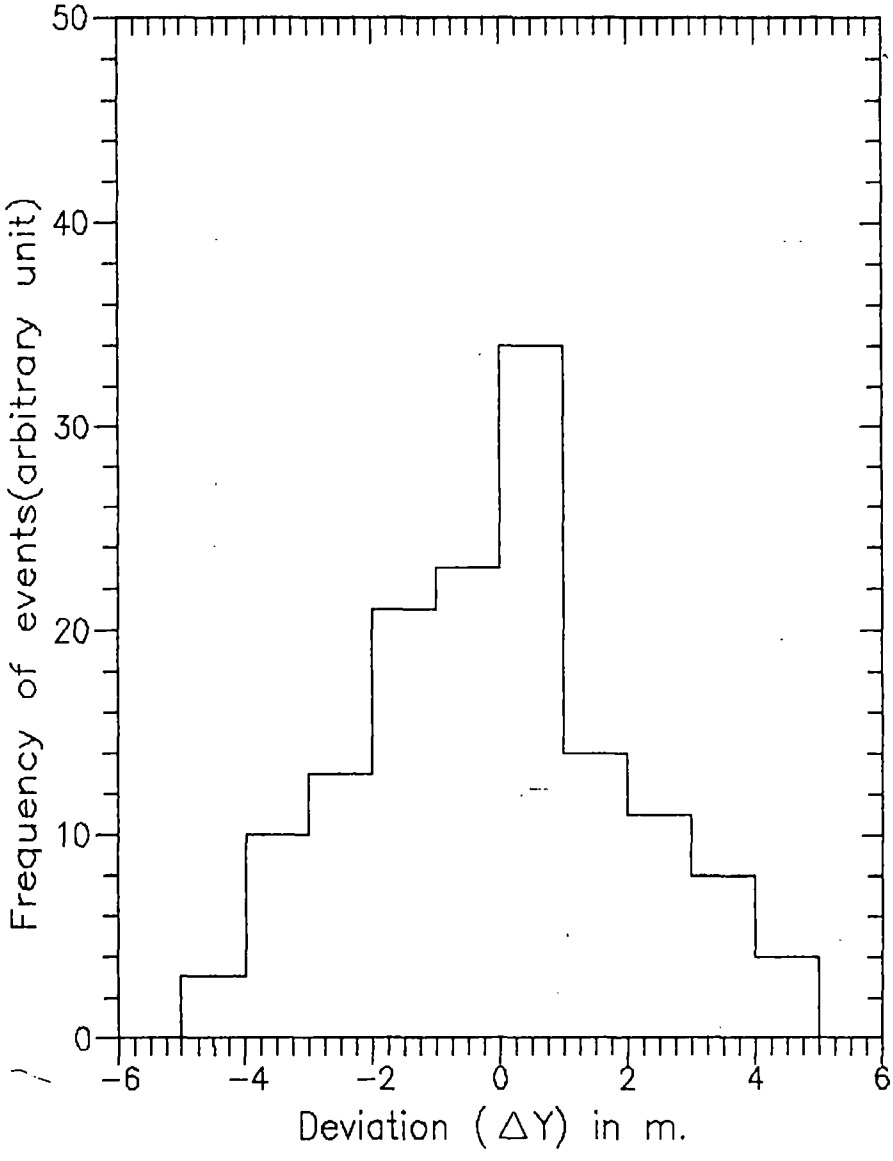

Fig.2.14. Frequency distribution of deviations in core location along the Y−axis

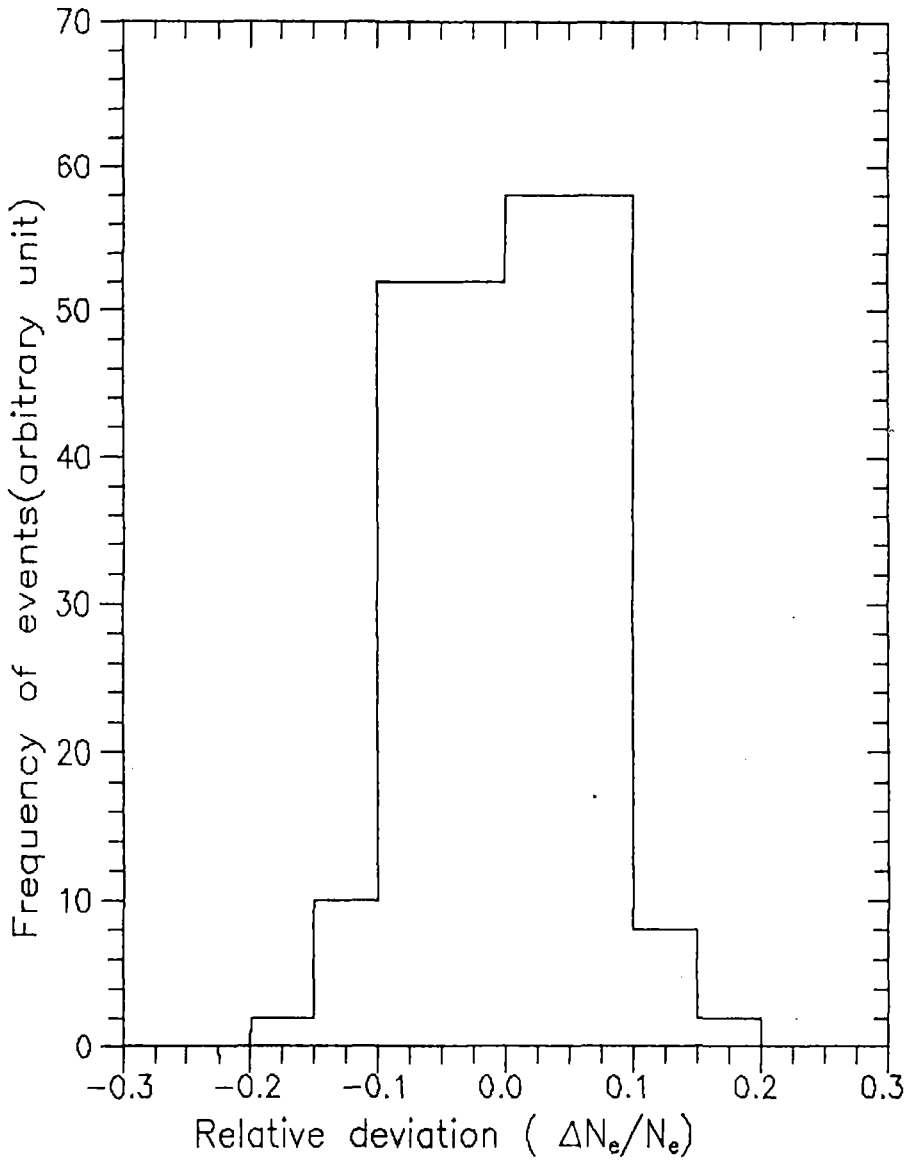

Fig.2.15. Frequency distribution of deviations in shower size

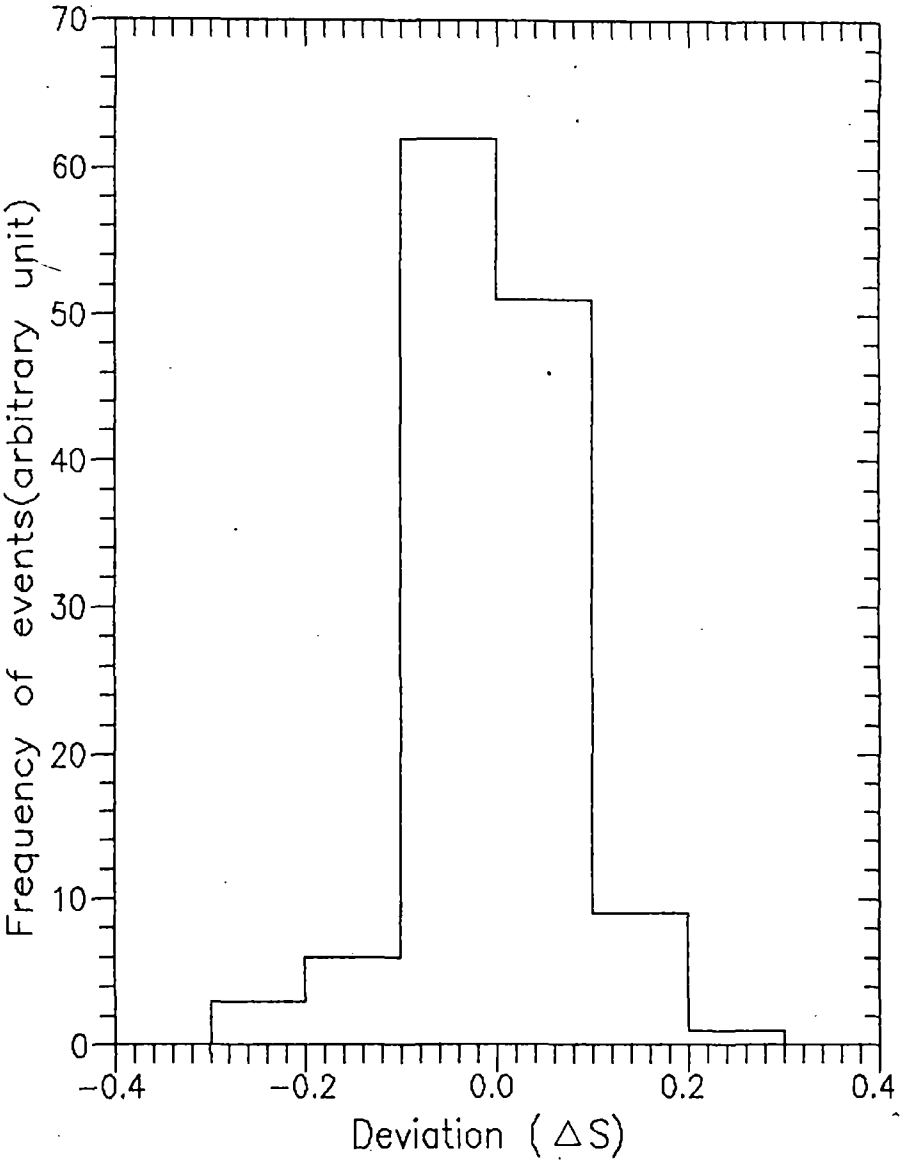

Fig.2.16. Frequency distribution of deviations in shower age

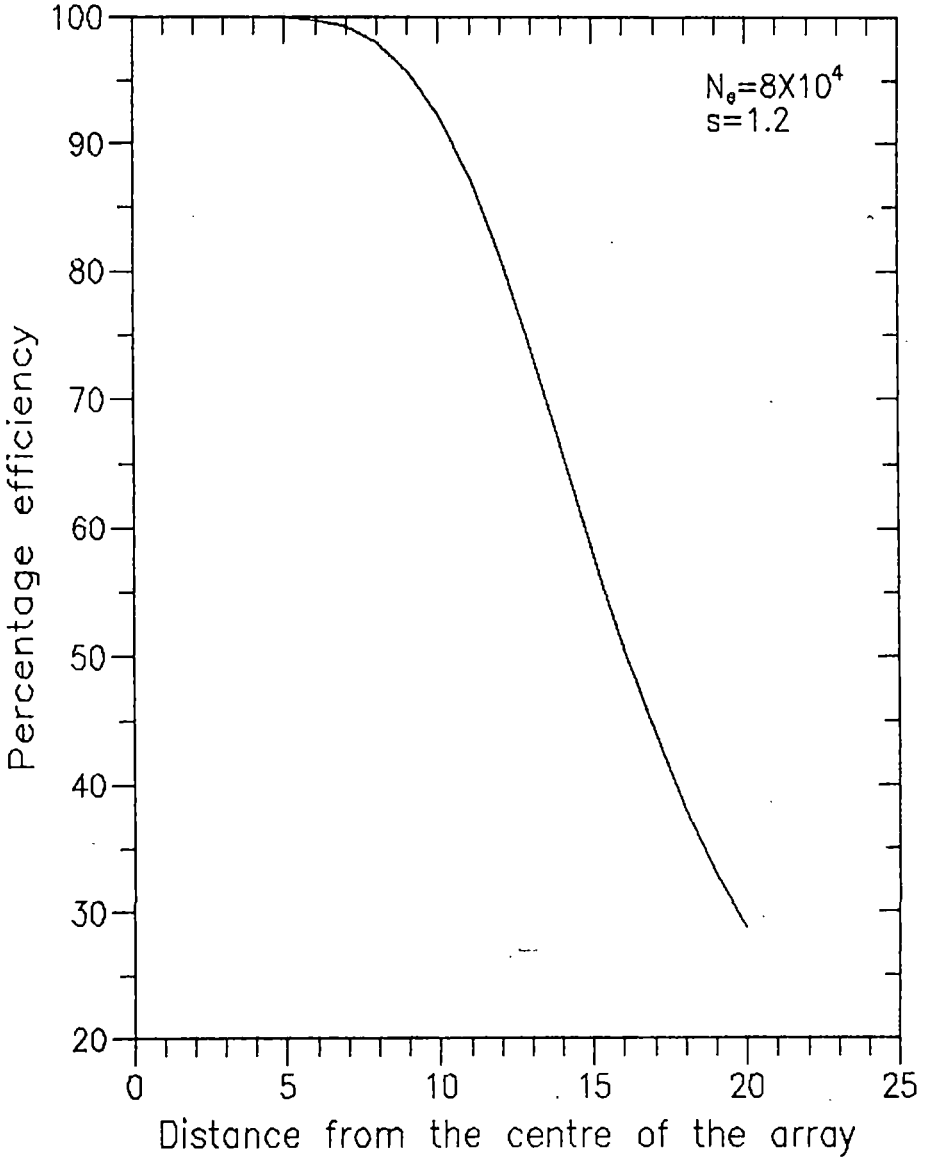

Fig.2.17. The detection efficiency of the array as a function of distance from the centre of the array for N_e=8x10^4 and s=1.2

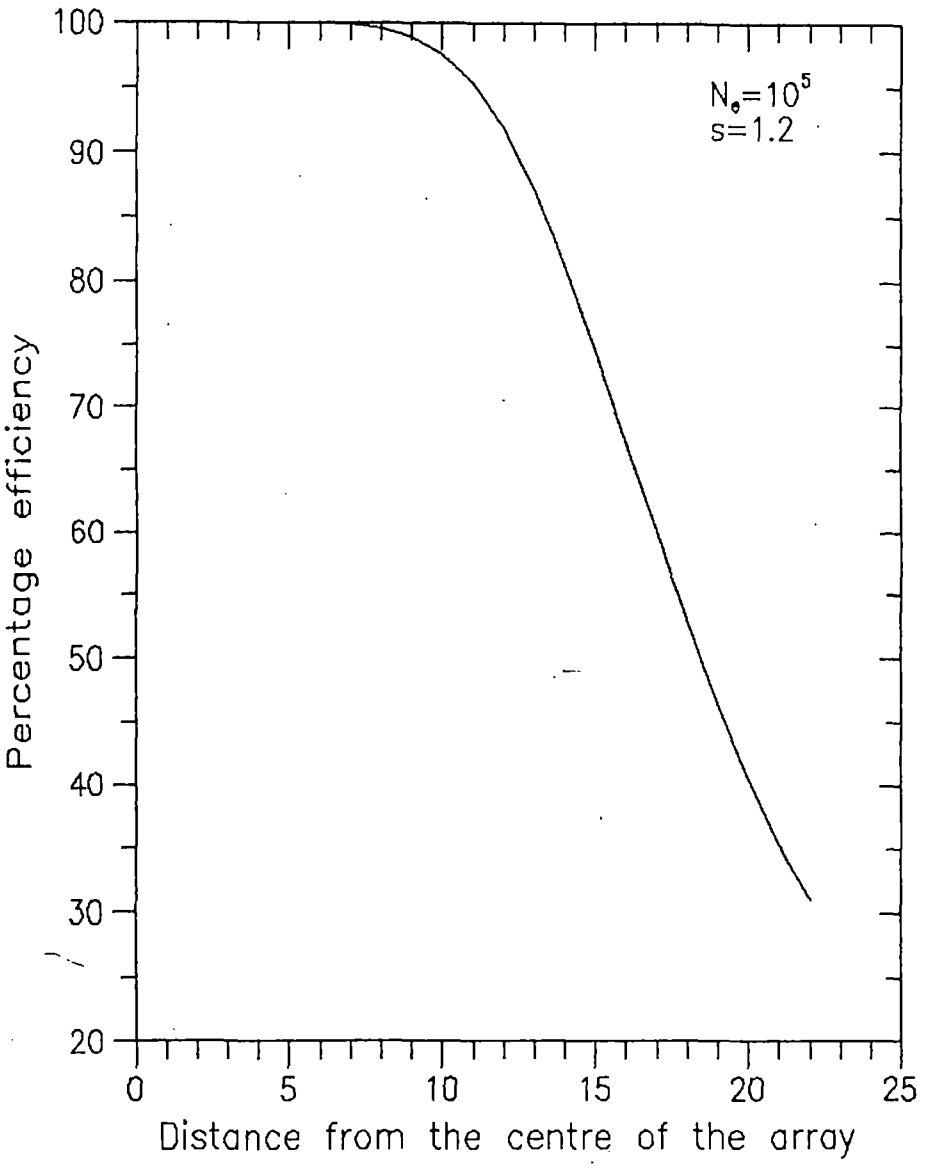

Fig.2.18. The detection efficiency of the array as a function of distance from the centre of the array for $N_e=10^5$ and s=1.2

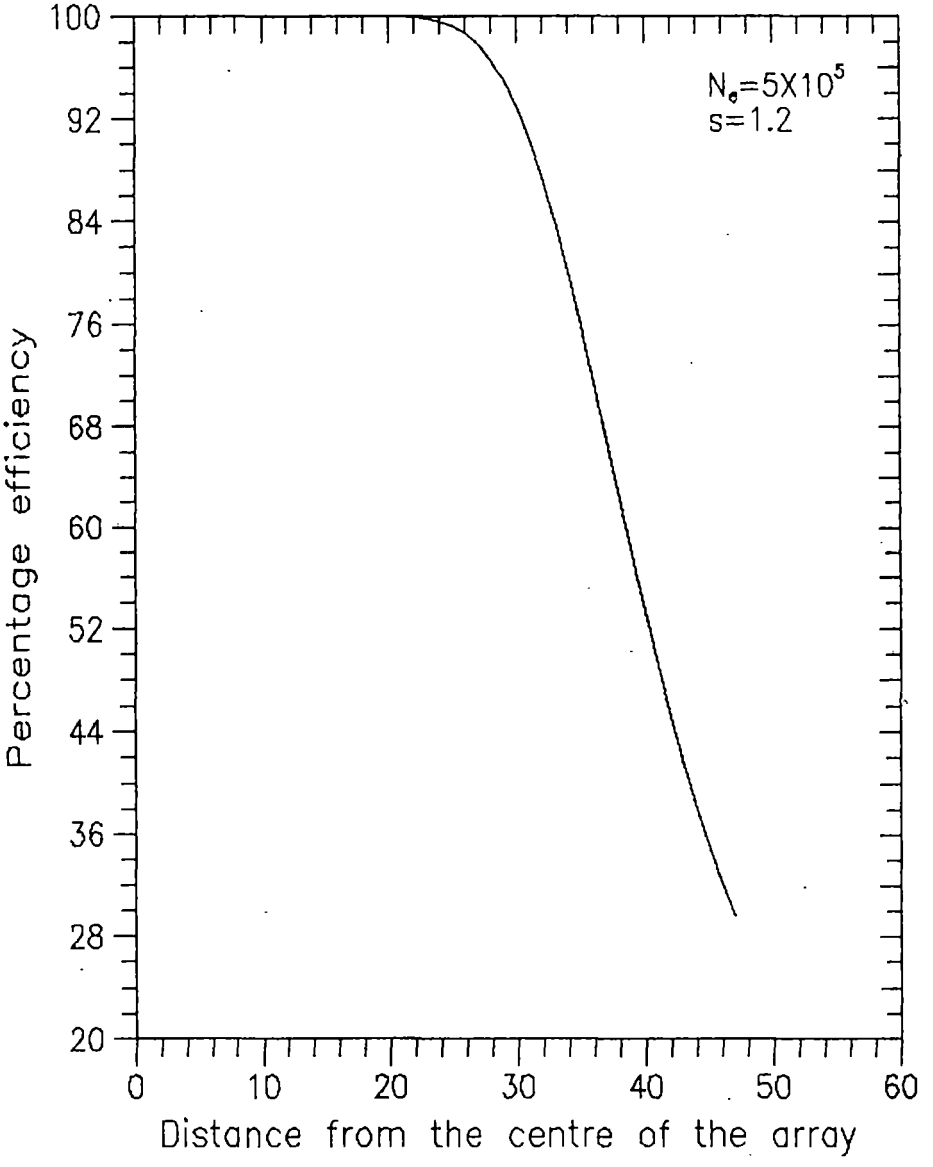

Fig.2.19. The detection efficiency of the array as a function of distance from the centre of the array for N_e=5x10^5 and s=1.2

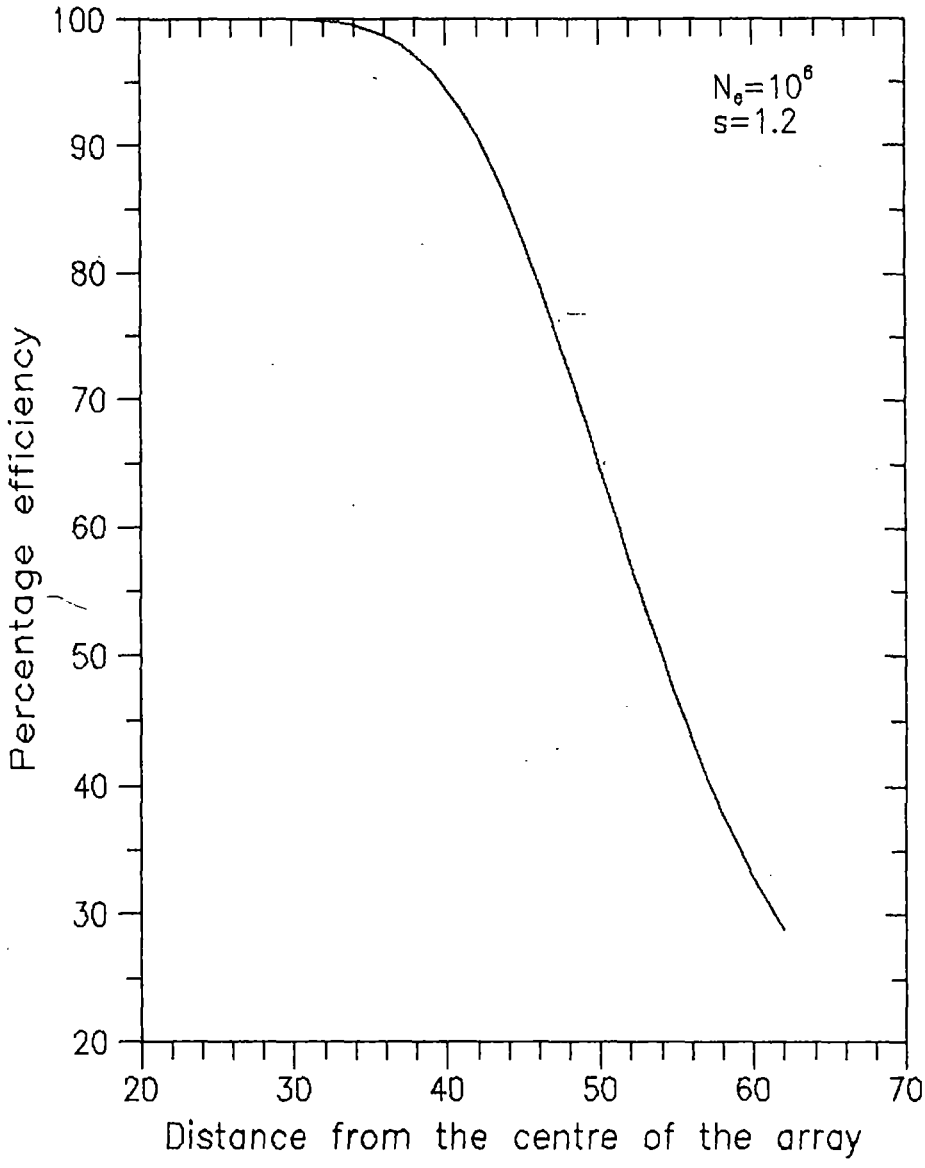

Fig.2.20. The detection efficiency of the array as a function of distance from the centre of the array for $N_e=10^6$ and s=1.2

Triggering probability of the EAS array:

Calculation of the average triggering probability is based upon the assumption that the number of particles that are detected in a detector follow Poissonian statistics and if this is so then the triggering probability P_i is given by

$$P_i = \exp(-\Delta_i.S_i) \sum_{n=m}^{\infty} (\Delta_i.S_i)^n / n! \quad \text{----------(2.11)}$$

where Δ_i is the particle density on the ith detector which is calculated by using Hillas function and S_i is the area of the ith detector whose particle threshold for detection is m.

The above relation is true only for detectors with no sampling errors , but in general the detectors have efficiencies that depend on both the number of particles incident on them and their particle threshold . If the efficiency is defined as $\varepsilon_i(n,m)$, where n is the number of particles incident on the detectors and m is the particle threshold , then equation 2.11 becomes

$$P_i = \exp(-\Delta_i.S_i) \sum_{n=0}^{\infty} [(\Delta_i.S_i)^n / n!] \, \varepsilon_i(n,m) \quad \text{---------- (2.12)}$$

A useful modification to equation 2.12 is to write in such a way that it is not necessary to sum over an infinite number of particles but only k terms where k is the number of particles at which ε_i becomes unity for the value of m in equation (2.12) and then

$$P_i = 1-\exp(-\Delta_i.S_i) \sum_{n=0}^{k} [\{(\Delta_i.S_i)^n / n!\}.\{1-\varepsilon_i(n,m)\}] \quad \text{----------(2.13)}$$

Equation 2.13 is used to measure the average triggering probability of the EAS array as a function of shower size for different radial distances .The variation of average triggering probability with shower size for core distances 20m,30m and 40m from the centre of the array are shown in fig.2.21.

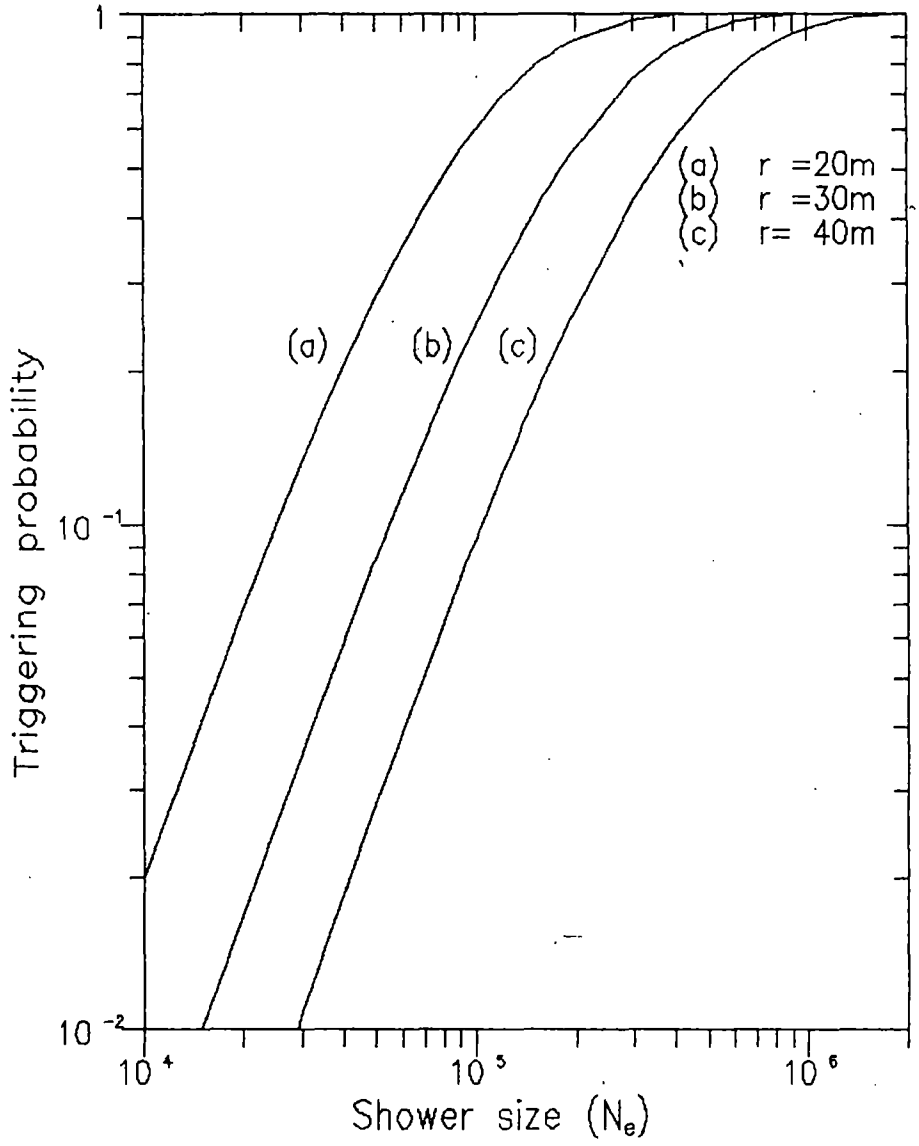

Fig.2.21. The average triggering probability for the array of detectors as a function of shower size for core distances 20m,30m and 40m

CHAPTER 3

EXPERIMENTAL RESULTS

The present experiment has been carried out on the North Bengal University campus (at an atmospheric depth ~ 1000 gcm^{-2}) by using the NBU air shower array comprising nineteen electron density detectors , eight fast timing detectors and two muon magnetic spectrographs. A total of 16,000 shower data associated with 2927 muon events have been collected carrying out the experiment during the period January 1994 to September 1995. Showers are detected in the size range 10^4 - $2.5x10^6$ particles . Showers having chi-square per degree of freedom greater than 6 are rejected as the fit of the observed data with fitting function is poor above 6 and for the same reason showers with age parameter greater than 1.6 or less than 0.7 are also rejected .The frequency distribution of shower size and shower age are shown in fig.3.1and fig.3.2.

The results of the experiment are presented here into two sections (section 3A and section 3B)

In the first section the results on the observations made on radial distribution of electrons , radial distribution and energy spectra of muons, variation of muon density to electron density ratio as a function of radial diastance, variation of total number of muons (N_μ) with shower size (N_e) are given .

The second section includes the results dealing with the variation of primary mass with the energy of the primary particle.

SECTION - 3A

3A.1 Determination of mean primary energy :

The primary energy of an EAS event is not possible to be determined precisely from the observed particle density distribution due to the presence of fluctuations in an EAS development . However the mean primary energy was determined by comparing the observed vertical shower size with the results of Monte Carlo model for proton primary at sea-level.

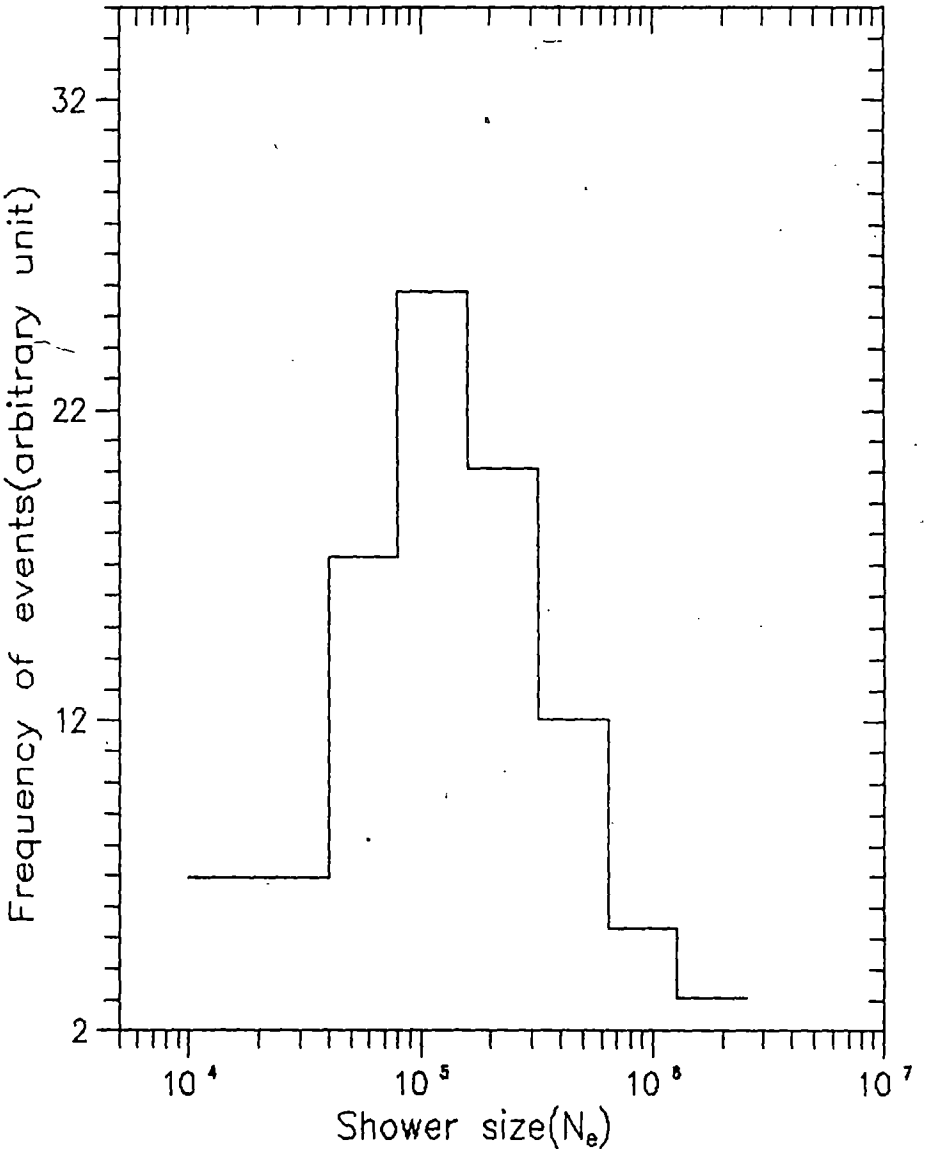

Fig.3.1. Frequency distribution of shower size of the observed shower events.

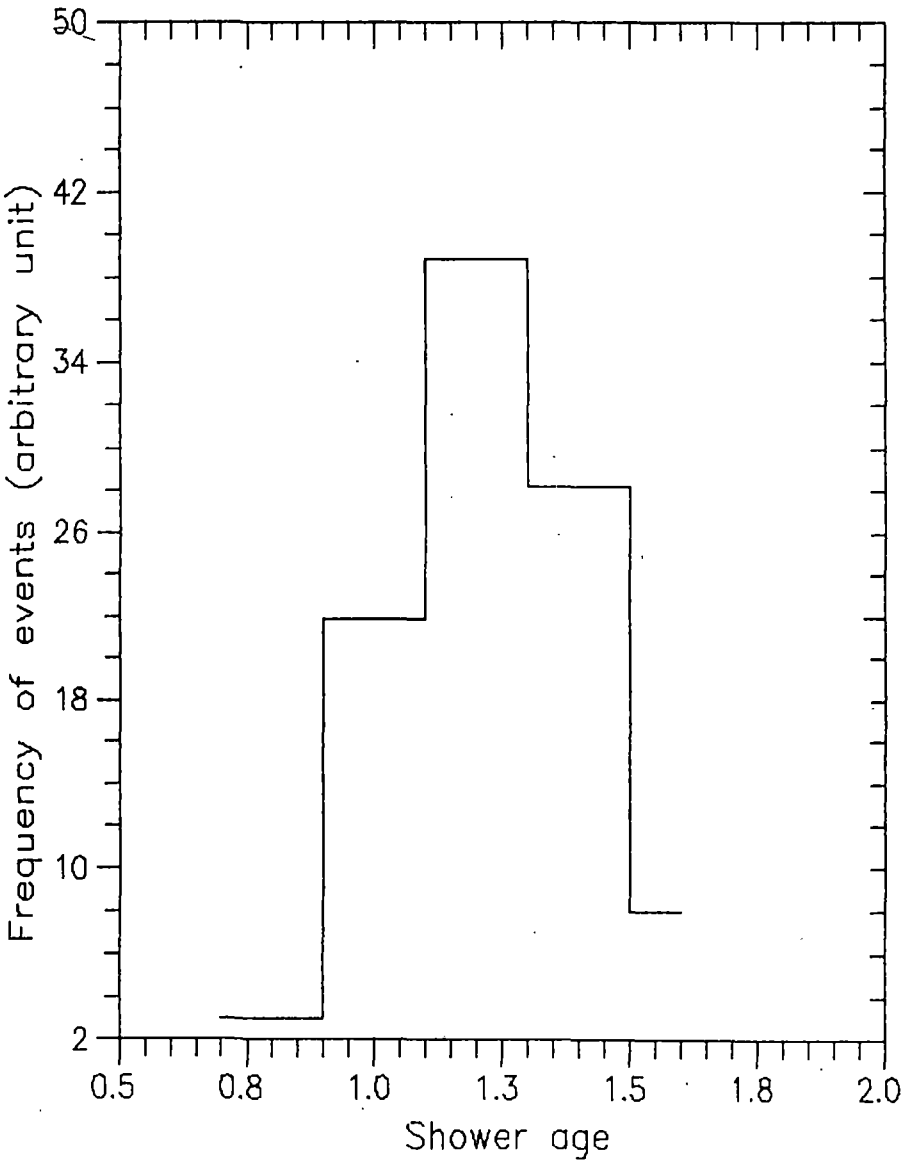

Fig.3.2. Frequency distribution of shower age of the observed shower events

For each shower of fixed size (N_e) and age (s) the mean energy of the primary particle (proton) (E_o) was obtained with a maximum error of 10% (which includes fluctuation in EAS development and the error in shower size measurement) from the energy scale established on the basis of hybrid Monte Carlo model (Trzupek et al [1]) for EAS at sea-level as given by

$$E_o(eV) = 3.03 \times 10^{10} \times N_e^{0.87} \quad \text{---------- (3.1)}$$

The mean primary energy was also obtained from the results of Monte Carlo simulations of EAS (Wrotniak and Yodh [2]) on the basis of different interaction models. For proton initiated shower and for the nuclear interaction model M-F00 , the relation between primary energy and shower size at sea-level is

$$E_o(eV) = 4.58 \times 10^{10} \times N_e^{0.84} \quad \text{---------- (3.2)}$$

In the analysis of the present experiment eqn.3.1 has been used to find out the primary energy from shower size.

3A.2. Radial distribution of electrons:

In the first step of the shower processing , the shower size N_e, the shower core Xo, Yo and the shower age s for each shower event are determined by fitting the measured particle densities to the fitting function (Hillas [3] function) by the chi-square minimisation procedure . Showers over the size range 10^4 - 2.5 x 10^6 particles are then divided into 8 groups with the size bins (1-2)x10^4 , (2-4)x10^4 , (4-8)x10^4 , (0.8-1.6)x10^5 , (1.6-3.2)x10^5 , (3.2-6.4)x10^5 , (0.64-1.28)x10^6 ,(1.28-2.56)x10^6 and for each group the whole radial range 0-45 m is again subdivided into 8 radial groups with distance bins (0-4)m ,(4-8)m ,(8-12)m ,(12-16)m ,(16-20)m ,(20-25)m ,(25-35)m , (35-45)m . The mean shower size , mean shower age for every shower size bin and mean core distances of different distance bins for a particular shower size bin are then calculated . For a particular shower size bin the mean electron density in a distance bin is determined following the relation

$$\Delta_e = 1/n \sum_i \Delta_{ei} \quad \text{----------(3.3)}$$

where n is the number of showers in that shower size bin as well as the distance bin. The transition effect arising from multiplication or absorption (absorption is predominant over multiplication)of shower particles in the finite thickness of a plastic scintillator in a density detector of the EAS array is taken into account and is corrected by using the relation as given by Asakimori et al [4] as

$$\Delta_c = \Delta_e(1.192 - 0.136 \log r)$$

where Δ_c and Δ_e are the corrected and measured densities respectively and r is the distance of the detector from the shower core.

The observed radial distribution of electrons for showers of sizes 1.09×10^5 , 4.48×10^5 and 1.79×10^6 along with the curves obtained from the Hillas function are shown in figs. 3.3 , 3.4 and 3.5. It is seen from the figures that the observed radial distributions up to the core distance of 45m are in good agreement with those predicted by Hillas et al [3].

3A.3.Measurement of muon density:

In the present experiment two identical magnetic spectrograph units separated by a distance of 4m are operated with the air shower array to detect the muon component in EAS.

The density of muons is calculated in the following way. The average muon density in near vertical showers as a function of radial distance from the shower core for each of the various shower groups in the shower size range 1.52×10^4 - 1.79×10^6 particles is defined as

$$\rho_\mu(\geq E_\mu, N_e, r) = n_\mu(\geq E_\mu, N_e, r) / [N_t(N_e, r).A'] \text{ ---------- } (3.4)$$

where $n_\mu(\geq E_\mu, N_e, r)$ is the total number of muons recorded in a particular distance interval (r) for a particular shower size (N_e) in a certain period of time above the threshold energy ($\geq E_\mu$) , N_t (N_e,r) represents the total number of showers of size N_e at the distance interval (r) recorded at the same time and A' is the effective area of the muon detector.The effective area of the muon detector A' is nearly same for all the observed muons since the maximum projected angle by the magnetic spectrograph is very low (i.e, near vertical)

3A.4. Radial distribution of muons:

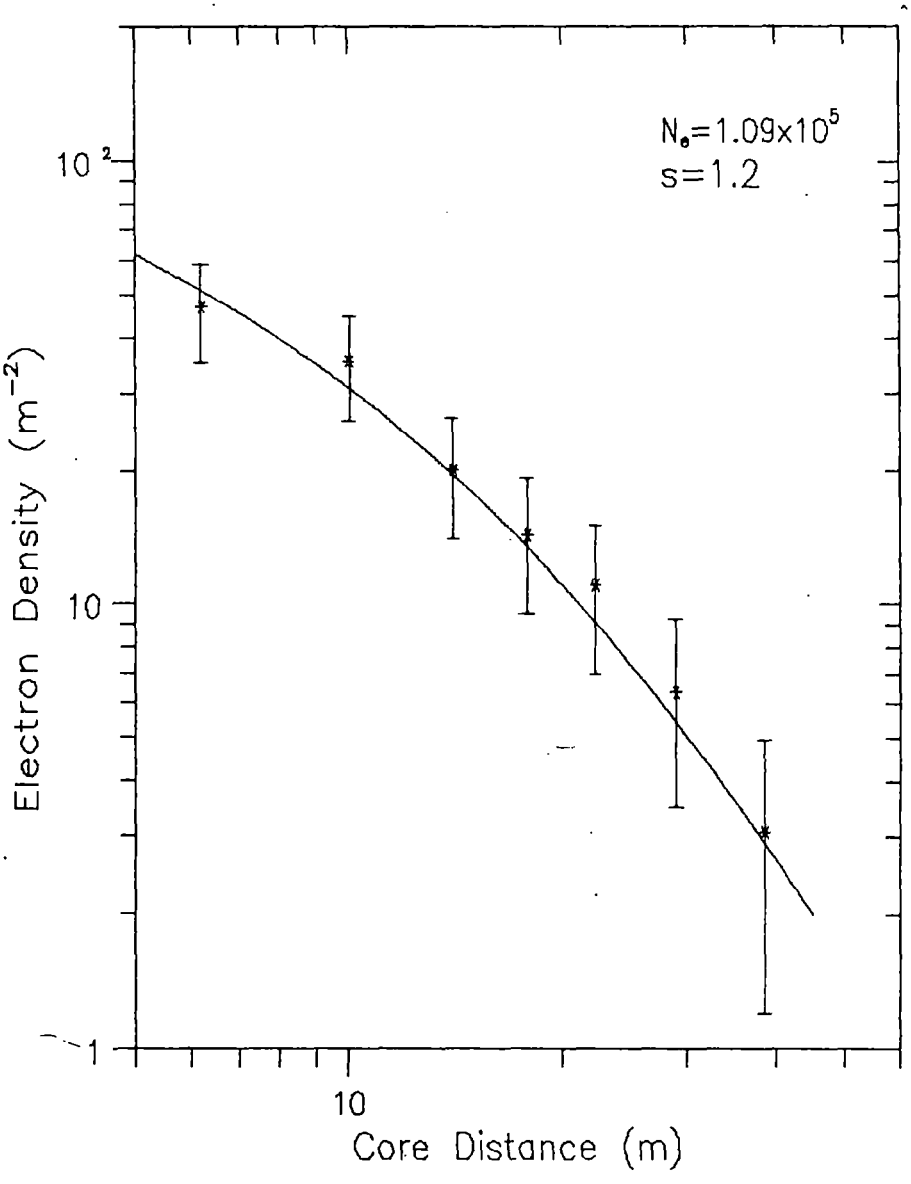

Fig.3.3. Observed radial distribution of EAS electrons compared with the Hillas function (solid line) for shower size 1.09×10^5 and shower age 1.2

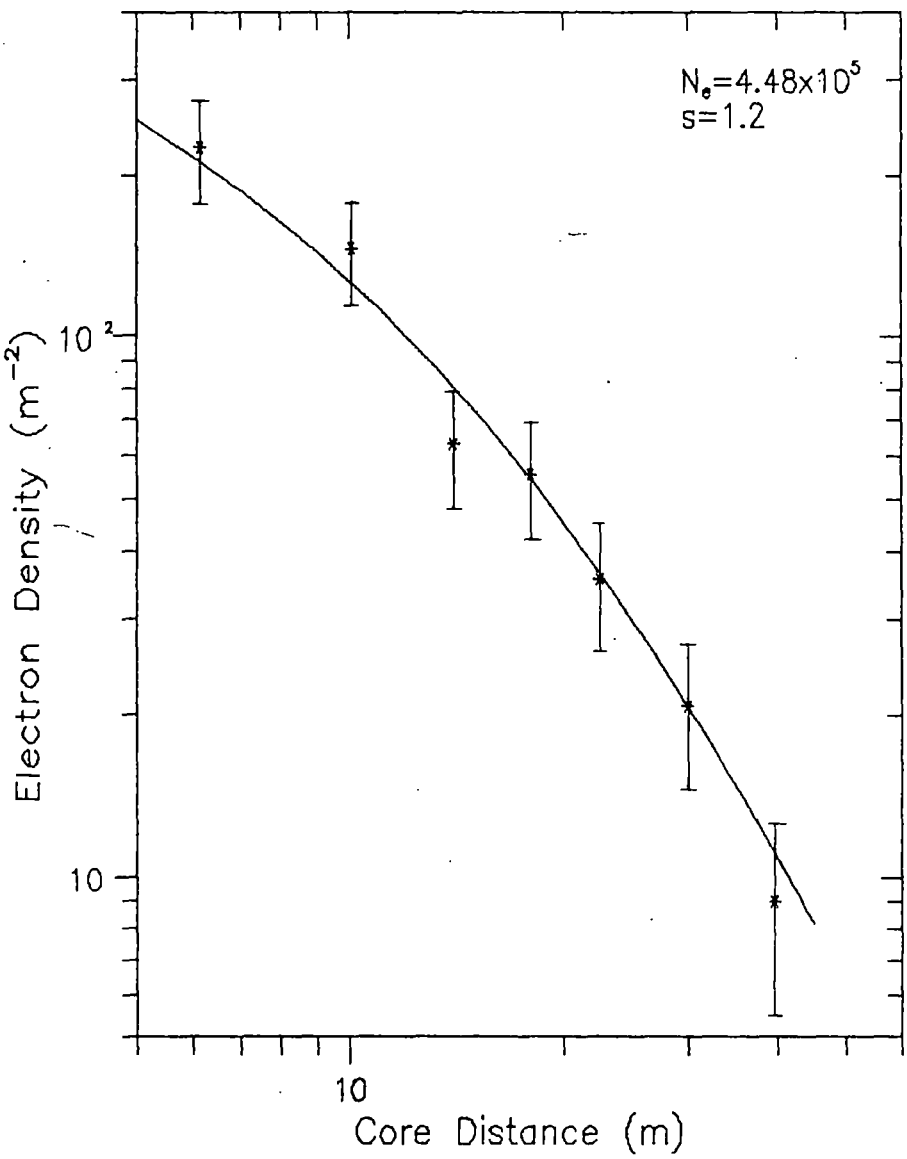

Fig.3.4. Observed radial distribution of EAS electrons compared with the Hillas function (solid line) for shower size 4.48×10^5 and shower age 1.2

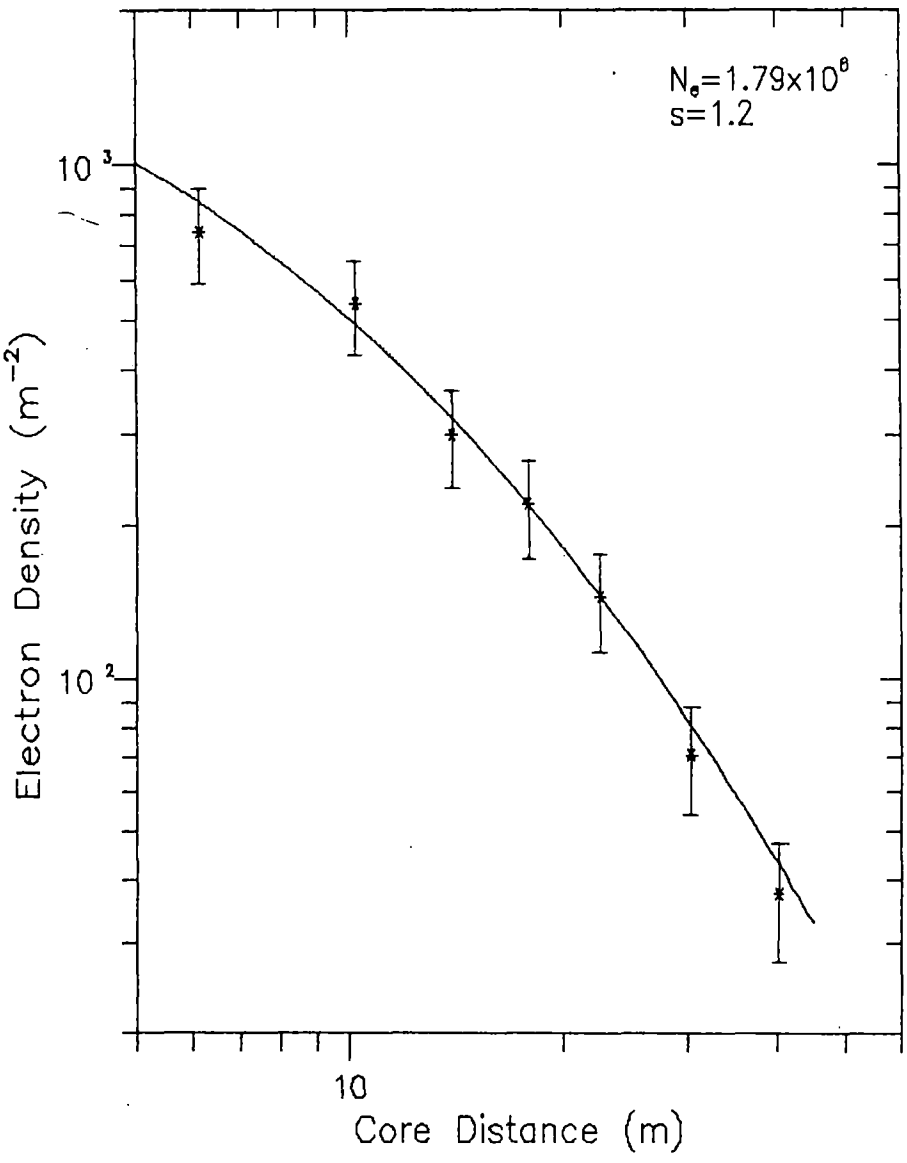

Fig.3.5. Observed radial distribution of EAS electrons compared with the Hillas function (solid line) for shower size 1.79×10^6 and shower age 1.2

In a particular shower group the muons are divided into groups in terms of chosen threshold energies ($\geq E_\mu$) and then each group is distributed into a number of bins with respect to radial distances from the shower core to determine the average muon density as a function of radial distance and threshold energy.

The density of muons for $E_\mu \geq 2.5$, 5 , 10 , 20 , 50 , 75 and 100 GeV are calculated using the equation (3.4) . The observed radial distribution of muons for different muon threshold energies and shower sizes are fitted to a relation of the form

$$\rho_\mu(\geq E_\mu, N_e, r) = A \, .r^{-\alpha(\geq E\mu)}.\exp(-r/r_o) \text{ --------- } (3.5)$$

where A , α and r_o are the fitting parameters . The values of A and α for different shower sizes and different threshold energies are given in table 3.1.

TABLE - 3.1

Values of α and A at different shower sizes and muon threshold energies

Muon threshold energies($\geq E_\mu$) in GeV	Shower sizes	α	A
2.5	3.15×10^4	0.337 ±0.067	0.441 ± 0.083
	5.97×10^4	0.344 ±0.067	0.702 ± 0.130
	1.09×10^4	0.373 ±0.068	1.157 ± 0.219
	2.21×10^5	0.392 ±0.067	1.975 ± 0.369
	4.48×10^5	0.434 ±0.066	3.597 ± 0.665
	9.02×10^5	0.386 ±0.069	4.923 ± 1.023
	1.79×10^6	0.339 ±0.085	6.548 ± 1.744
5	3.15×10^4	0.360 ± 0.065	0.421 ± 0.076
	5.97×10^4	0.368 ± 0.070	0.673 ± 0.132
	1.09×10^4	0.422 ± 0.066	1.179 ± 0.217
	2.21×10^5	0.444 ± 0.066	2.040 ± 0.377
	4.48×10^5	0.468 ± 0.068	3.519 ± 0.676

	9.02×10^5	0.456 ± 0.064	5.391 ± 0.986
	1.79×10^6	0.386 ± 0.087	6.232 ± 1.697
10	3.15×10^4	0.471 ± 0.070	0.486 ± 0.095
	5.97×10^4	0.483 ± 0.067	0.784 ± 0.145
	1.09×10^5	0.510 ± 0.063	1.273 ± 0.222
	2.21×10^5	0.538 ± 0.062	2.203 ± 0.384
	4.48×10^5	0.564 ± 0.062	3.827 ± 0.667
	9.02×10^5	0.566 ± 0.070	6.117 ± 1.230
	1.79×10^6	0.497 ± 0.089	7.595 ± 2.115
20	5.97×10^4	0.572 ± 0.074	0.763 ± 0.158
	1.09×10^5	0.599 ± 0.065	1.280 ± 0.230
	2.21×10^5	0.664 ± 0.064	2.454 ± 0.438
	4.48×10^5	0.730 ± 0.063	4.782 ± 0.852
	9.02×10^5	0.740 ± 0.073	7.772 ± 1.702
	1.79×10^6	0.747 ± 0.076	12.214 ± 2.778
50	5.97×10^4	0.808 ± 0.080	0.922 ± 0.205
	1.09×10^5	0.848 ± 0.077	1.524 ± 0.327
	2.21×10^5	0.892 ± 0.075	2.707 ± 0.566
	4.48×10^5	0.942 ± 0.072	4.932 ± 1.002
	9.02×10^5	0.975 ± 0.077	8.693 ± 2.011
	1.79×10^6	0.970 ± 0.077	13.342 ± 3.078
75	5.97×10^4	0.960 ± 0.078	0.989 ± 0.214
	1.09×10^5	1.014 ± 0.084	1.680 ± 0.393
	2.21×10^5	1.047 ± 0.080	2.953 ± 0.663
	4.48×10^5	1.098 ± 0.083	5.311 ± 1.242
	9.02×10^5	1.126 ± 0.073	9.115 ± 1.913
	1.79×10^6	1.101 ± 0.085	12.447 ± 3.176
100	1.09×10^5	1.110 ± 0.091	1.654 ± 0.417
	2.21×10^5	1.161 ± 0.081	3.051 ± 0.690
	4.48×10^5	1.233 ± 0.083	5.679 ± 1.316

9.02×10^5	1.286 ± 0.083	10.794 ± 2.552
1.79×10^6	1.257 ± 0.082	14.455 ± 3.557

The radial distribution of muons along with the curves obtained from the fitting function (3.5) at various shower sizes for each of the muon threshold energies from 2.5 to 100 GeV are shown in figs. 3.6 to 3.11.

Some observed results on energy spectra of muons along with those obtained from Khrenov and Linsley [5] function are also shown in figs. 3.12 , 3.13 , 3.14 and 3.15.and it is seen that the observed energy spectra of muons are in good agreement with the results of Khrenov and Linsley.

3A.5. Comparison of radial distribution of muons with calculations:

The observed radial distribution of muons for $N_e=9.02\times10^5$ and $E\mu \geqslant 10$ GeV are compared in fig.3.16 with the calculated results of Greisen [6] distribution function as given by

$$\rho_\mu(\geqslant E_\mu, N_e, r)=(14.4.r^{-0.75})(N_e/10^6)^{0.75}(1+r/320)^{-2.5}\,(51/(E_\mu+50))(3/(E_\mu+12))^{0.14r^{0.37}} \quad \text{---------- (3.6)}$$

and the results of Khrenov and Linsley [5] distribution function as given by

$$\rho_\mu(\geqslant E_\mu, N_e, r) = \{5\times10^3/(E_\mu+250)^{1.4}\}.r^{-0.55\eta^{0.1}}\,\psi^{0.07}\exp(-\eta^{0.62}\, r/80)\psi^{0.78} \quad \text{---------- (3.7)}$$

where $\eta = (E_\mu+2)/12$ and $\psi = N_e/(2\times10^5)$.

Equation (3.6) is valid for N_e in the range 10^5-10^8 , $E_\mu \leqslant 500$ GeV and equation (3.7) is valid for N_e in the range 3×10^4-10^6 , E_μ in the range 50 GeV- 6×10^3 GeV. Fig.3.16 shows that the observed radial muon density distributions are in good agreement with the distributions of Khrenov and Linsley but are flatter than Greisen's prediction.

3A.6.Comparison of radial distribution of muons with other experimental data:

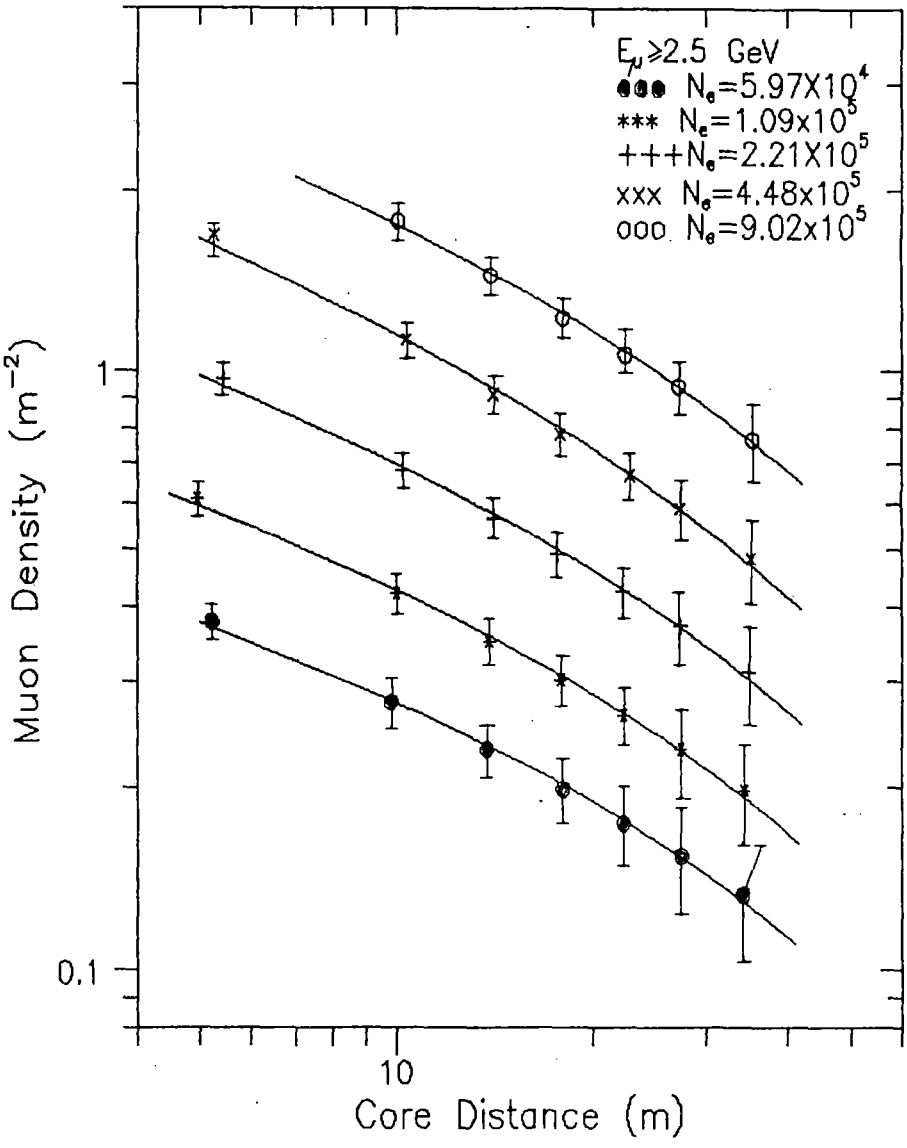

Fig.3.6. Observed radial distribution of EAS muons for muon threshold energy 2.5 GeV and for various shower sizes . The least-squares fit to the data are shown as solid lines.

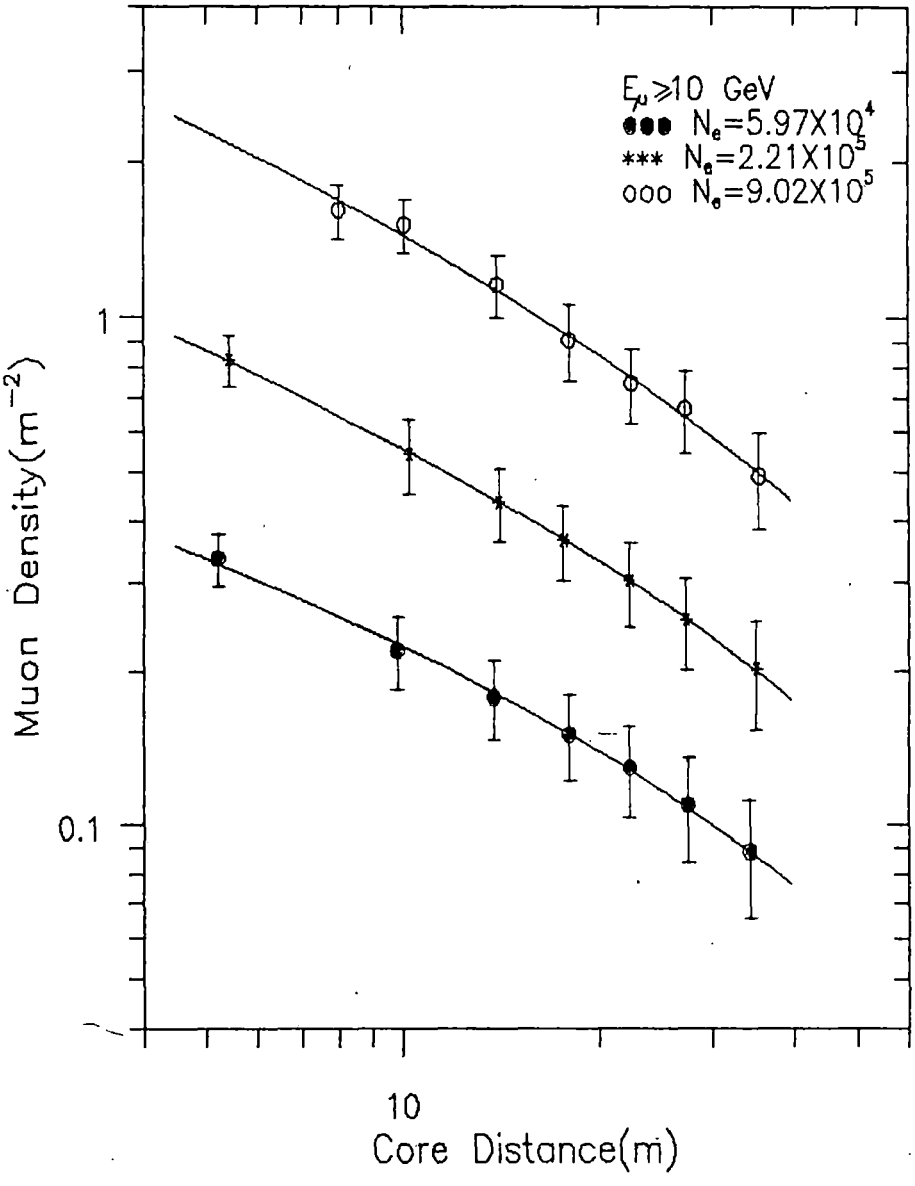

Fig.3.7. Observed radial distribution of EAS muons for muon threshold energy 10 GeV and for various shower sizes . The least-squares fit to the data are shown as solid lines.

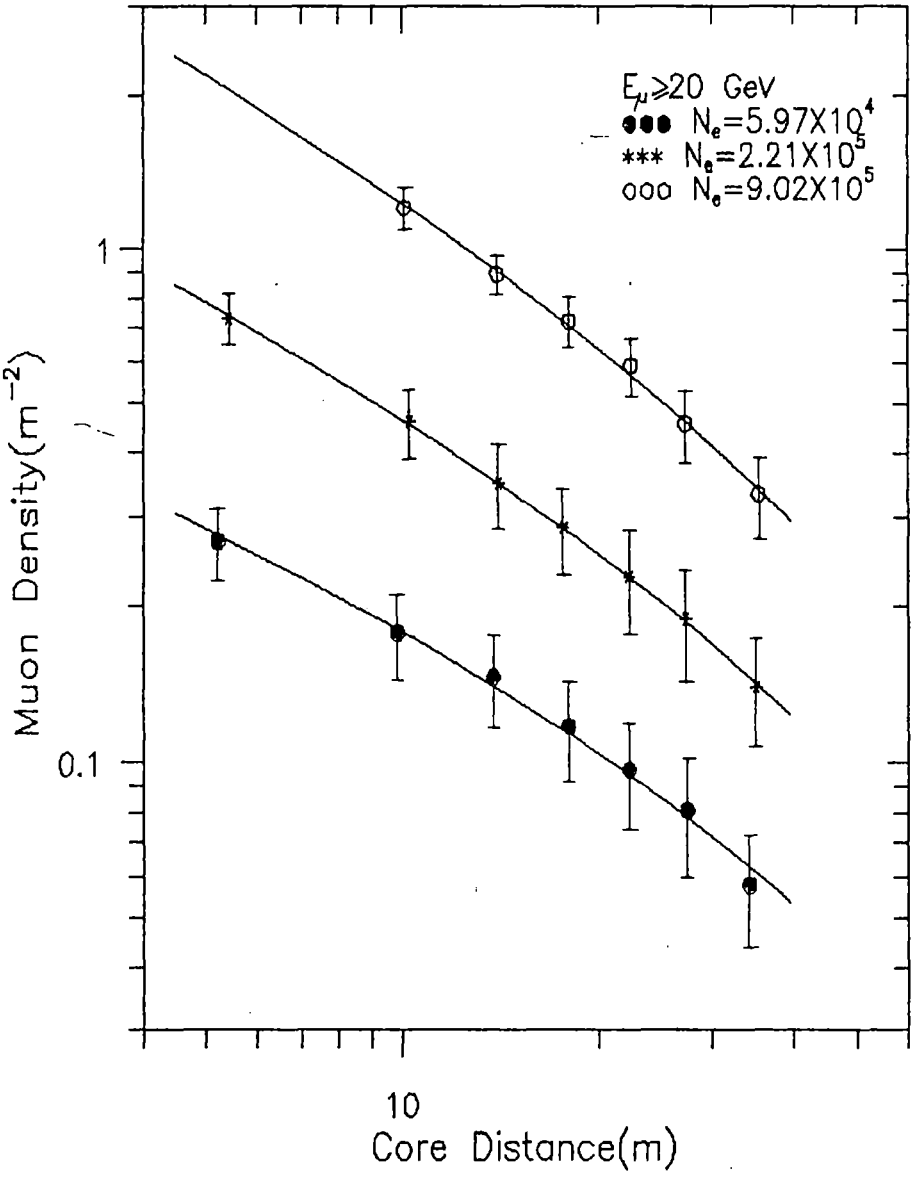

Fig.3.8. Observed radial distribution of EAS muons for muon threshold energy 20 GeV and for various shower sizes . The least-squares fit to the data are shown as solid lines.

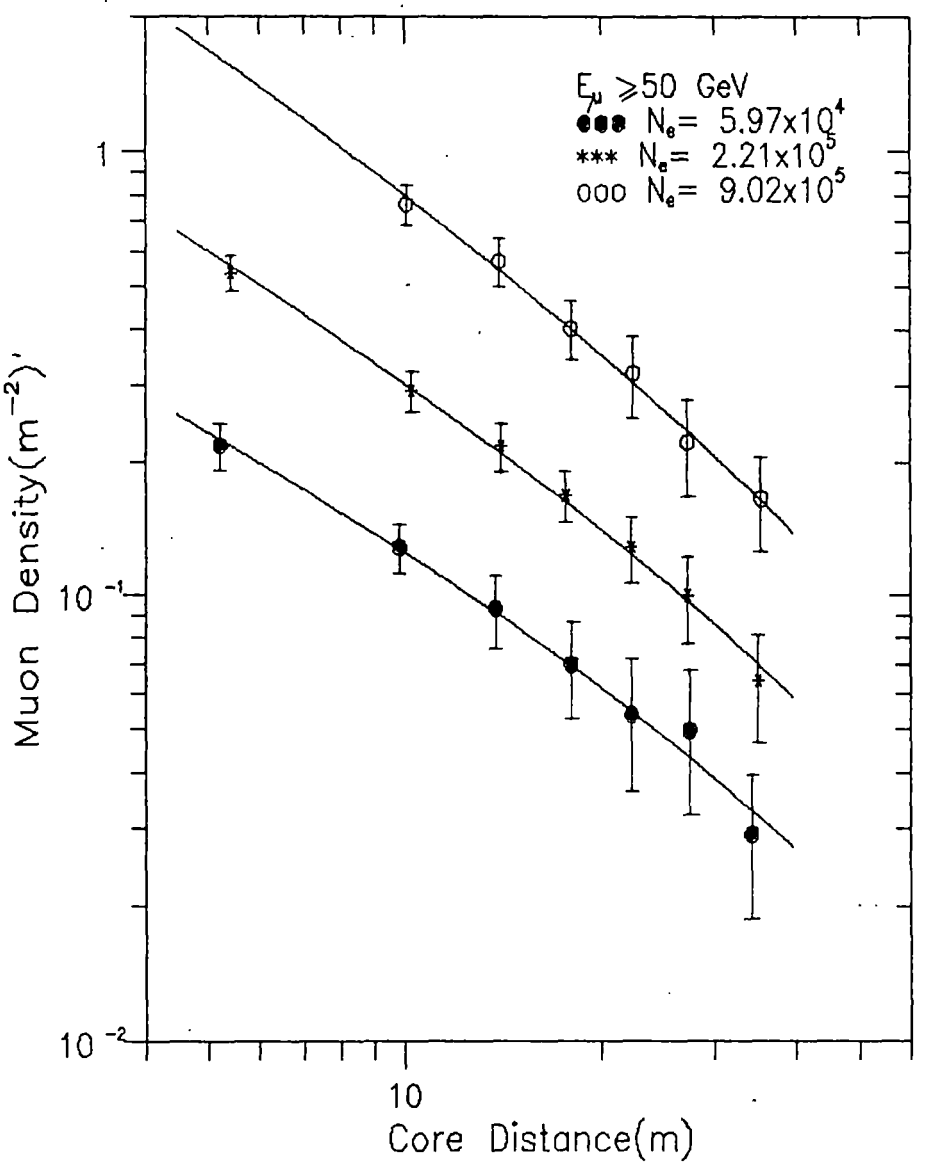

Fig.3.9. Observed radial distribution of EAS muons for muon threshold energy 50 GeV and for various shower sizes . The least-squares fit to the data are shown as solid lines.

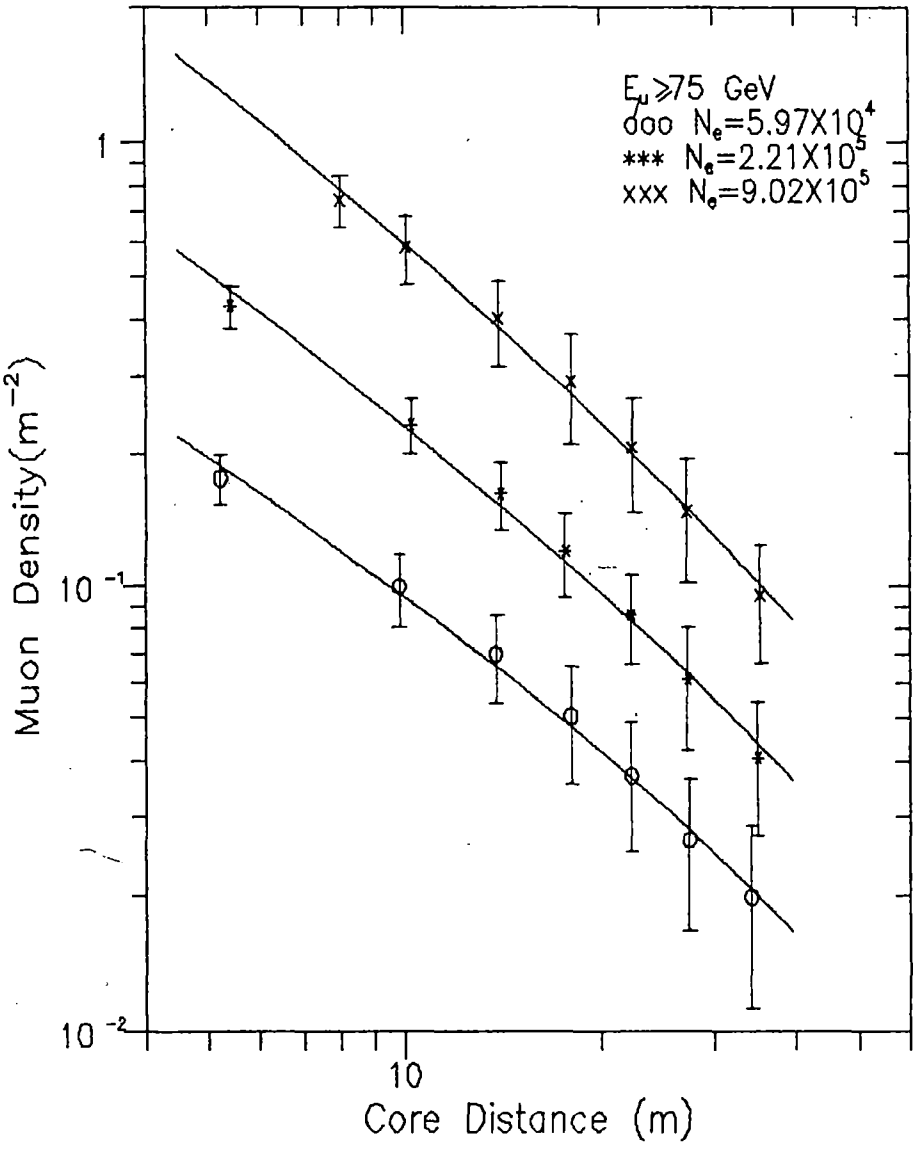

Fig.3.10. Observed radial distribution of EAS muons for muon threshold energy 75 GeV and for various shower sizes . The least-squares fit to the data are shown as solid lines.

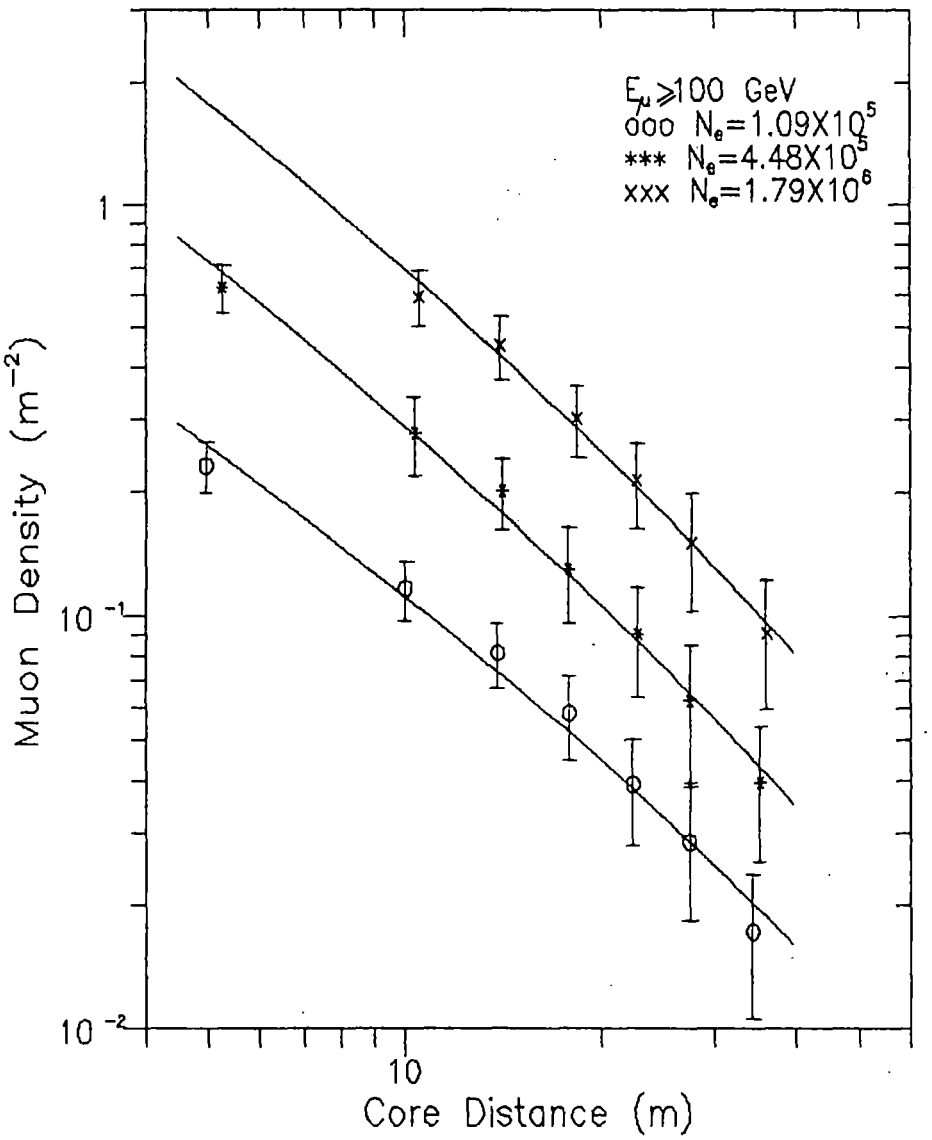

Fig.3.11. Observed radial distribution of EAS muons for muon threshold energy 100 GeV and for various shower sizes . The least-squares fit to the data are shown as solid lines.

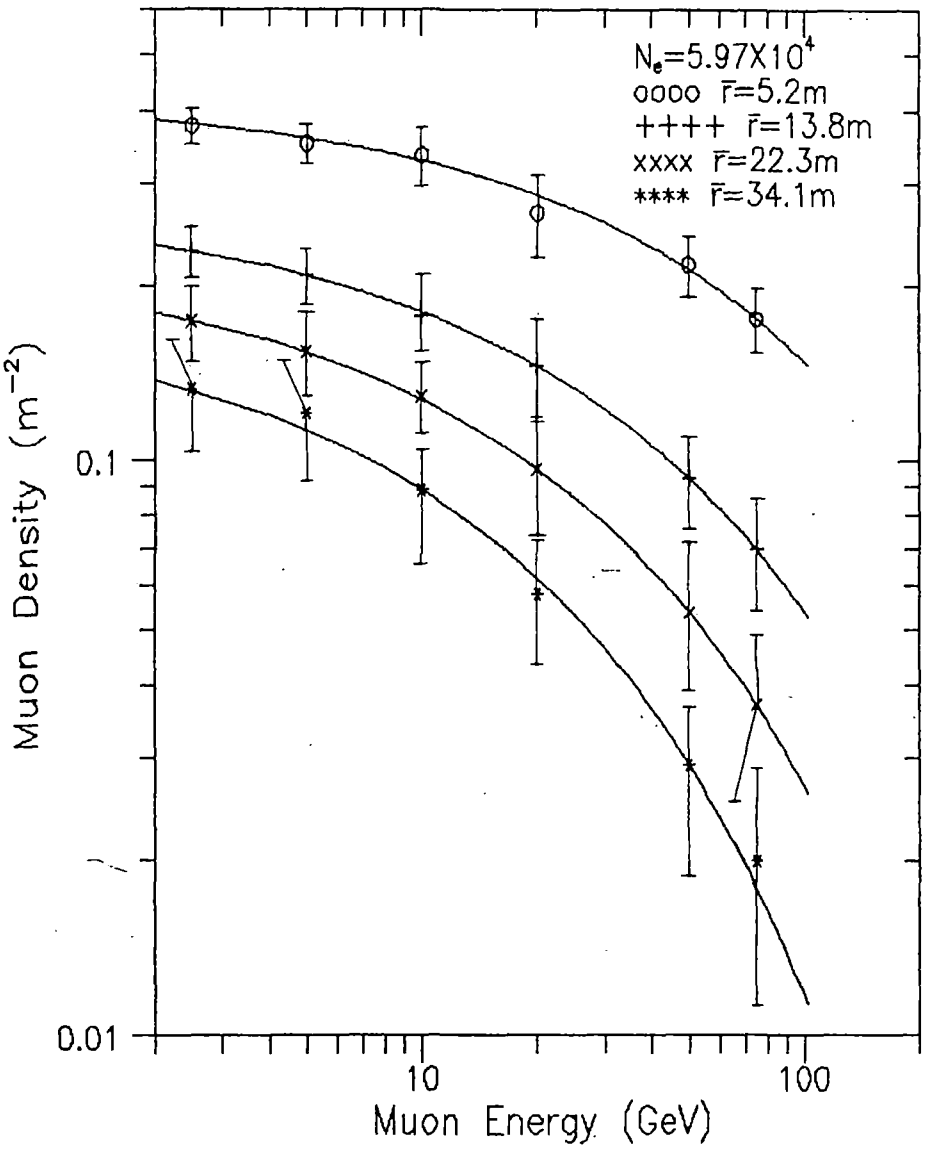

Fig.3.12. Variation of muon density with muon energy at various radial distances.

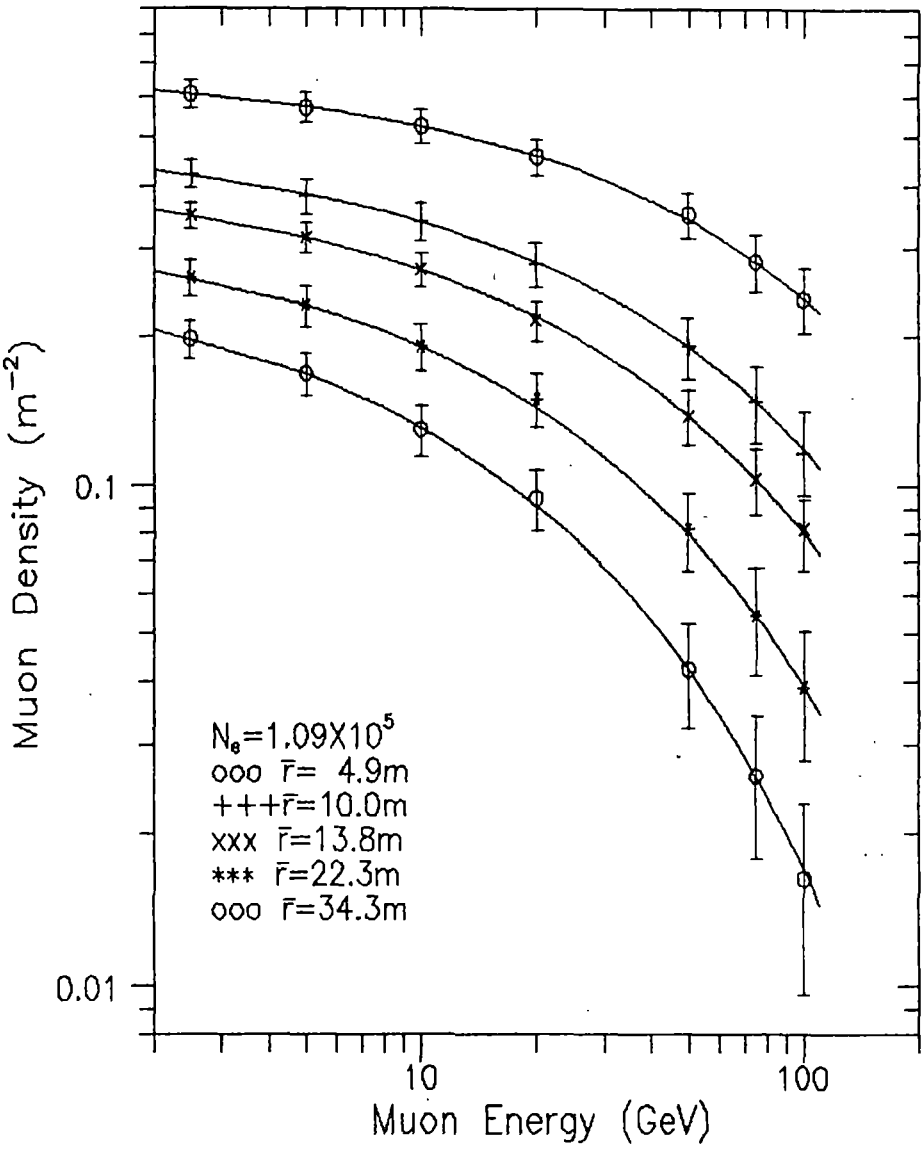

Fig.3.13. Variation of muon density with muon energy at various radial distances.

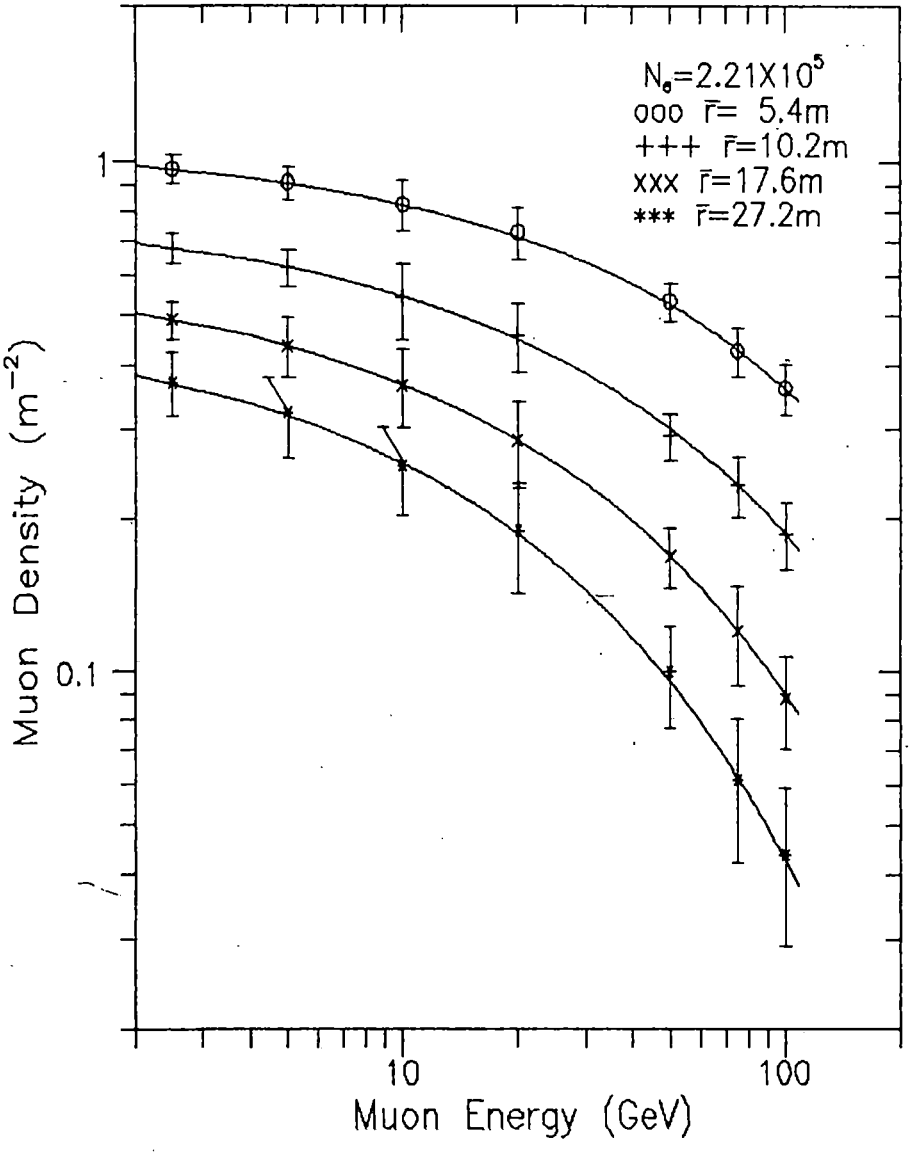

Fig.3.14. Variation of muon density with muon energy at various radial distances.

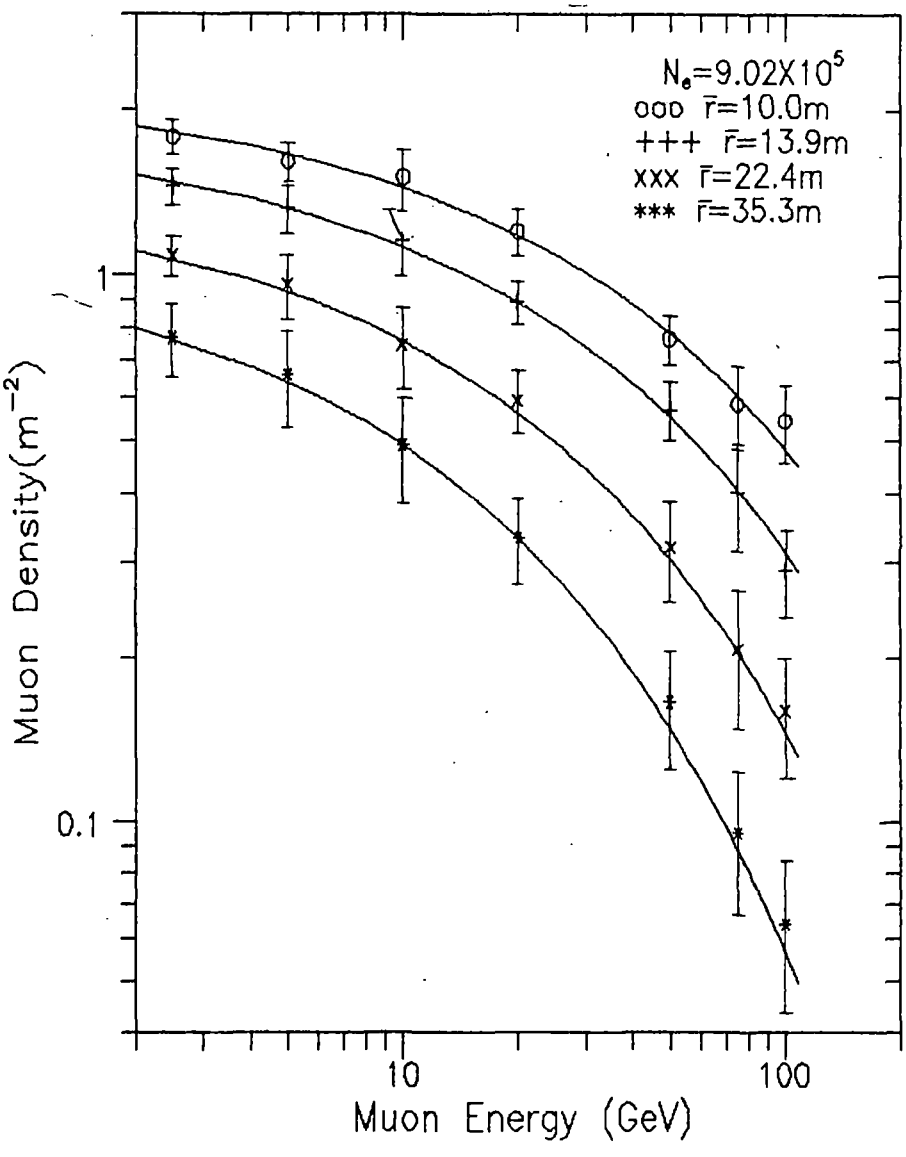

Fig.3.15. Variation of muon density with muon energy at various radial distances.

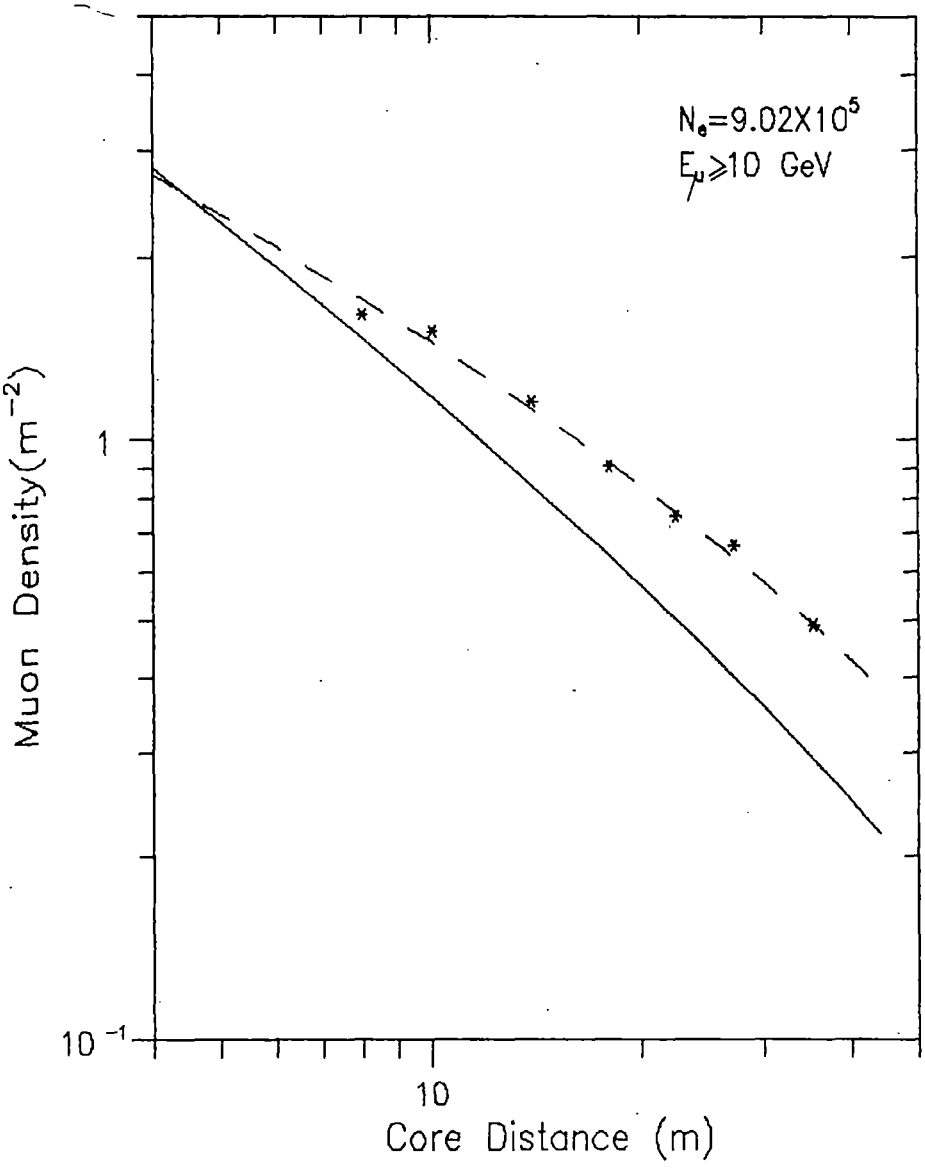

Fig.3.16. Observed radial muon density distribution along with the distributions using Greisen function (solid line) and Linsley function (dashed line) for shower size 9.02x10^5 and muon threshold energy 10 GeV

The radial density distribution of muons obtained from the present experiment are shown along with the experimental results of Khrenov (1961) [7] ,Khrenov (1966) [8] and Earnshaw et al [9] in fig.3.17 for $E_\mu \geq 10$ GeV and $N_e \sim 10^6$. It is seen from the figure that the observed radial distribution of muons are in close agreement with the results of Khrenov (1961) and Earnshaw et al. In fig.3.18 we have compared our results on radial distribution of muons with the experimental results of Rada et al [10] and Atrashkevich et al [11] for $E_\mu \geq 50$ GeV and $N_e \sim 10^6$. The experimental data of Rada et al deviate from our data whereas our data show a good agreement with the experimental results of Atrashkevich et al (Moscow group). For the same shower size but for $E_\mu \geq 100$ GeV , our radial distribution of muons also agree with the experimental results of Vashkevich et al [12] (Moscow group) which is shown in fig.3.19.

3A.7. Comparison of the measured radial density distribution of muons with Monte Carlo simulation result:

The radial density distribution of muons obtained from the Monte Carlo simulation results of S.Mikocki et al [13] for primary proton and the measured radial muon density distribution for primary energy $\sim 10^{15}$ eV and $E_\mu \geq 10$ GeV are shown in fig.3.20.It is seen from fig.3.20 that the observed radial muon density distribution is flatter compared to the distribution for primary proton.

3A.8. Variation of muon density to electron density ratio as a function of radial distance :

The variation of muon density to electron density ratio as a function of radial distance for primary energy 1.3×10^{15} eV and for $E_\mu \geq 2.5$ GeV has been studied and compared with the calculated results of S.Mikocki et al [13] on the basis of Monte Carlo simulation technique for primary (proton) energy 10^{15} eV and for $E_\mu \geq 1$ GeV which is shown in fig.3.21.

3A.9. Variation of muon size (N_μ) with shower size (N_e) :

The total number of muons above the threshold energy E_μ in a shower of size N_e was calculated by using the relation

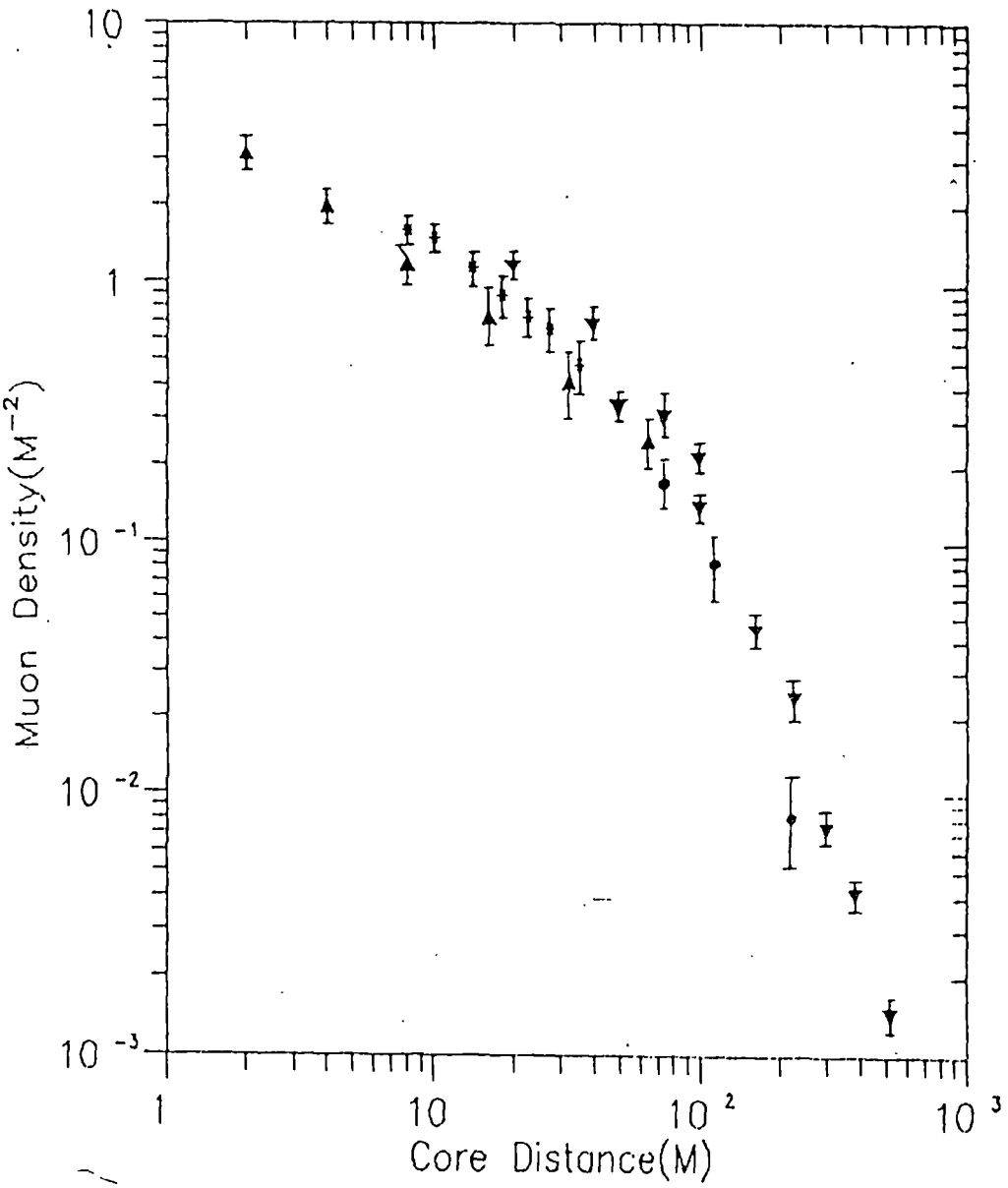

Fig.3.17. A comparison of the observed radial density distribution of muons of the present experiment (*) with the experimental results of Khrenov [5] (▲),Khrenov [6] (•) and Earnshaw et al [7] (▼) for $N_e \sim 10^6$ and $E_\mu \geqslant 10$ GeV

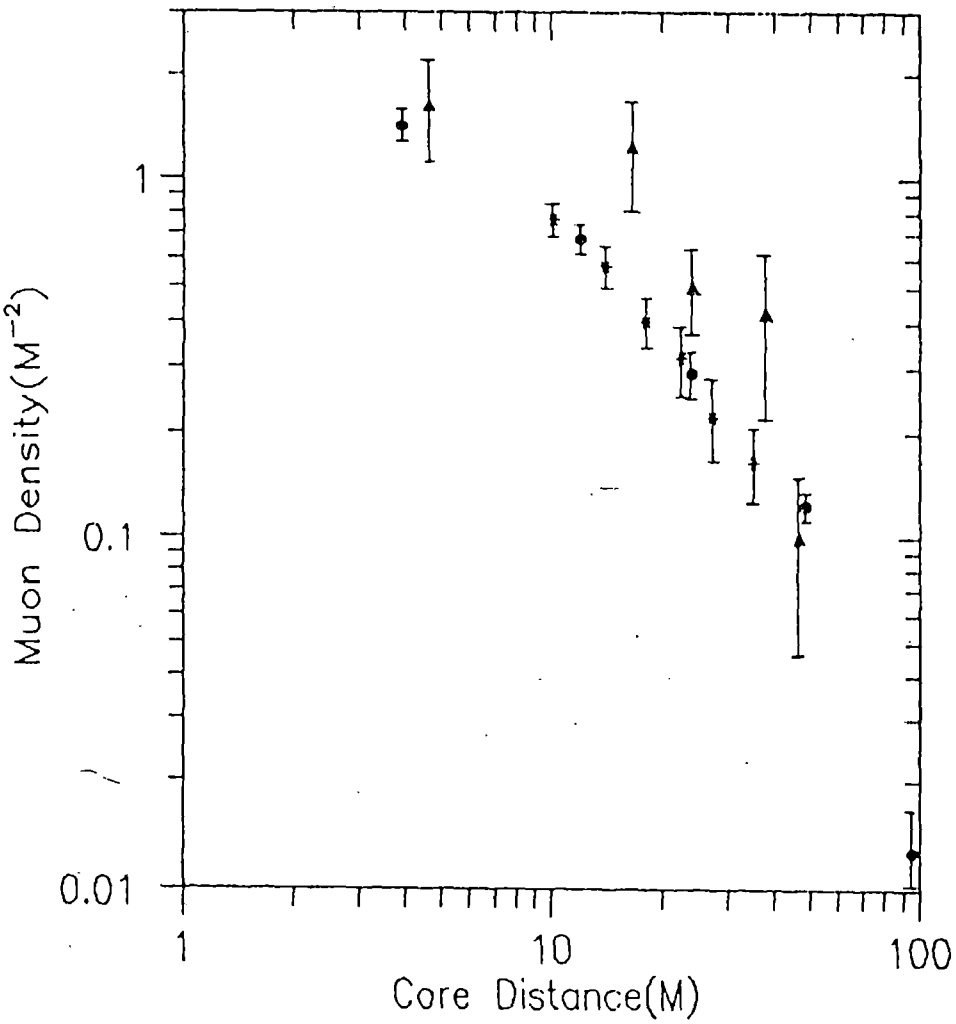

Fig.3.18. A comparison of the observed radial density distribution of muons of the present experiment (*) with the experimental results of Rada et al [8] (▲) and Atrashkevich et al [9] (•) for $N_e \sim 10^6$ and $E_\mu \geqslant 50$ GeV

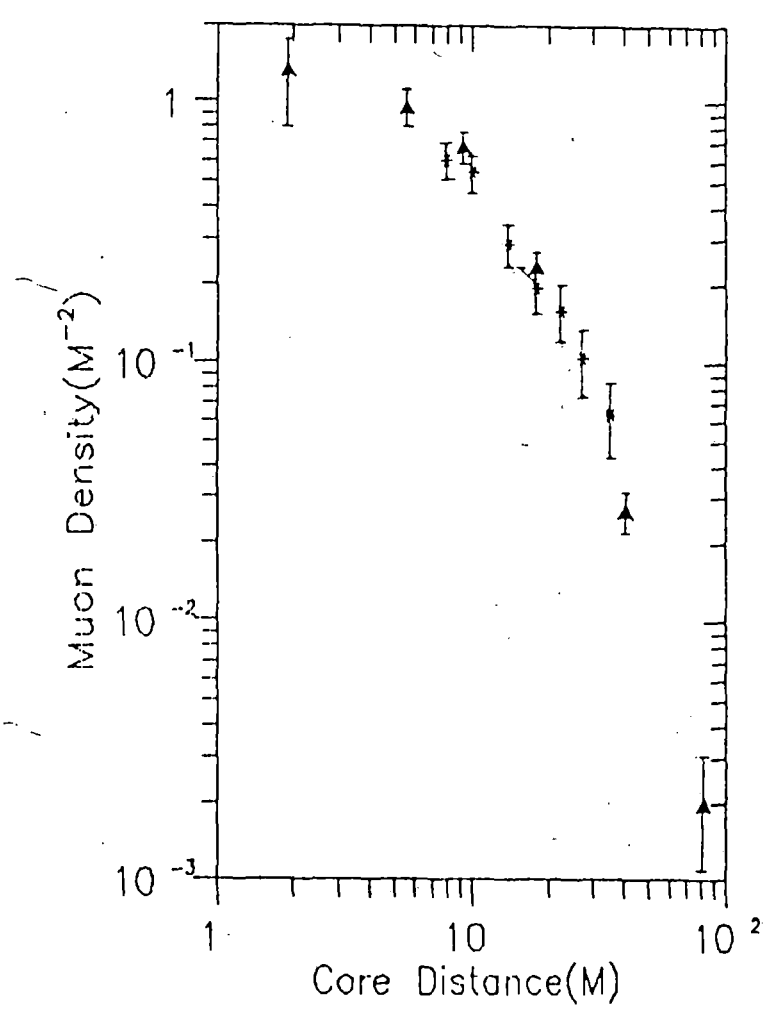

Fig. 3.19. A comparison of the observed lateral distribution of muons with the experimental results of Vashkevich et al [12] (▲) and the present experiment (*) for $N_e \sim 10^6$ and $E_\mu \geq 100$ GeV.

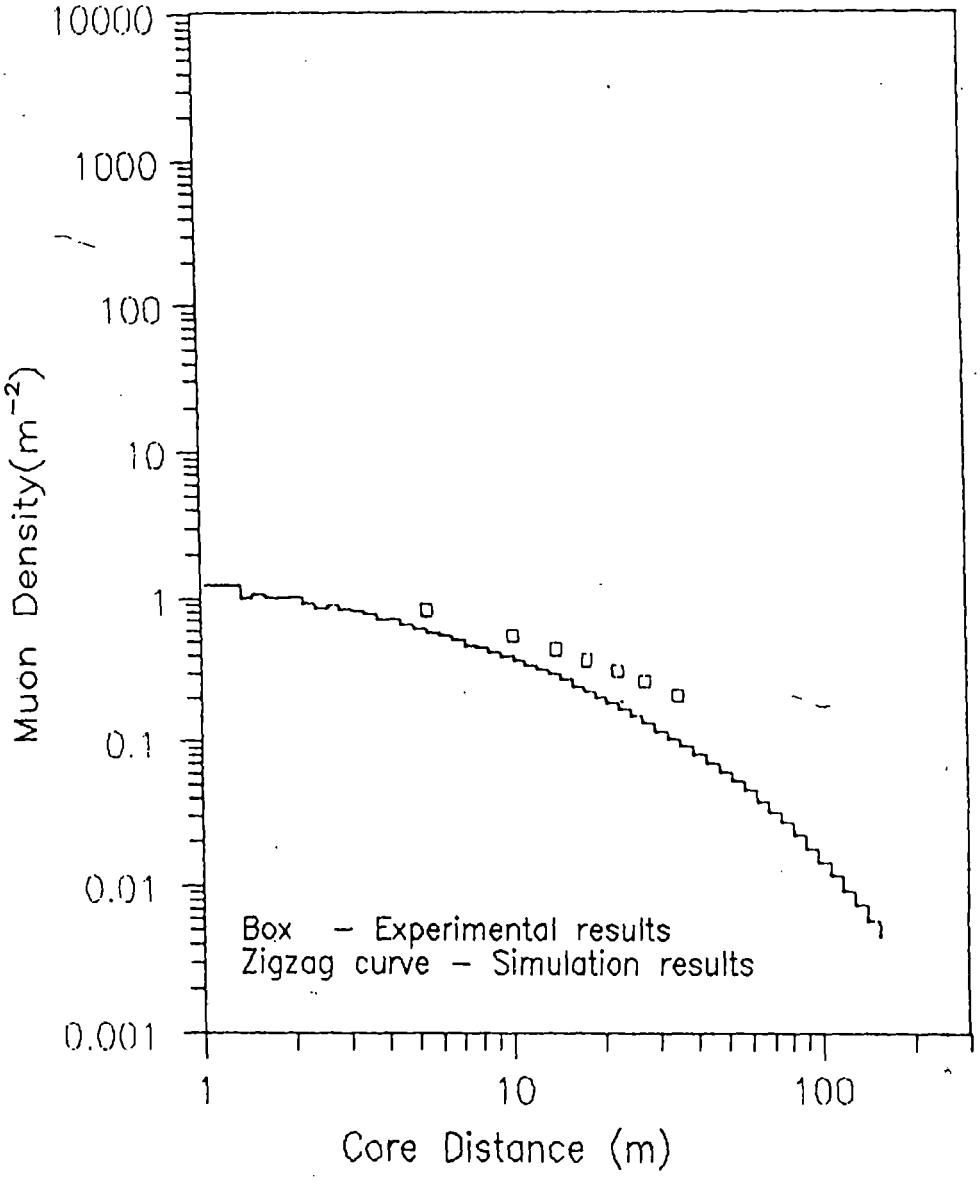

Fig.3.20. A comparison of the observed radial density distribution of muons for primary energy $\sim 10^{15}$ eV and muon threshold energy 10 GeV with the corresponding calculated results of Mikocki et al [13] for proton primary.

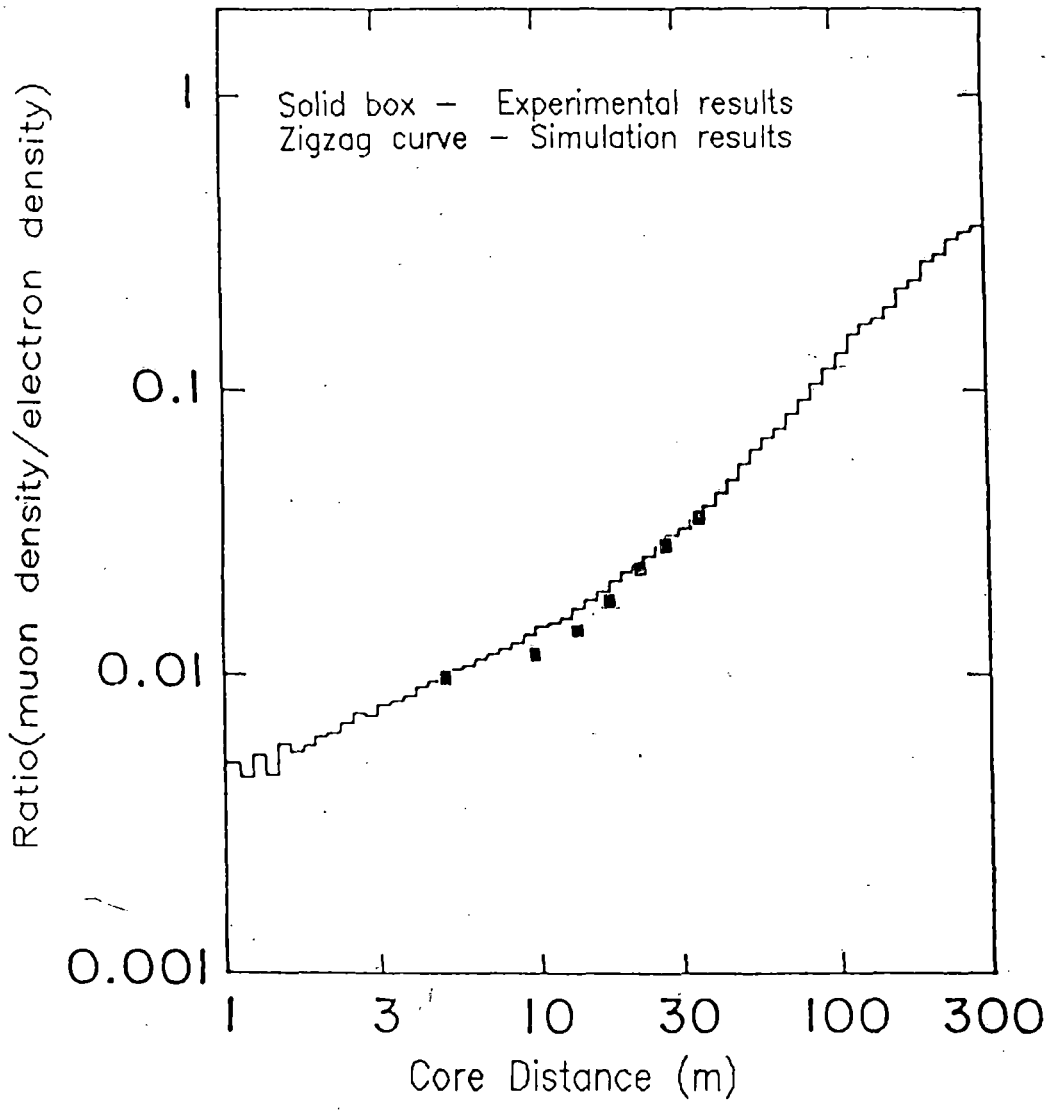

Fig.3.21. A comparison of the observed variation of muon density to electron density ratio as a function of radial distance for primary energy 1.3×10^{15} eV and muon threshold energy 2.5 GeV with the calculated results of Mikocki et al [13] for proton primary of energy 10^{15} eV and muon threshold energy 1 GeV.

$$N_\mu(\geq E_\mu, N_e) = \int_0^\infty \rho_\mu(\geq E_\mu, N_e, r)\, 2\pi r\, dr \quad \text{---------- (3.8)}$$

where $\rho_\mu(\geq E_\mu, N_e, r)$ is the density of muons with muon threshold energy $\geq E_\mu$ in a shower of size N_e at a distance r from the shower core and to calculate N_μ the functional form of ρ_μ as in equation (3.5) is considered . Then equation (3.8) becomes

$$N_\mu(\geq E_\mu, N_e) = 2\pi A \int_0^\infty r^{-\alpha+1} \exp(-r/r_o)\, dr \quad \text{---------- (3.9)}$$

The variation of muon size with shower size for muon threshold energies 2.5, 10, 20, 50 and 100 GeV are shown in fig.3.22 . The variation can be represented by a power law given by

$$N_\mu = AN_e^{\alpha} \quad \text{---------- (3.10)}$$

The values of α and A for different muon threshold energies are given in table 3.2.

TABLE - 3.2

Values of a and A for different muon threshold energies

Muon threshold energies ($\geq E_\mu$) in GeV	α	A
2.5	0.656	3.373
10	0.642	2.394
20	0.594	2.780
50	0.599	1.173
100	0.601	0.465

The observed variation of muon size with shower size for $E_\mu \geq 2.5$ GeV is compared with the Monte Carlo simulation results of Wrotniak and Yodh [14] calculated on the basis of nuclear interaction model M-F01 for proton primary and RM-F00 for iron primary for $E_\mu \geq 2$ GeV in fig.3.23.

Fig.3.24 shows the observed N_μ-N_e variation together with the calculated results of Hillas [15] at sea-level for muons of energy above 10 GeV . In this calculation the transport equations have been solved with the more accurate data from the accelerators by using the Feynman-Yan scaling model. The inelastic cross-

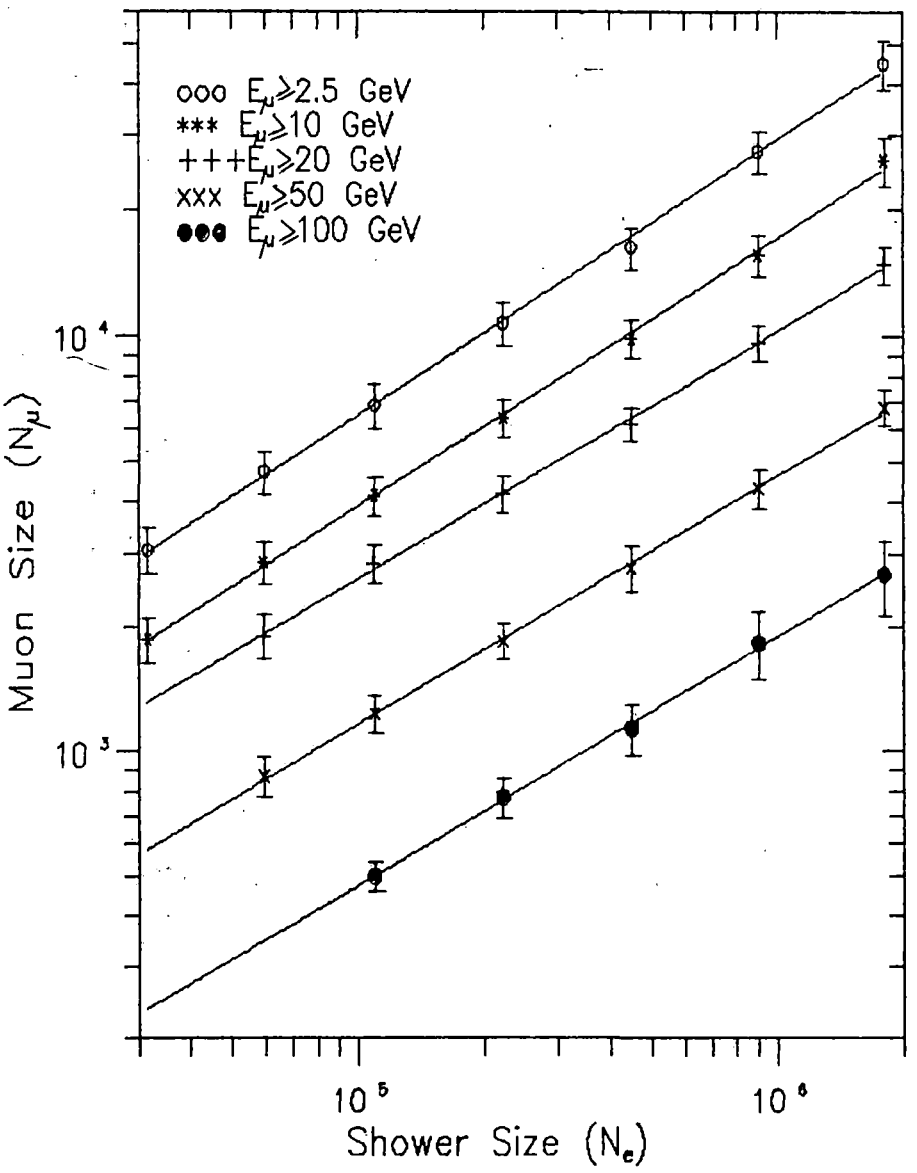

Fig.3.22. Variation of muon size with shower size for different muon threshold energies . The solid lines are the best fit to the data

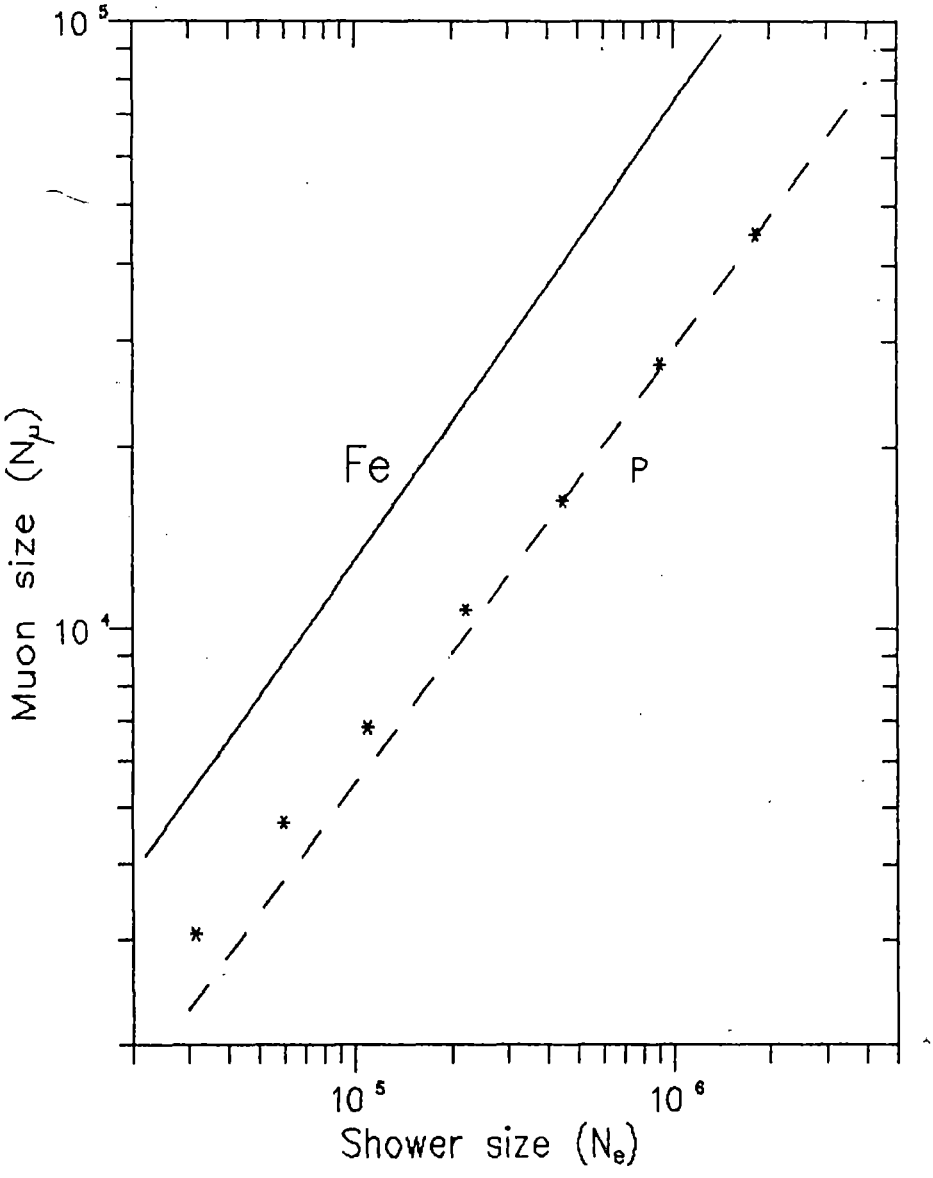

Fig.3.23. A comparison of the present results (star marks) of muon size dependence on shower size for $E_\mu \geqslant 2.5$ GeV with the corresponding Monte Carlo simulation results of Wrotniak and Yodh for $E_\mu \geqslant 2$ GeV using M-F01 model for proton primary (dashed line) and RM-F00 model for iron primary (solid line)

sections for collisions of hadron 'i' on nucleons are assumed to rise as follows at high energy :

$$\sigma_{in,inel} = \sigma_i [\ 1+0.0273\ u + 0.01u^2\ \theta(u)]\ ,$$

where $u=\ln(E/200GeV)$; $\theta(u) = 0$ if $u<0$, 1 if $u\geq 0$

For protons , pions and kaons σ_i is 32.2, 20.3 and 17.5 mb.The model calculations are shown as a stippled band , covering the range from proton primaries at the lower edge to iron primaries at the top, with solid circles (●) making the results of the mixed composition . From fig.3.24 it is seen that the observed N_μ–N_e variation for the shower size range 3.15 $x10^4$- 1.79 $x10^6$ particles is very close to the calculated results of Hillas for mixed composition.

Comparison have also been made of the experimentally observed N_μ-N_e variation with the Monte Carlo simulation results of Bourdeau et al [16] for $E_\mu \geq 10$ GeV in fig.3.25 . Scaling model is considered in the simulation work with particular attention to the following conditions and the consequences of their admixture

(i) rising p-air cross-section

(ii)shortened radiation length in e.m.cascades

(iii)mixed primary composition and modulation of the galactic confinement according to the Larmor radius of different nuclei.

It is seen from fig.3.25 that the primary composition in the shower size range 3.15 $x10^4$ - 1.79 $x10^6$ particles is neither purely proton nor iron rather mixed.

SECTION - 3B

In the previous section of this chapter the observed variations of total number of muons (N_μ) with shower size at different muon threshold energies have been studied and compared with different Monte Carlo simulation results . These comparisons seem to indicate that the composition of primary mass in the shower size range 3.15 $x10^4$ - 1.79 $x10^6$ particles is mixed .

Here the characteristics of the radial muon density distribution at fixed shower size and the variation of muon density with shower size at fixed radial distance for various muon threshold energies have been determined to draw conclusion about the change of the primary mass with the change of the energy of the primary particle in the knee energy region.

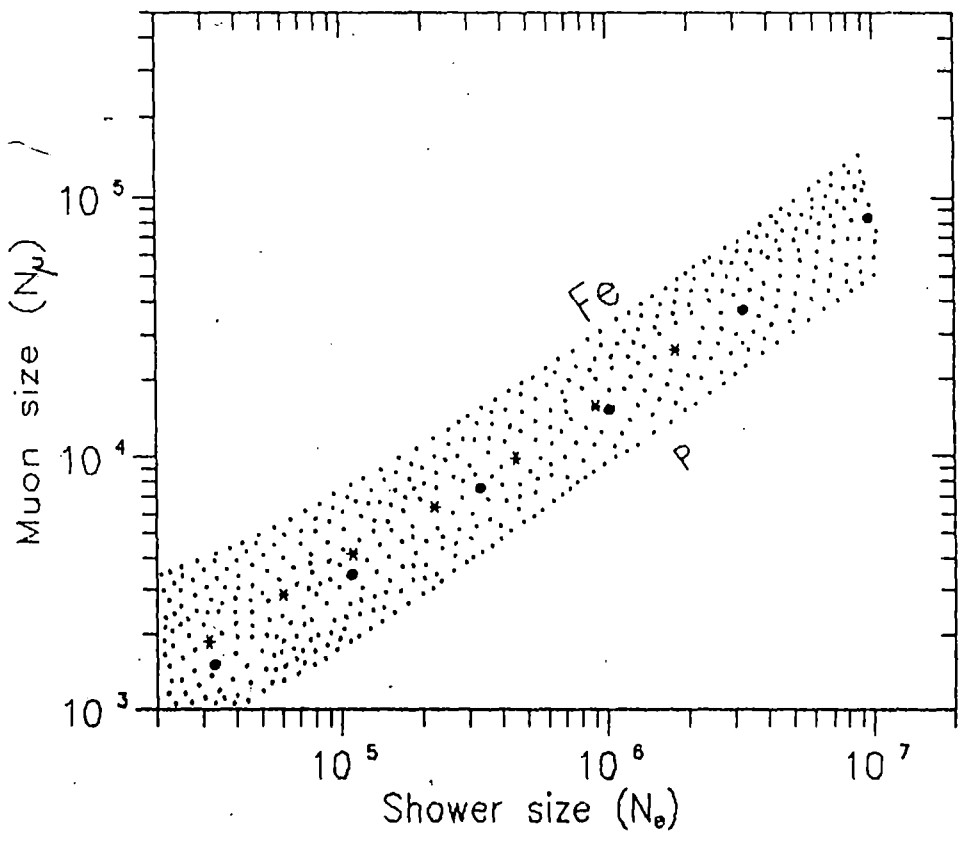

Fig.3.24. A comparison of the present results (*) of muon size dependence on shower size with the calculated results of Hillas [15] for $E_\mu \geq 10$ GeV

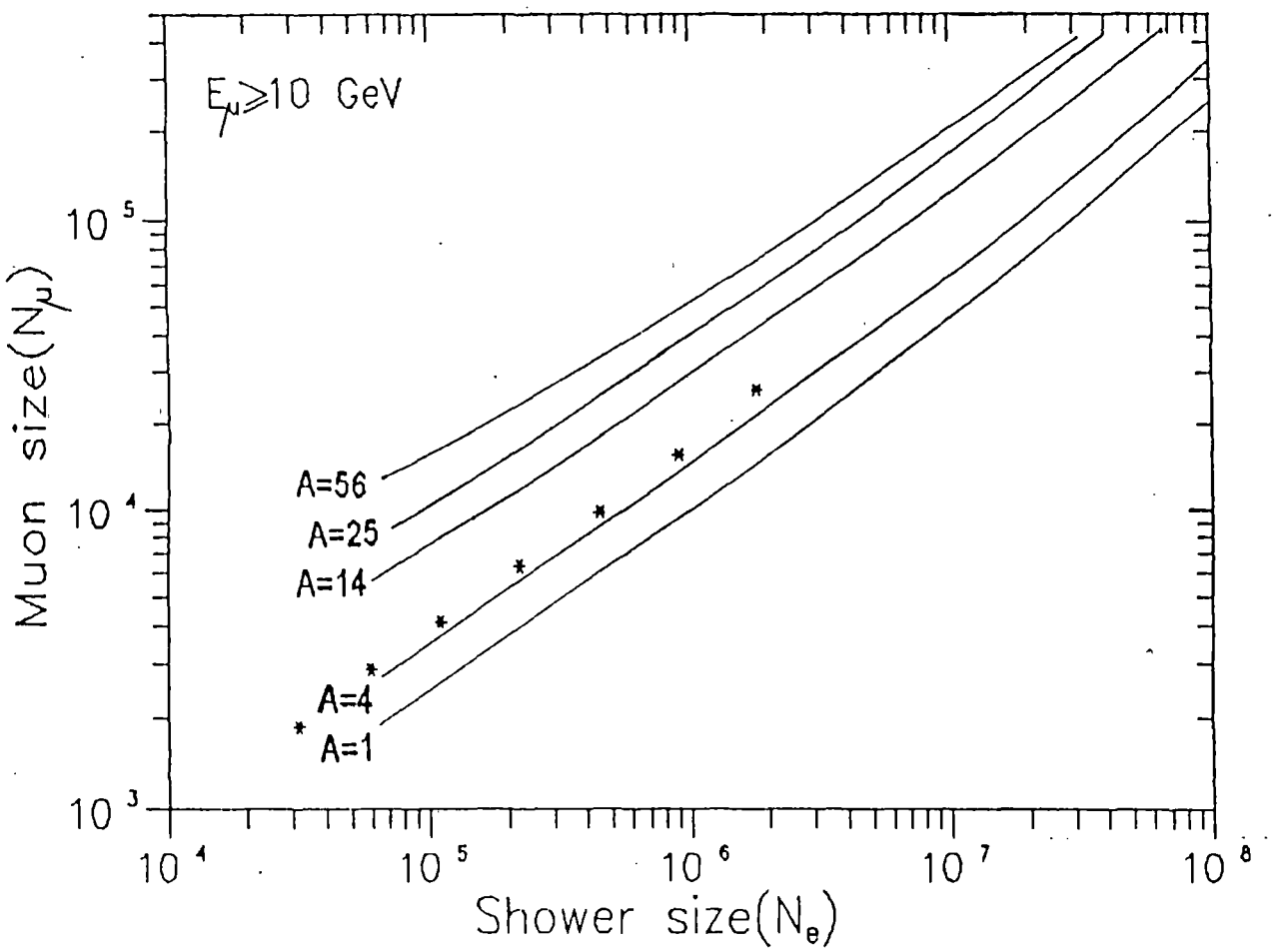

Fig.3.25. A comparison of the present results (*) of muon size dependence on shower size with the calculated results of Bourdeau et al [16] for $E_\mu \geq 10$ GeV and for different primary mass numbers

3B.1. The dependence of muon density on shower size :

The variation of muon density at fixed radial distances has been studied as a function of shower size at various muon threshold energies by assuming a dependence of the form given by

$$\rho_\mu(\geq E_\mu, r) \sim N_e^{\beta(E_\mu, r)} \qquad \text{---------- (3.11)}$$

The fit to the observed data has yielded the results shown in figs.3.26 , 3.27 , 3.28.It is seen that at a fixed muon threshold energy β decreases slowly with radial distance for all shower sizes in the range 3.15 $x10^4$ - 1.79 $x10^6$ particles and the trend of variation of β with radial distance is similar for all muon threshold energies .All these results together seem to indicate that the muon distribution function does not change with primary energy.The values of the exponent (β) obtained by fitting the observed data are given in table 3.3.

TABLE - 3.3

Values of the exponent (β) at different distance ranges for various muon energies

Muon energy (GeV)	β (for r=8-12m)	β(for r=30-40m)
2.5	0.692 ± 0.009	0.653 ± 0.012
10	0.699 ± 0.010	0.655 ± 0.013
50	0.661 ± 0.011	0.587 ± 0.021

3B.2. Muon density dependence on radial distance:

The measured radial distribution of muons in showers of various sizes can also be fitted to a relation of the form

$$\rho_\mu(\geq E_\mu, N_e, r) \sim r^{-\alpha(\geq E\mu)} \qquad \text{———————— (3.12)}$$

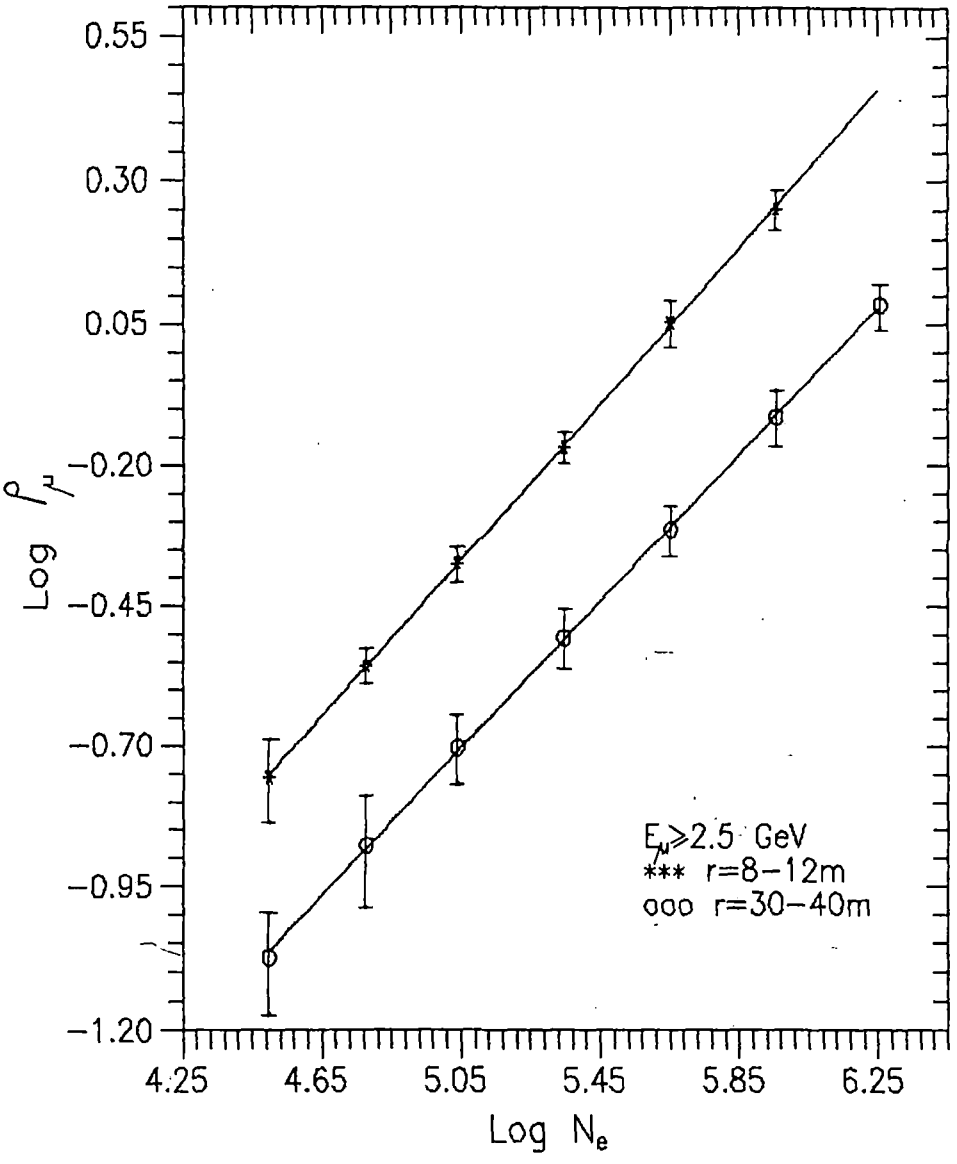

Fig.3.26. Variation of muon density at radial distance ranges 8−12m and 30−40m with shower size at muon threshold energy 2.5 GeV

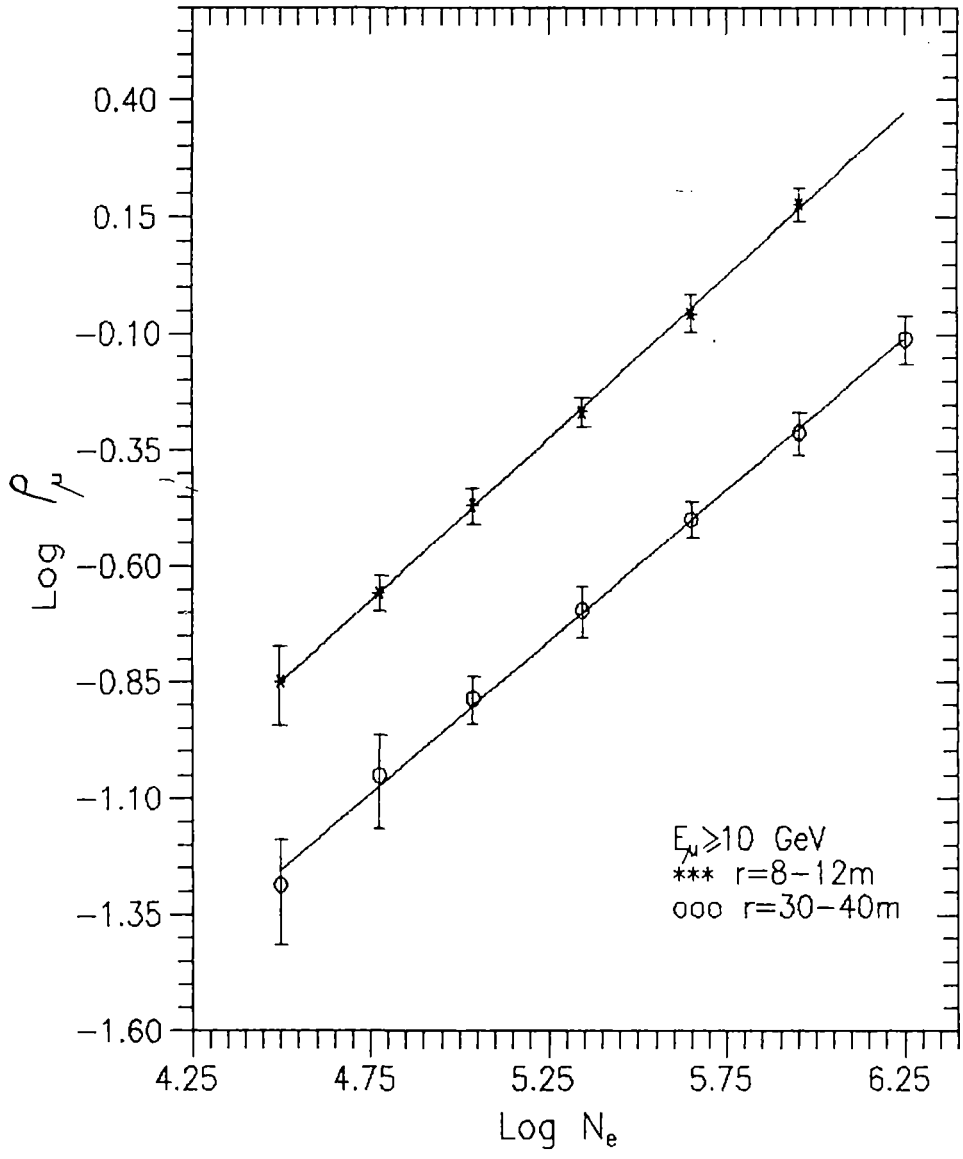

Fig.3.27. Variation of muon density at radial distance ranges 8−12m and 30−40m with shower size at muon threshold energy 10 GeV

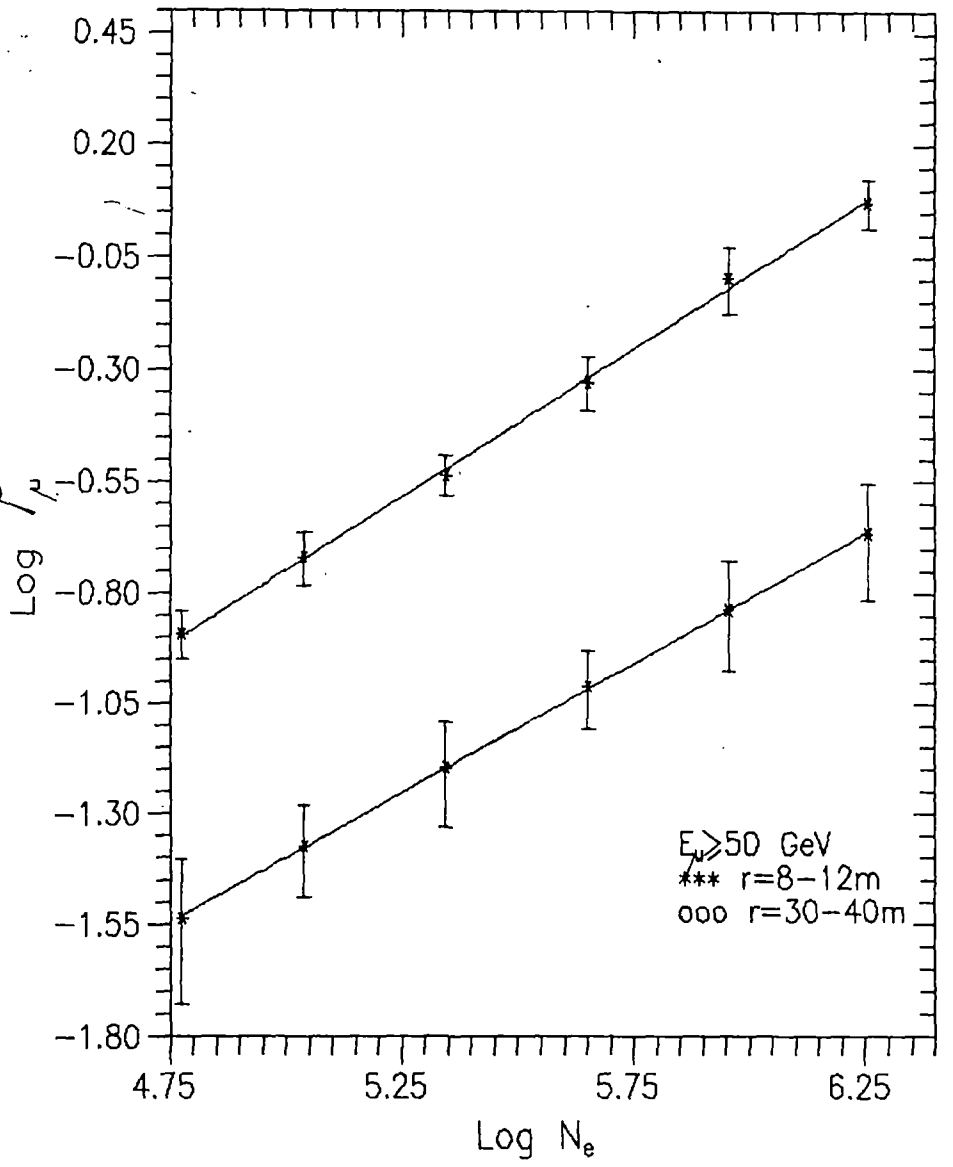

Fig.3.28. Variation of muon density at radial distance ranges 8−12m and 30−40m with shower size at muon threshold energy 50 GeV

A plot of this function for $N_e = 4.48 \times 10^5$ and $E_\mu \geq 2.5$ GeV is shown in fig.3.29 as an example .The value of α derived from this plot is 0.647. From fig.3.29 it is seen that except for the last radial bin ($\bar{r}$=34.1m) the shower cores were inside the edges of the array where the efficiency of the array is large. For the last radial bin , which is also close to the array boundary , obviously , the error of r and N_e are comparetively large but the overall effect of these errors on determination of α is small . The least square fitted line obtained from the plot of log ρ_μ vs. log r at various N_e for a particular muon threshold energy gives the values of α .

Values of α from the fit of the data for $E_\mu \geq 2.5$ GeV and $E_\mu \geq 10$ GeV are shown as a function of N_e in fig.3.30 and 3.31. The trend of α vs. N_e curves show that α is a function of N_e for N_e in the range 5.97×10^4 particles (primary energy 4.3×10^{14} eV) - 9.02×10^5 particles (primary energy 4.6×10^{15} eV) and becomes constant at higher shower sizes . For a lighter composition of the Primary Cosmic Rays it is expected to have steeper showers and hence large values of α.Therefore such a variation of α with N_e possibly indicates that the effective primary mass is decreasing from 4.3×10^{14}eV to around 4.6×10^{15}eV.

Y.Kawamura et al [17] and M.Ichimura et al [18] have derived similar conclusions about the primary mass in the knee energy region from direct observations from their new emulsion chamber experiments . From an analysis of low energy EAS muons Blake et al [19] reported similar trend for average primary mass in the primary energy region 6.0×10^{14} - 5×10^{15} eV.

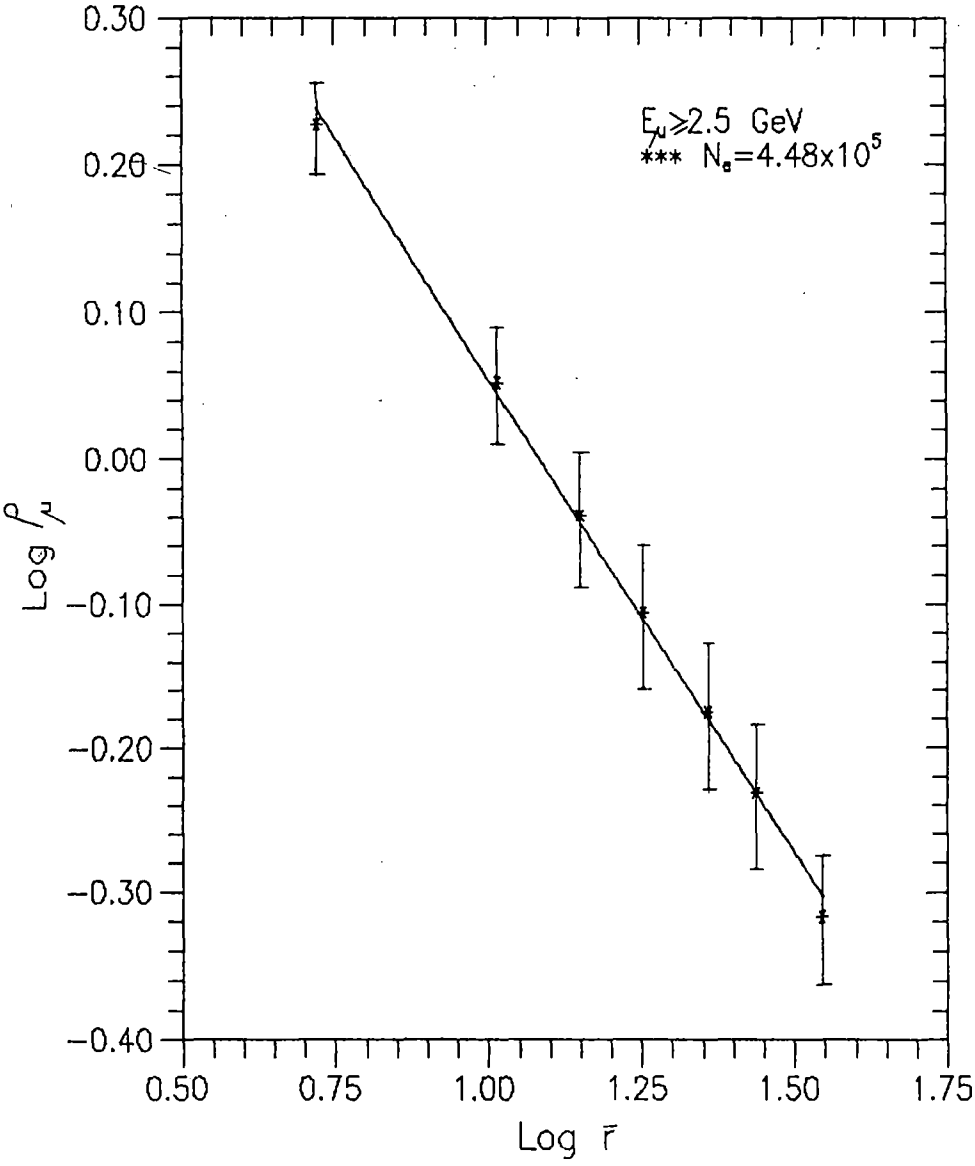

Fig.3.29. Variation of muon density with radial distance range for $N_e = 4.48 \times 10^5$

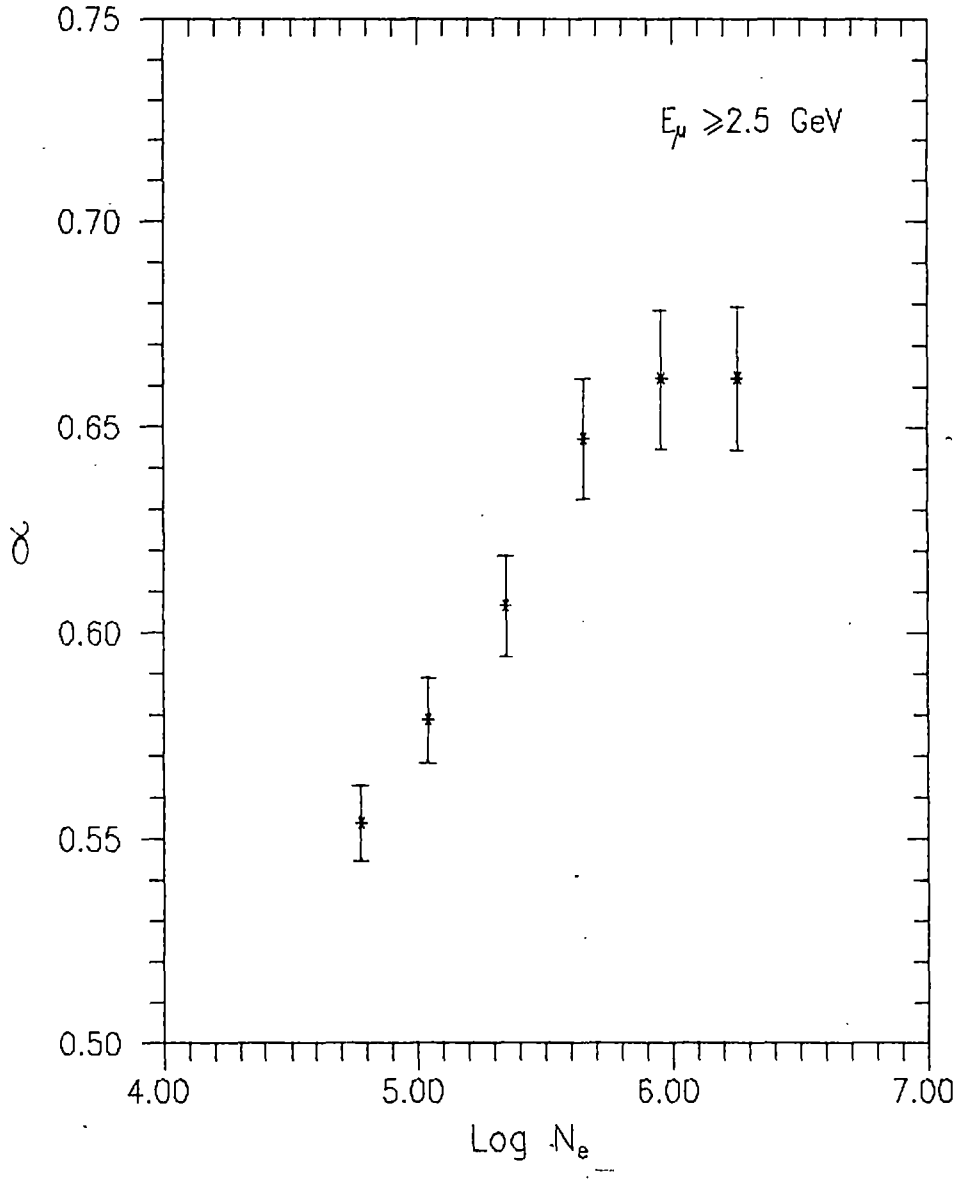

Fig.3.30. Variation of α with shower size (N_e) at the muon threshold energy 2.5 GeV.

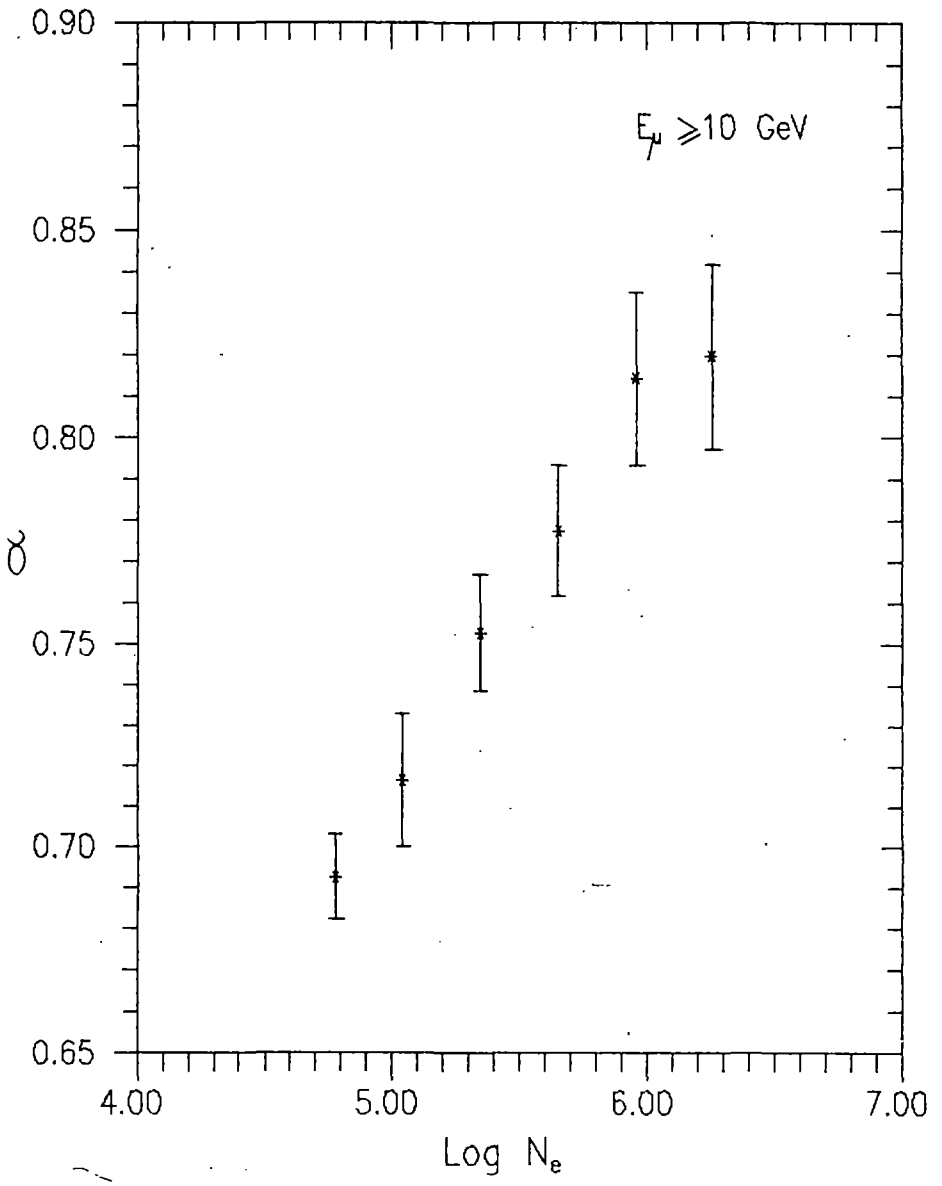

Fig.3.31. Variation of α with shower size (N_e) at the muon threshold energy 10 GeV.

CHAPTER 4

SUMMARY , DISCUSSION AND CONCLUSIONS

In the present study , the electrons and muons in Extensive Air Showers have been detected by the NBU air shower array operating near sea-level.Radial electron density distribution is determined by using **19** scintillation detectors located at various points (Fig.1.1) covering an area of ~ 1200 m^2 and the momenta of muons have been measured by two shielded magnet spectrographs separated from each other at a distance of 4m . The muons having momenta in the range 2.5 GeV/c - 100 GeV/c have been taken for analysis in the present study . Results obtained from the analysis of the measured data are compared with the experimental results of other EAS experiments as well as Monte Carlo simulation results based on different high energy interaction models to draw conclusion about the primary mass composition.

The first chapter of the thesis presents an introduction to EAS phenomena with special emphasis on the discussion on detection of EAS muons to extract information about the Primary Cosmic Ray mass composition . A brief review of the previous works particularly concerned with the composition of primary mass is also given in this chapter.

The details of the present experiment for detection of EAS electrons and muons of various energies are discussed in the second chapter . Analysis of EAS data for the estimation of air shower parameters and errors in the estimated shower parameters are also included in this chapter . The chapter includes the description of the operation of the whole data acquisition system consisting of shower selection system , timing data handling system , density data handling system and muon data handling system . The χ^2 - minimisation procedure for the estimation of air shower parameters and the artificial shower analysis for the measurement of errors on the estimated shower parameters have been given . The sensitivity of the EAS array of detecting showers at different N_e and s have also been discussed in terms of the computed detection efficiency and triggering probability in the same chapter.

Experimental results are presented , discussed and compared with the experimental results of other EAS groups in the third chapter

Various Monte Carlo simulation results based on different high energy interaction models are also presented to compare with the present experimental results in this chapter. The main results of the present study with conclusions as presented in the third chapter are the following

(1) The mean energy of the Primary Cosmic Ray particle (protons) is obtained from the energy scale established on the basis of hybrid Monte Carlo model (Trzupek et al , as referred to in the third chapter) at sea-level.

Similar such relation between the primary energy and shower size was obtained from the calculated results of Wrotniak and Yodh (as referred to in the third chapter) using Monte Carlo simulation results has also been given.

(2) The measured radial distribution of electrons in EAS of various shower sizes in the radial range 0-40m have been presented and compared with the distributions obtained from Hillas (as referred to in the third chapter) structure function . It has been observed that the Hillas function represents a good fit to the observed density distribution in 0-40m radial range.

(3) A comparison of the measured radial muon density distribution has been made with the experimental results of Khrenov (1961), Khrenov (1966) , Earnshaw et at , Rada et al , Atrashkevich et al and Vashkevich et al.(all are referred to in the third chapter) It is seen that the measured muon density distribution agrees well with those of Khrenov (1961) and Earnshaw et al for $E_\mu \geq 10$ GeV and with the results of Atrashkevich et al but for $E_\mu \geq 50$ GeV. Again for $E_\mu \geq 100$ GeV the measured radial muon density distribution agrees with those reported by Vashkevich et al.

Measured radial density distribution of muons have also been compared with the calculated results using Greisen distribution function and Khrenov and Linsley distribution function .It is seen that the radial muon density distribution agrees well with the distribution of Khrenov and Linsley but deviates from the Greisen's predictions.

(4) Results on the energy spectra of EAS muons at different shower sizes and radial distances have been presented.

(5) Comparison of the observed variation of muon density to electron density ratio as a function of radial distance with the Monte Carlo simulation results calculated by S.Mikocki et al (as referred to in the third chapter) has been made.

(6) The observed variation of the total number of muons (N_μ) with shower size (N_e) for $E_\mu \geq 2.5$ GeV has been compared with the Monte Carlo simulation results calculated by Wrotniak and Yodh (as referred to in the third chapter)on the basis of nuclear interaction model MF01 for proton primary and RM-F00 for iron primary for $E_\mu \geq 2$ GeV . For $E_\mu \geq 10$GeV, the observed N_μ-N_e variation has been compared with the calculated results of Hillas (as referred to in the third chapter) based on Feynman-Yan scaling model.Comparison has also been made of the observed N_μ-N_e variation for $E_\mu \geq 10$ GeV with the Monte Carlo simulation of Bourdeau et al.

All these comparisons show that the observed N_μ-N_e variations are close to the simulated results for mixed composition of the Primary Cosmic Ray.

(7) The variation of muon density with shower size at fixed radial distances and at various muon threshold energies has been studied and it is seen that the radial muon density distribution at low and high muon energies does not change with the primary energy.

(8) Finally, the variation of muon density with radial distance in showers of various sizes has been investigated . These variations show that the radial muon density distribution steepens in the primary energy range 4.3×10^{14}-4.6×10^{15} eV indicating that the effective primary mass decreases between 4.3×10^{14} and 4.6×10^{15} eV.

All these results discussed above seem to indicate that the primary mass composition is mixed in the primary energy range 2.48×10^{14} - 8.34×10^{15} eV (shower size range 3.15×10^{4} - 1.79×10^{6} particles) and the effective primary mass decreases with the primary energy in the energy range 4.3×10^{14} - 4.6×10^{15} eV.

REFERENCES:

Chapter - 1

[1] Greisen K., Annu.Rev.Nucl.Sci.,10(1960)63.

[2] Nishimura J. and Kamata K., Prog.Theor.Phys., 5(1950)899 , 6(1951)628 7(1952)185.

[3] Hara T., Hatano Y., Hasebe N., Hayashida N., Jogo N.,Kamata K.,Kawaguchi S., Kifune T., Nagano M. and Tanahashi G., Proceedings of the 16th International Conference on Cosmic Rays,Kyoto,13(1979)148

[4] Dedenko L.G., Nesterova N.M., Nikolsky S.I., Stamenov I.N. and Janminchev V.D., Proceedings of the 14th International Conference on Cosmic Rays, Munich, 8(1975)2731

[5] Linsley J., Proceedings of the 13th International Conference on Cosmic Rays, Denver, 5(1973)3215

[6] Kaneko T., Aguirre C., Toyoda Y., Nakatani H., Jadot S., Mackeown P.K., Suga K., Kakimoto F., Mizumoto Y., Murakami K., Nishi K., Nagano M. and Kamata K., Proceedings of the 14th International Conference on Cosmic Rays, Munich, 8(1975)2747.

[7] Capdevielle J.N., Procureur R. and Gawin J., Proceedings of the 18th International Conference on Cosmic Rays, Bangalore, 11(1983)307.

[8] Lagutin A.A., Pljasheshnikov A.V. and Uchaikin V., Proceedings of the 16th International Conference on Cosmic Rays, Kyoto, 7(1979)18

[9] Hillas A.M. and Lapikens J., Proceedings of the 15th International Conference on Cosmic Rays, Plovdiv, 8(1977)460

[10] Trzupek A., Lu Y. and Poirier J., Proceedings of the 23rd International Conference on Cosmic Rays, Calgary, 4(1993)359.

[11] Cowsik R., Tonwar S.C., Viswanath P.R., Ellsworth R.W., Goodman J.A., Ito A.S., Streitmatter R.E. and Yodh G.B., Proceedings of the 17th International Conference on Cosmic Rays, Paris, 1981

[12] Yodh G.B., Proc.Rencontre Moriond , 16th,1981, Reprint pp.81-230

[13] Peters B., Nuo. Cim. 22(1961)800

[14] Zatsepin G.T., Nikolsky S.I. and Khristiansen G.B., Proceedings of the 8th International Conference on Cosmic Rays, Jaipur,4(1963)100

[15] Hillas A.M., Proceedings of the 16th International Conference on Cosmic Rays, Kyoto, 8(1979)7.
[16] Karakula S., Osborne J.L. and Wdowczyk J., J.Phys., A7(1974)437
[17] Balasubrahmanyan V.K. and Ormes J.F., Ap.J., 186,109,1973
[18] Juliusson E., Ap.J., 191,331,1974
[19] Ormes J.F., Fisher A., Hagen F., Maehl R. and Arnes J.F., Proceedings of the 14th International Conference on Cosmic Rays, Munich, 1(1975)245.
[20] Lezniak J.A. and Webber W.R., Ap.J., 223,676,1978.
[21] Kempa J., Samorski M., Wdowczyk J., Proceedings of the 24th International Conference on Cosmic Rays, Rome, 2(1995)681.
[22] McCusker C.B.A., Peak L.S. and Rathgeber M.A., Proceedings of the 11th International Conference on Cosmic Rays, Budapest, 3(1969)527.
[23] Samorski M., Staubert R., Trumper J. and Bohm E., Proceedings of the 12th International Conference on Cosmic Rays, Hobert, 3(1971)959.
[24] Sivaprasad K., Ph.D. thesis, University of Bombay, India (1971).
[25] Acharya B.S., Ph.D. thesis, University of Bombay, India,1983.
[26] Andam A.A., Craig M.A.B., Chantler M.P., McComb T.J.L.,Orford K.J., Turver K.E. and Walley G.M., Proceedings of the 17th International Conference on Cosmic Rays, Paris, 6(1981)57
[27] Linsley J. and Watson A.A., Phys.Rev.Lett., 46(1981)459.
[28] Walker R. and Watson A.A., J.Phys., G8(1982)1131.
[29] Yodh G.B., Goodman J.A. and Tonwar S.C., Proceedings of the 18th International Conference on Cosmic Rays , Bangalore,2(1983)106.
[30] Stamenov J.N., Ushev S.Z. and Janminchev V.D., Proceedings of the 18th International Conference on Cosmic Rays, Bangalore, 2(1983)111.
[31] Nikolsky S.I. and Stamenov J.N., Proceedings of the 18th International Conference on Cosmic Rays, Bangalore, 2(1983)115.
[32] Muraki Y., Proceedings of the 19th International Conference on Cosmic Rays, La Jolla, 2(1985)178.
[33] Dawson B.R., Prescott J.R. and Clay R.W., Proceedings of the 19th International Conference on Cosmic Rays, La Jolla , 2(1985)230.
[34] Cho C., Higashi S., Hiraoka N., Ozaki S., Sato T., Suwada T., Takahashi T. and Umeda H., Proceedings of the 19th International Conference on Cosmic Rays, La Jolla, 7(1985)115.

[35] Blake P.R. and Tummey S.P., Proceedings of the 23rd International Conference on Cosmic Rays, Calgary, 4(1993)363.

Chapter -2

[1] Basak D.K., Chakraborti N., Ghosh B., Goswami G.C. and Chaudhuri N., Nucl.Instrum.Methods , 227,167,1984.
[2] Sarkar S.K., Ph.D. thesis , University of North Bengal , India, 1987.
[3] Goswami G.C., Ghosh B., Ghoshdastidar M.R., Sengupta S.K. and Chaudhuri N., Nucl. Inst. Methods , 192,375,1982.
[4] Goswami G.C., Ghosh B., Ghoshdastidar M.R., and Chaudhuri N., Nucl.Inst. Methods,199,505,1982.
[5] Hillas A.M. and Lapikens J., Proceedings of the 15th International Conference on Cosmic Rays, Plovdiv,8(1977)460.
[6] Bhattacharyya B., Bhadra A., Mukherjee A., Saha G., Sanyal S., Sarkar S., Ghosh B. and Chaudhuri N., IL Nuovo Cimento , 18C(1995)325.
[7] Greisen K., Annu.Rev.Nucl.Sci.,10(1960)63.
[8] Capdeville J.N., Gawin J. and Procureur J., Proceedings of the 15th International Conference on Cosmic Rays , Plovdiv,8(1977)341.

Chapter-3

[1] Trzupek A., Lu Y. and Poirier J., Proceedings of the 23rd International Conference on Cosmic Rays, Calgary,4(1993)359.
[2] Wrotniak J.A. and Yodh G.B., Proceedings of the 19th International Conference on Cosmic Rays, La Jolla, 7(1985)1.
[3] Hillas A.M. and Lapikens J., Proceedings of the 15th International Conference on Cosmic Rays, Plovdiv, 8(1977)460.
[4] Asakimori K., Hara T., Maeda T., Nishijima K., Toyoda Y., Kamamoto K., Yoshida M., Kameda T. and Mizushima K., Proceedings of the 17th International Conference on Cosmic Rays, Paris, 11(1981)301.

[5] Khrenov B.A. and Linsley J., Proceedings of the 17th International Conference on Cosmic Rays, Paris, 10(1981)354.
[6] Greisen K., Ann.Rev., Nuc. Sci., 10(1960)63.
[7] Khrenov B.A., Soviet Phys., JEPT,14(1961)1001.
[8] Khrenov B.A., Jour.Nucl.Phys., USSR, 1(1965)540.
[9] Earnshaw J.C., Orford K.J., Rochester G.D., Somogyi A.J., Turver K.E. and Walton A.B., Proc., Phys.Soc., 90,91,1967.
[10] Rada R.S., Smith A.C., Stewart T.R., Thompson M.G., Treasure M.W., Nuovo Cimento Soc. Ital.Fis.A 54(1979)208.
[11] Atrashkevich V.B., Ermakov G.G., Fomin Yu A., Garipov G.G., Iljina N.P., Kalmykov N.N., Khrenov B.A., Khristiansen G.B. et al., Proceedings of the 18th International Conference on Cosmic Rays, Bangalore,11(1983)229.
[12] Vashkevich V.V., Ermakov G.G., Ermolov P.F., Kulikov G.V., Rukovichkin V.P., Solovyeva V.I., Sulakov V.P., Fomin Yu.A. et al ., Soviet J. Nucl. Phys.,Engl.Transl, 47(1988)1054.
[13] Mikocki S. and Trzupek A., Private communication , Grand-90-820.
[14] Wrotniak J.A., Yodh G.B., Proceedings of the 19th International Conference on Cosmic Rays, La Jolla,7(1985)1.
[15] Hillas A.M., Proceedings of the 16th International Conference on Cosmic Rays , Kyoto,9(1979)13.
[16] Bourdeau M.F., Capdevielle J.N., Guedj A., Procureur J., Proceedings of the 16th International Conference on Cosmic Rays, Kyoto,9(1979)155.
[17] Kawamura Y. et al , Phy.Rev.D40,729,1989.
[18] Ichimura M. et al., ICRR Report 287,92-95,1992.
[19] Blake P.R. and Tummey S.P., Proceedings of the 23rd International Conference on Cosmic Rays, Calgary, 4(1993)363.

IL NUOVO CIMENTO VOL. 18 C, N. 3 Maggio-Giugno 1995

A New Lateral Distribution Function for Electrons in Extensive Air Showers (EAS) Detected near Sea Level.

B. BHATTACHARYYA, A. BHADRA, A. MUKHERJEE, G. SAHA, S. SANYAL
S. SARKAR, B. GHOSH and N. CHAUDHURI
High Energy and Cosmic Ray Centre, North Bengal University, India

(ricevuto il 5 Luglio 1994; revisionato il 13 Marzo 1995; approvato il 7 Aprile 1995)

Summary. — A detailed analysis of Extensive Air Showers in the size range 10^4–10^6 particles detected near sea level has yielded a new distribution function for the radial distribution of EAS electrons. The goodness-of-fit criteria applied to the present and already existing similar distribution functions confirm that the present function is appropriate in EAS at radial distances beyond 20 m from the shower axis.

PACS 94.40.My – Cascade studies (*e.g.*, extensive air showers).

1. – Introduction.

There has been a number of recent studies on the lateral structure of Cosmic-Ray Extensive Air Showers (EAS) with a view to distinguishing between Primary-Cosmic-Ray (PCR) protons or nuclei-initiated EAS and ultra-high-energy cosmic gamma-ray photon-initiated EAS. In both kinds of EAS a photon-electron cascade develops together with a nucleon cascade longitudinally from the atmospheric depths to which the initiating particles penetrate to make their first nuclear collisions. A photon-electron cascade in EAS with radial symmetry is described laterally at a distance r from the EAS axis by expressing the shower particle density $\Delta(r)$ by

$$\Delta(r) = \frac{N}{r_0^2} f(r/r_0, s), \tag{1}$$

with the shower particle density defined as

$$\Delta(r) = \frac{\Delta N}{(r_0^2)\, 2\pi (r/r_0)\, d(r/r_0)},$$

where N is the total number of particles (size) in EAS; $f(r/r_0, s)$ the lateral structure

function of the EAS; s the age of the electron-photon cascade in the EAS and r_0 the unit of distance chosen for measuring the radial distance of any point in EAS from the EAS axis.

An exact form of the function $f(r/r_0, s)$ is necessary to determine the EAS parameters (shower axis location coordinates (x_0, y_0), shower size N, and shower age s) from a number of measured densities $\Delta(r)$ at various radial distances r from the EAS axis.

A critical analysis of several forms of $f(r/r_0, s)$ used in EAS work in the last four decades was given by Basak *et al.* [1]. The form of $f(r/r_0, s)$ referred to as NKG distribution function was first introduced by Greisen [2] to represent the theoretical results of Nishimura and Kamata [3]. The various forms of $f(r/r_0, s)$ in use [4] are the NKG form and the different modifications [5-13] of the NKG form to take care of the discrepancies with measurement of $\Delta(r)$ *vs.* r observed over a wide range of r.

The purpose of the present paper is to determine, from the experimentally observed lateral particle density distribution, the radial ranges in which three extensively used forms of $f(r/r_0, s)$ are valid on the basis of rigorous «goodness of fit» criterion. A new form for $f(r/r_0, s)$ has also been derived from such analysis of the observed sea level EAS data on $\Delta(r)$ in individual EAS.

2. – EAS data collection and method of analysis.

A closely packed well-defined EAS array operating near sea level at the North Bengal University (26°45′ N) has 35 unshielded scintillation detectors to measure shower particle density $\Delta(r)$ in individual EAS. Eight (8) of these detectors are used to measure relative time delays between their output pulses to determine the arrival directions of the detected EAS. The angular accuracy in direction measurement is within 2° and the error in the EAS axis location is about 1 m.

The shower parameters are determined by fitting a chosen function $f(r/r_0, s)$ to the observed radial distribution of the densities $\Delta(r)$ by minimizing with respect to each of the shower parameters simultaneously the entity defined as

$$\chi^2(x_0, y_0, N, s) = \sum_{i=1}^{n} W_i(\Delta_i^o - \Delta_i^e)^2 . \tag{2}$$

Here Δ_i^o, Δ_i^e are the observed and expected particle densities at the i-th detector in the EAS array and the weight factor W_i of the i-th density data point is the inverse of the variance of the i-th point density Δ_i^e. If the fitting function $f(r/r_0, s)$ is chosen appropriately to predict densities $\Delta_i^e(r)$, a good fit of $f(r/r_0, s)$ to the observed densities $\Delta_i^o(r)$ can be obtained by minimizing χ^2 and hence the constants and parameters in the fitting function can be determined. The number of data points in an EAS is denoted by n.

The method of searching for the minimum value of $\chi^2(x_0, y_0, N, s)$ with respect to each of the EAS parameters simultaneously is the gradient search method in the direction of steepest descent. For fitting the observed density $\Delta^o(r)$ *vs.* r distribution in individual EAS, three forms of the function $f(r/r_0, s)$ have been tried. These are: NKG function $f_{\mathrm{NKG}}(r/r_0, s)$ [2], Hillas function $f_{\mathrm{H}}(r/r_0, s)$ [14] and Capdevielle function $f_{\mathrm{C}}(r/r_0, s)$ [15]. The steepest-descent iterative process of minimizing χ^2 was done by the gradient search method and when the minimum of the χ^2-hypersurface

was attained the gradient was reduced to one-half of its former value. This procedure was repeated until the χ^2-value between two successive steps was close enough to a preassigned value.

3. – Results.

Results of a sample of some five thousand recorded EAS events with more than 50% detectors registering particle densities have been analysed shower-size-wise by the standard χ^2 minimization procedure discussed above in sect. 2. The mean of the minimum of the χ^2-values represents the goodness of fit of the observed density distribution of particles in EAS of given size to the fitting function chosen to describe the data.

3·1. *Least-square fitting to the observed density* $\Delta^0(r)$ *data using* NKG *function* $f_{\mathrm{NKG}}(r/r_0, s)$ *for* $\Delta^e(r)$. – The shower parameters N and s determined on the basis of $f_{\mathrm{NKG}}(r/r_0, s)$ (eq. (3)) are given in table I.

$$\Delta^e(r) = \frac{N}{r_0^2} f_{\mathrm{NKG}}(r/r_0, s) = \frac{N}{r_0^2}\left[C(s)\left(\frac{r}{r_0}\right)^{s-2}\left(1+\frac{r}{r_0}\right)^{s-4.5}\right], \tag{3}$$

where the photon-electron cascade parameter s is a measure of the development of EAS down to the depth of observation in the atmosphere. Theoretically this shower age parameter s is a function of depth t (measured in radiation unit), the energy of the initiating particle and the radial range r of an EAS. $C(s)$ is the normalization constant to be determined by the fitting procedure, $r_0 = 79$ m (Moliere unit of displacement at sea level).

The observed probability distribution P_χ corresponding to ν degrees of freedom for the reduced chi square $\chi^2_\nu (= \chi^2/\nu)$ for a given shower size over the whole radial range is shown in fig. 1 and for the range 0–20 m in fig. 2.

3·2. *Least-square fitting to the density* $\Delta^0(r)$ *data using Hillas function* $f_{\mathrm{H}}(r/r_0, s)$. – The observed probability distribution for the reduced χ^2_ν for the same shower size is given in fig. 3 and fig. 4 when $f_{\mathrm{H}}(r/r_0, s)$ (derived from Monte Carlo simulation data) given below (eq. (4)) was used for fitting the EAS density data

$$\Delta^e(r) = \frac{N}{r_0^2} f_{\mathrm{H}}(r/r_0, s) = \frac{N}{r_0^2}\left[C(s)\left(\frac{r}{r_0}\right)^{a_1 + a_2(s-1)}\left(1+\frac{r}{r_0}\right)^{b_1 + b_2(s-1)}\right], \tag{4}$$

where the constants r_0, a_1, a_2, b_1, b_2 are the fitting parameters.

TABLE I.

Range of estimated shower size N (No. of particles)	Radial range of density $\Delta^0(r)$ (measurement in metres)	Range of best-fitting values of s
$(1–5)\cdot10^4$	0–120	0.90–1.35
$(5–9)\cdot10^4$	0–120	0.90–1.35
$(1–5)\cdot10^5$	0–120	0.90–1.35

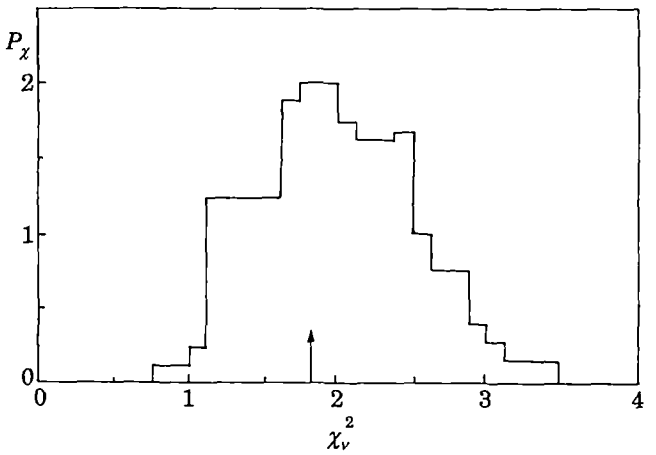

Fig. 1. – The observed probability distribution P_χ for the reduced chi square χ_ν^2 using the NKG function in the radial range 0–120 m.

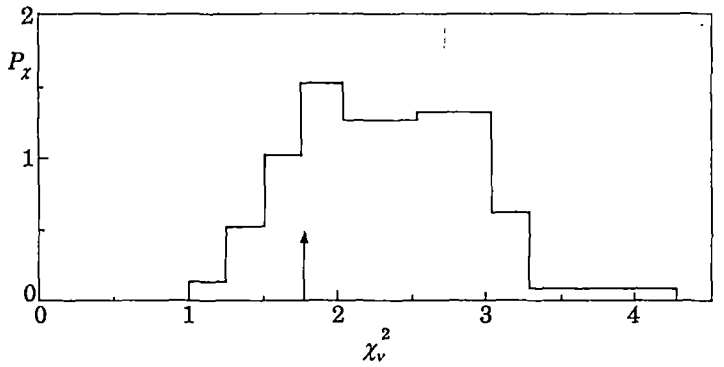

Fig. 2. – Same as in fig. 1, but for the radial range 0–20 m.

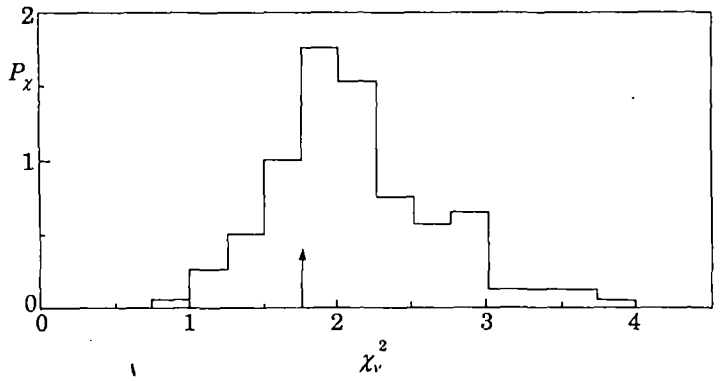

Fig. 3. – Same as in fig. 1, but using Hillas function.

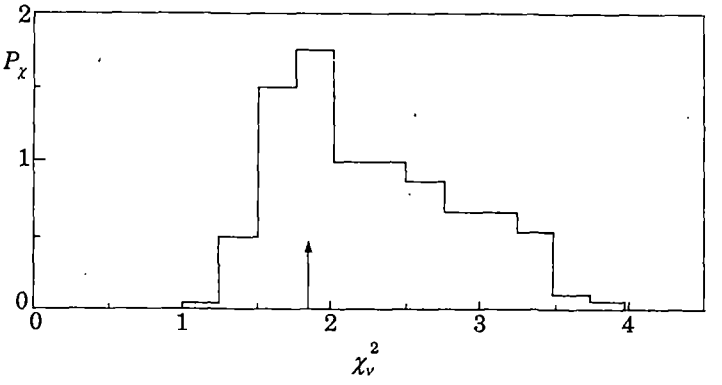

Fig. 4. – Same as in fig. 1, but using Hillas function in the radial range 0–20 m.

3·3. *Least-square fitting to the density* $\Delta^0(r)$ *data using* $f_C(r/r_0, s)$. – Capdevielle *et al.* [15] assumed that the shower age parameter in the fitting function should be the «effective age» for radial development of shower and defined it as

$$s(r) = \alpha \log \beta(r/r_0) + s_l\,, \qquad \text{for} \qquad r \leqslant 150 \text{ m} \tag{5}$$

where s_l is the longitudinal age parameter at the level of observation and α, β, s_l are constants at sea level for a given shower size.

The observed probability distribution for the reduced χ_ν^2 for the same shower size using the $f_C(r/r_0, s)$ (eq. (6)) for fitting the density data is given in fig. 5 and fig. 6.

$$\Delta^e(r) = \frac{N}{r_0^2} f_C(r/r_0, s) = \frac{N}{r_0^2}\left[C(s)\left(\frac{r}{r_0}\right)^{s(r)-2}\left(1+\frac{r}{r_0}\right)^{s(r)-4.5}\right], \tag{6}$$

where $r_0 = 79$ m (Moliere unit of displacement at sea level). The summary of χ_ν^2 results from the distribution in fig. 2 to 6 and similar such other distributions (not shown) are given in table II and III.

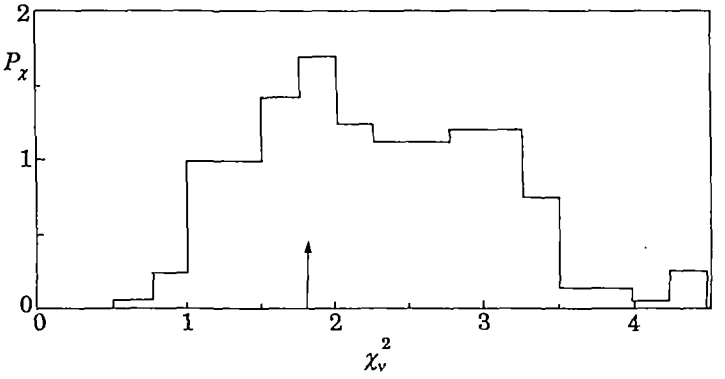

Fig. 5. – Same as in fig. 1, but using Capdevielle function.

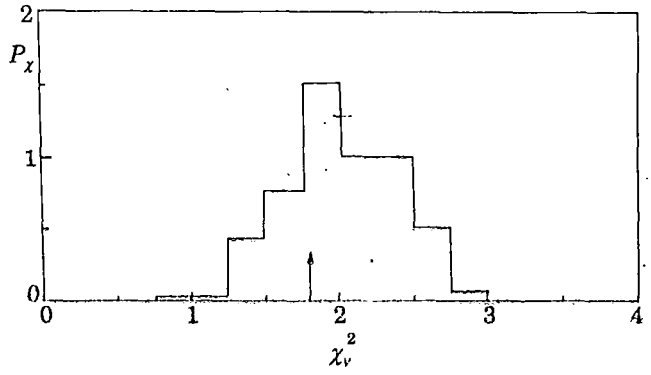

Fig. 6. – Same as in fig. 1, but using Capdevielle function in the radial range 0–20 m.

TABLE II. – *Mean values of the reduced* χ^2_ν *from fig.* 1, 3 *and* 5 *for the distribution functions (for* EAS *radial range* 0–120 m).

$f_{NKG}(r/r_0, s)$	$f_H(r/r_0, s)$	$f_C(r/r_0, s)$	Proposed $f'(r/r_0, s)$
1.81	1.77	1.80	1.72

TABLE III. – *Mean values of the reduced* χ^2_ν *in different radial ranges in* EAS *for distribution functions.*

EAS radial ranges in metres	$f_{NKG}(r/r_0, s)$	$f_H(r/r_0, s)$	$f_C(r/r_0, s)$	Proposed function (eq. (7))
0–20	1.77	1.82	1.80	1.83
20–80	1.79	1.77	1.76	1.77
80–120	1.83	1.55	1.82	1.45

4. – Proposed radial distribution function.

The present shower data have also been analysed by using a new distribution function $f'(r/r_0, s)$ (proposed) (eq. (7)) which incorporates two features:

1) the dependence of radial shower age on radial distance and

2) the unit of distance r_0 is taken as the parameter of the fitting function instead of choosing for it a constant value of 79 m (Moliere unit of displacement at sea level).

$$(7)\quad \Delta^e(r) = \frac{N}{r_0^2} f'(r/r_0, s) = \frac{N}{r_0^2}\left[C(s)\left(\frac{r}{r_0}\right)^{-0.53 + 1.54(s(r)-1)}\left(1 + \frac{r}{r_0}\right)^{-3.39 + 0.01(s(r)-1)}\right],$$

where $s(r) = \alpha \ln \beta(r/r_0) + s_1$, for $r \leqslant 150$ m. Here r_0, α, β and s_1 are the fitting parameters.

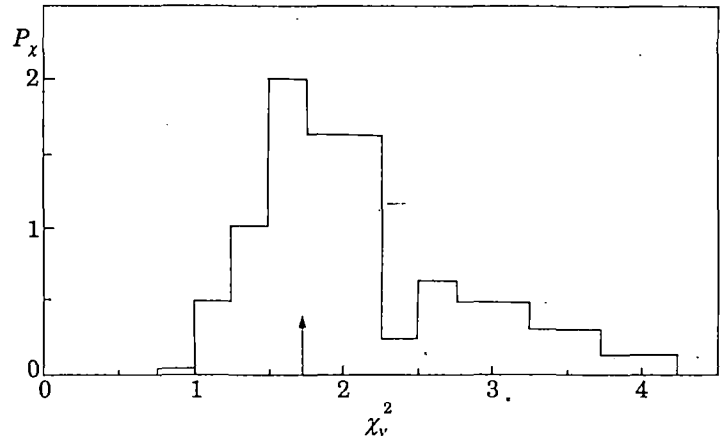

Fig. 7. – Same as in fig. 1, but using the proposed function.

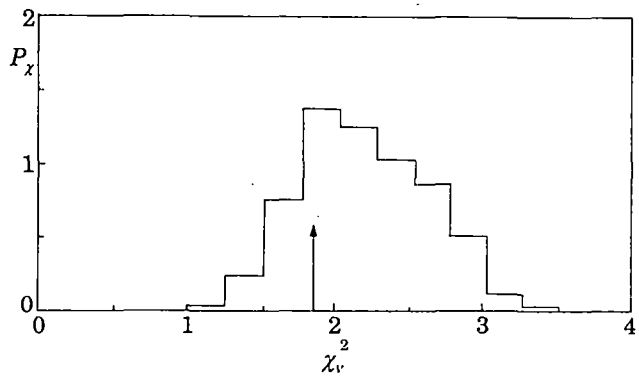

Fig. 8. – Same as in fig. 1, but using the proposed function in the radial range 0–20 m.

Some results for the probability distribution for χ_ν^2 using eq. (7) are shown in fig. 7 and fig. 8. The mean values of χ_ν^2 for the same shower size in the whole region and in three different radial ranges 0–20 m, 20–80 m, 80–120 m are given in table II and III, respectively.

5. – Discussion and conclusion.

It is necessary to touch upon a few points in connection with the present air shower measurements and analysis. The transition effect arising from multiplication or absorption (absorption is predominant over multiplication) of shower particles in the finite thickness of a plastic scintillator in a density detector of the EAS array was taken into account by correcting the observed density in the manner discussed previously by Basak *et al.* [1, 16] and Asakimori *et al.* [17, 18]. The shape of the average lateral distribution function and the value of the local shower age parameter s measured [1, 16-18] by using thin plastic scintillators is not much dependent on the transition effect near cores of showers in the size range $\sim 10^5$ particles.

The cores of EAS striking the detecting points within the well-defined periphery of the EAS array were located by fitting the measured particle densities registered at the struck detectors to eq. (3) for interpolation of the measured density readings. It has been checked that shower cores thus located are insensitive to the interpolation function chosen. With a close-packed (small detector spacing) well-defined detector array as in the present experiment, the uncertainty in the shower core location from the measured density readings is expected to be minimum compared to what is expected from a detector arrangement with large spacings.

The weighting factor W_i in eq. (2) is the inverse of the variance σ_i^2 (which describes the uncertainty of the i-th data point evaluated by assuming Poisson distribution). Consequently the fits obtained with different lateral distribution function (l.d.fs) will not depend on the detector spacing of an array with well-defined perimeter, the weighting factor W_i and the shower core location procedure.

To obtain a fit of the measured density data of a recorded EAS event to a fitting function (l.d.f) with several parameters, the gradient search method of least squares was used for determining simultaneously the optimum values of the parameters which give a minimum to the function χ^2 (eq. (2)) defined with that l.d.f. This

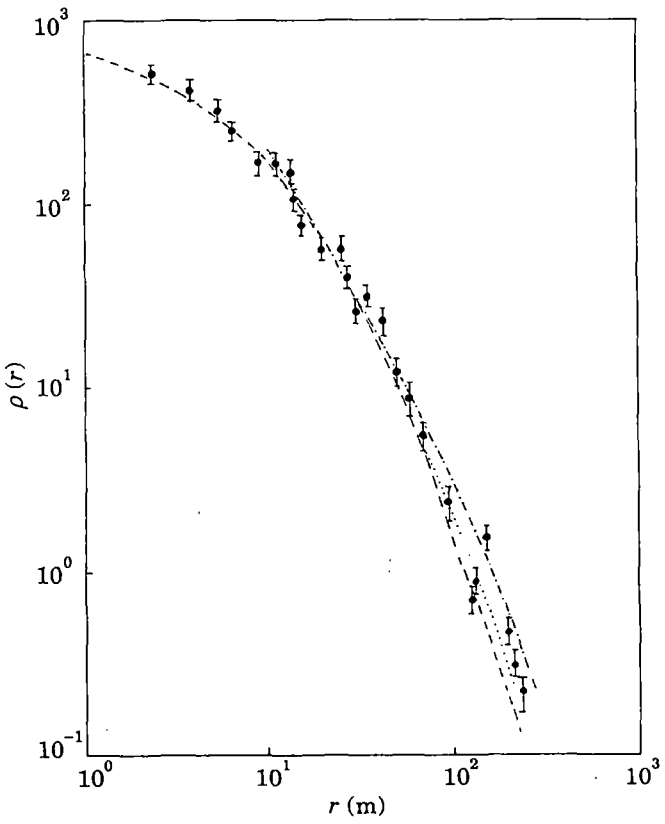

Fig. 9. – Observed lateral electron density distribution along with the theoretical distributions using Hillas (dashed line), Capdevielle (dot-dashed line) and the proposed function (dotted line) in the radial range 0–120 m. $N = 6 \cdot 10^6$, $s = 1.25$.

procedure is expected to obtain a best fit for the multiparameter l.d.f to a large number of density readings in a registered EAS event from a large sample of EAS of fixed size N. The probability distribution for χ^2 as well as the χ^2-values found in the present work by the gradient search method are larger than the expected values due to large intrinsic fluctuations from shower to shower and random sample of density data of an individual EAS with small values of «sample standard deviation σ_i». The error in attaining χ^2-minima by the gradient search with steepest-descent iterative procedure adopted in the present work may contribute to the size of χ^2-near minima.

The results of the fit with different l.d.fs are shown in fig. 9 to indicate the extent to which the present experimental data could discriminate them.

It is seen from table II that $f_H(r/r_0, s)$ among the three distributions (f_{NKG}, f_H, f_C) considered above is the best fit to the observed density distribution in the whole 0–120 m radial range of EAS. The results of the reduced χ^2_ν test (table III) for the three successive smaller radial ranges in an EAS of the same size as that used in table II show a varying degree of goodness of fit of the observed data to the same fitting function. Whereas $f_{NKG}(r/r_0, s)$ represents a good fit to 0–20 m radial range, in the 20–80 m radial range $f_C(r/r_0, s)$ shows a slight improvement over $f_H(r/r_0, s)$ which is best in the 80–120 m range. None of these three functional forms can give a reasonably good fit to the observed data in the whole range 0–120 m.

The choice of $s(r)$ variation with r and the choice of r_0 as an adjustable parameter of the fitting function in place of Moliere unit of displacement at sea level are adjusted in the radial range 20–80 m and 80–120 m. In the 80–120 m range the function under eq. (7) gives the better fit to the observed data ($\chi^2_\nu = 1.45$) than the fits obtained by other functions (eq. (1) to (3)). The result of the χ^2_ν-test (table II) made over the whole shower range 0–120 m shows that the proposed function (eq. (7)) is better than any other fitting functions considered above.

The measured age parameter $\bar{s}$ (table I) of an EAS of given size is the mean of the s-values obtained at the χ^2 minima using eq. (3) or eq. (4) as the fitting function. The relation between the values of $\bar{s}$ and s_l values obtained by the analysis using eq. (7) as the fitting function is

$$s_l = \bar{s} + s_c\,, \qquad \text{for} \qquad r \leqslant 120 \text{ m}\,, \tag{8}$$

with $s_c = 0.15$–0.3.

This experimental relation has been obtained from the analysis over the radial range 0–120 m in muon-rich normal EAS initiated presumably by PCR protons or nuclei. However this form is applicable to recorded EAS events of similar shower size having arrival directions from specific stellar point sources of ultra-high-energy gamma-ray photons. From the measured $\bar{s}$-values of such EAS events, one can determine s_l values from relation (8). This determination together with a determination of muon size and hadron size simultaneously in such EAS may unambiguously identify such events as ultra-high-energy gamma-ray photon-initiated events. This relation gives a comparison of the performance of the proposed function (eq. (7)) with the NKG function or Hillas function in terms of the measured longitudinal age parameter s_l and the measured $\bar{s}$ which represents the shower age parameter of a given shower size that one obtains from a best fit of the data with $f_{NKG}(r/r_0, s)$ or $f_H(r/r_0, s)$.

Recently the lateral distributions of particles in simulated EAS have also been studied by using cosmic atomic nuclei and cosmic gamma-ray photons [14, 19, 20]. In the simulation work of Mikocki *et al.*, the lateral distribution of particles in EAS of size range 10^5–10^6 particles at sea level was studied using NKG formula (eq. (3)) as

the fitting function. Their χ^2_ν test for the simulation over the radial range 0–100 m yielded, at the minimum value of $\chi^2_\nu (\simeq 6)$ and the fitting parameters, $r_0 = 41$ m and $\bar{s} = 1.29$–1.35. These results show that $f_{\mathrm{NKG}}(r/r_0, s)$ is not an appropriate fitting function for the observed $\Delta(r)$ distribution over a wide radial range in EAS.

In conclusion it may be stated that the proposed function for radial particle density distribution in EAS can be applied to analyse small- and medium-size EAS of the radial range extending to 120 m at least. It can be also used to derive the longitudinal age parameter s_l from the measured shower age parameters $\bar{s}$.

REFERENCES

[1] BASAK D. K., BHATTACHARYYA B. and CHAUDHURI N., *Nuovo Cimento C*, **13** (1990) 677.
[2] GREISEN K., *Annu. Rev. Nucl. Sci.*, **10** (1960) 63.
[3] NISHIMURA J. and KAMATA K., *Prog. Theor. Phys.*, **5** (1950) 899; **6** (1951) 628; **7** (1952) 185.
[4] PROCUREUR J. and STAMENOV J. N., *J. Phys. G.*, **13** (1987) 1579; NIKOLSKY S. I., STAMENOV J. N. and USHEV S. Z., *J. Phys. G.*, **13** (1987) 883; DEDENKO L. G., *Proceedings of the XXIII International Conference on Cosmic Rays*, Vol. 4 (Calgary, 1993), p. 231.
[5] KHRISTIANSEN G. B., KULIKOV G. B. and SOLOVIEVA V. I., *Proceedings of the XVII International Conference on Cosmic Rays*, Vol. 6 (Paris, 1981), p. 39.
[6] KAWAGUCHI S., SUGA K., SAKUYAMA H., *Proceedings of the XIV International Conference on Cosmic Rays*, Vol. 8 (1975), p. 2826.
[7] DEDENKO L. G., NESTEROVA N. M., NIKOLSKY S. I., STAMENOV I. N. and JANMINCHEV V. D., *Proceedings of the XIV International Conference on Cosmic Rays*, Vol. 8 (Munich, 1975), p. 2731.
[8] KANEKO T., AGUIRRE C., TOYODA Y., NAKATANI H., JADOT S., MACKEOWN P. K., SUGA K., KAKIMOTO F., MIZUMOTO Y., MURAKAMI K., NISHI K., NAGANO M. and KAMATA K., *Proceedings of the XIV International Conference on Cosmic Rays*, Vol. 8 (Munich, 1975), p. 2747.
[9] LINSLEY J., *Proceedings of the XV International Conference on Cosmic Rays*, Vol. 12 (Plovdiv, 1977), p. 56.
[10] HARA T., HATANO Y., HASEBE N., HAYASHIDA N., JOGO N., KAMATA K., KAWAGUCHI S., KIFUNE T., NAGANO M. and TANAHASHI G., *Proceedings of the XVI International Conference on Cosmic Rays*, Vol. 13 (Kyoto, 1979), p. 148.
[11] LAGUTIN A. A., PIJASHESHNIKOV A. V. and UCHAIKIN V. V., *Proceedings of the XVI International Conference on Cosmic Rays*, Vol. 7 (Kyoto, 1979), p. 18.
[12] CHUDAKOV A. E., DZHAPPUEV D. D., LIDVANSKY A. S. and TIZENGAUZEN V. A., *Proceedings of the XVI International Conference on Cosmic Rays*, Vol. 8 (Kyoto, 1979), p. 217.
[13] NAGANO M., HARA T., HATANO Y., NAYASHIDA N., KAWAGUCHI S., KAMATA K., KIFUNE T. and MIZUMOTO Y., *J. Phys. G.*, **10** (1984) 1295.
[14] HILLAS A. M. and LAPIKENS J., *Proceedings of the XV International Conference on Cosmic Rays*, Vol. 8 (Plovdiv, 1977), p. 460.
[15] CAPDEVIELLE J. N., GAWIN J. and PROCUREUR J., *Proceedings of the XV International Conference on Cosmic Rays*, Vol. 8 (Plovdiv, 1977), p. 341.
[16] BASAK D. K. and CHAUDHURI N., *Nuovo Cimento C*, **9** (1986) 846.
[17] ASAKIMORI K., HARA T., MAEDA T., NISHIJIMA K., TOYODA Y., KAMAMOTO K., YOSHIDA M., KAMEDA T. and MIZUSHIMA K., *Proceedings of the XVII International Conference on Cosmic Rays*, Vol. 11 (Paris, 1981), p. 301.
[18] ASAKIMORI K., MAEDA T., KAMEDA T., MIZUSHIMA K. and MISAKI Y., *Proceedings of the XIX International Conference on Cosmic Rays*, Vol. 7 (La Jolla, 1985), pp. 107; 179.
[19] STAMENOV J. N., *Proceedings of the XX International Conference on Cosmic Rays*, Vol. 8 (Moscow, 1987), p. 258.
[20] MIKOCKI S., GRESS J. and PIORIER J., *Proceedings of the XXI International Conference on Cosmic Rays*, Vol. 9 (Adelaide, Australia, 1990), p. 1.

Study of electrons simultaneously with muons in Extensive Air Showers (EAS) initiated by Primary Cosmic Rays of energy 10^{14}-10^{16} eV

C. Chakrabarti, D. Chanda, G. Saha, A. Mukherjee, A. Bhadra
S. Sanyal, S. K. Sarkar, B. Ghosh, N. Chaudhuri.
High Energy & Cosmic Ray Centre.
North Bengal University
Darjeeling, India

Abstract.

An air shower experiment performed with the provision of direct measurement of both low and high energy muons simultaneously by magnet-spectographs has yielded radial muon density distributions at various measured muon energies and radial electron density distributions as a function of known shower size of measured age. The characteristics of these distributions in terms of the measured shower parameters have been determined to draw conclusions about the mass of the primaries of EAS.

1.- Introduction:

The initial results of the first set of measurements of both the electron and muon distributions in EAS in the size range 10^4 - 10^6 particles (primary energy range 2.2×10^{14} - 4.8×10^{15} eV) have been presented in the previous ICRC sessions (1983, 1985, 1987, 1990) by the NBU group. The direct measurements of muon energies by two magnet-spectographs of the NBU EAS array provide accurate data to form a base for comparison with the predictions of different EAS models for various primary compositions. The present report presents the final results of our first experiment.

2.- Method:

The method was same as we described in previous reports (1983, 1985, 1987, 1990). The magnet-spectographs for recording muons were operated in coincidence with the EAS array of particle density detectors and timing detectors under a fixed set of selection criteria. The average electron and muon densities in each of various narrow shower size bins in the

shower size range 10^4-10^6 particles was obtained as a function of r and muon energy E_μ (not exceeding E_μ). These results yield radial distributions for muon density with energy not exceeding E_μ as well as the muon energy spectrum at various muon distances r over the range 0-120 m .

3.-Results:

3·1:-The measured muon energy spectrum.
The muon energy spectra have been measured for various average shower sizes. For average shower size $\bar{N}_e = 2.2 \times 10^4$ particles($\bar{s} = 1.25$) in the radial range 0-100 m the muon energy spectrum fits to :

$$N_\mu(\geq E_\mu) \sim E_\mu^{\alpha_\mu(r)} \qquad \text{--- (1)}$$

where $\alpha_\mu(r)$ changes from 0.26 at about 5 m to 1.01 at about 90 m showing the degree of dependence of energy spectrum of muons on the distances from the EAS axis .

3·2:-Muon density dependence on average shower size $\bar{N}_e$.
For different threshold muon energies and the radial distances from the EAS axis, the results of muon density dependence on shower size fit to :

$$\rho_\mu(\geq E_\mu, r) \sim N_e^{\beta(E_\mu, r)} \qquad \text{--- (2)}$$

The exponent β is weakly dependent on r and the threshold muon energy E_μ. For example for muons of energy exceeding 10 GeV at r between 16 and 32 m, the value of β is 0.72 whereas for $E_\mu > 100$ GeV for the same value of r between 16 and 32 m, the value of β is 0.68 .

It is further seen (fig.1) that for low energy muons in showers of size less than $10^{5.25}$ particles the exponent β decreases with r increasing whereas in larger showers of $\bar{s}$ greater than $10^{5.25}$ particles, β increases with r. For high energy muons β decreases with r in showers of size below and above $10^{5.25}$ particles. At different radial distances and for different low muon thereshold energies β changes around the shower size $10^{5.25}$ particles. Such variation of β implies that the muon radial distribution function changes with the primary energy. The measured muon

lateral distribution for each shower size and muon energy exceeding E_μ in the radial range between 0 and 120 m shows a fit to the form

$$\rho_\mu(\geq E_\mu, r, N_e) \sim r^{-k(\geq E_\mu)} \exp(-r/r_o) \quad \text{---} \quad (3)$$

This shows that the muon lateral distribution function depends on muon energy threshold. The exponent k has the values in the range 0.26 - 1.22 .

The measured data of muon density also fit to a single parameter form :

$$\rho_\mu(\geq E_\mu, r, N_e) \sim r^{-\alpha(\geq E_\mu)} \quad \text{---} \quad (4)$$

values of α within an error range 8-10 % from the fit of the data for $E_\mu \geq 2.5$ GeV. are shown as a function of N_e in fig.2 . The trend of α vs. E_o (the conversion of shower size to primary energy E_o is in accordance with the energy scaling factor of Aliev et. al.[1] and Trzupek et. al.[2]) curve shows that α is a function of energy up to 2×10^{15} eV and becomes constant at higher energies. Such a variation of α with E_o implies that the effective primary mass is decreasing with increasing energy over the range 10^{14} - 10^{15} eV and becomes constant at higher energies.

3.3-Radial distribution of electrons compared with radial distribution of muons:
The radial muon density distribution in young developing showers ($s \leq 1.0$) as well as in old decaying showers ($s \geq 1.0$) is flatter compared to the radial electron density distribution which is shown in fig.3 for $N_e = 3.3 \times 10^5$. The muon densities in old showers are high than those in younger showers of the same size by a factor two.

4.-Discussion.

The properties of the measured radial distribution of muon density in EAS as a function of primary energy in the range 10^{14} - 10^{15} eV indicate continuously decreasing primary mass composition. The measured value and shape of the radial distribution for muons and electrons at small and large distances from the EAS axis are similar to the Monte Carlo results obtained for primary proton initiated EAS (Poirier et al.[3])

References

[1] Aliev N et al 18th ICRC 7(1985)191
[2] Trzupek A.et al 23rd ICRC 4(1993)359
[3] Poirier J.Gress J,Mikocki S ? t. ICRC 9(1990)120

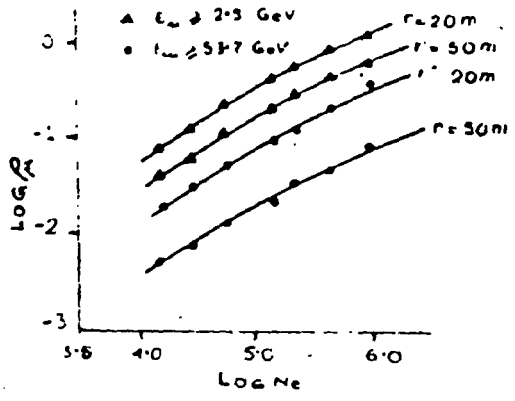

Fig 1

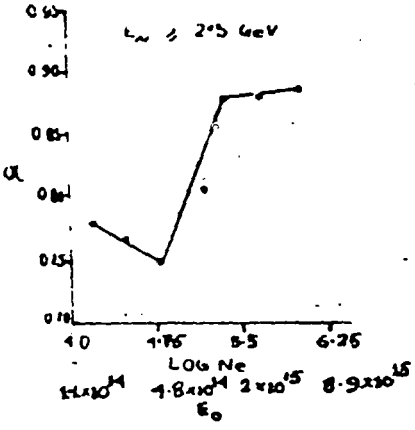

Fig 2

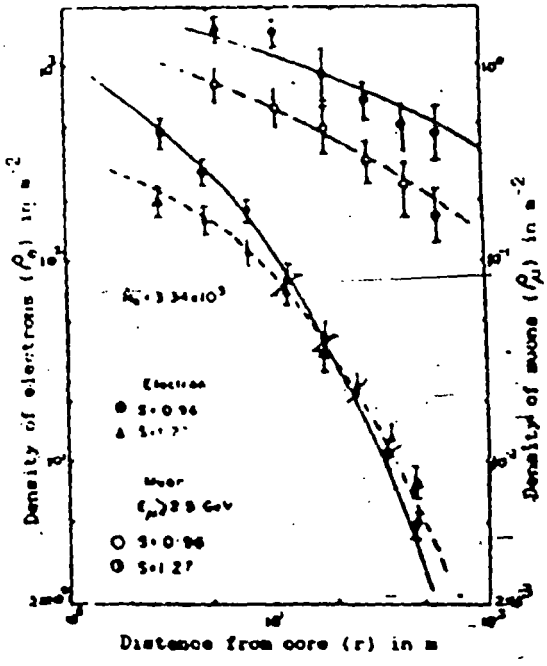

Fig 3

Figure Captions

Fig.1. Variation of muon density at radial distances 20 m & 50 m with shower size (vertical showers) at $E_\mu \geq 2.5$ & 53.7 GeV

Fig.2. Variation of α with N_e at $E_\mu \geq 2.5$ GeV

Fig.3. Electron and muon lateral density distributions for old decaying and young developing vertical showers.

Low And High Energy Muons In Extensive Air Showers Of Size 10^4 To 10^6 Particles

C. Chakrabarti, D. Chanda, G. Saha, A. Mukherjee, A. Bhadra, S. Sanyal, R. K. Chhetri, S. K. Sarkar, B. Ghosh and N. Chaudhuri.

High Energy and Cosmic Ray Center
North Bengal University
Darjeeling
India-734 430

Abstract

Accurately measured energy spectra and radial distributions of low and high energy muons in Extensive Air Showers (EAS) are presented and compared with Monte Carlo calculations assuming specific hadronic interaction characteristics of primary protons with air nuclei in the primary energy range $2.2X10^{14}$ - $4.8X10^{15}$ eV.

I-Introduction:

Knowledge of radial distribution together with energy distribution of muons in EAS is of fundamental importance as such data have explicit energy dependence and are expected to be sensitive to both the primary cosmic ray composition and the characteristics of hadronic interaction with air nuclei.

This paper contains accurately measured data on low and high energy muons detected in association with EAS at sea level. By direct and accurate measurement of muon energy over a wide range of energy and radial distance from the EAS axis, the present experiment provides a firmer base for comparing with the theoretical predictions for different primary compositions.

II-Experiment and Method:

The experimental set up consists of an air shower array of 32 electron detectors and two

magnet spectrographs for recording and measuring muon momenta accurately in association with individual EAS incident on the array. The description of the array system and spectrographs was given by Basak et al. (1). Low and high energy muons in the range of 2.5 - 200 GeV in EAS of size 10^4 to 10^5 particles (primary energy range $2.2X10^{14}$ - $4.8X10^{15}$ eV, determined by using the energy scaling factor of N.Aliev et al.(2)and A.Trzupek et al.(3)) were recorded by the two spectrographs simultaneously with the recording of the EAS events by the array. The EAS parameters such as shower size(Ne),age paramete(s), EAS axis location and the radial distance of each recorded muon were determined by the method of least squares.

The recorded muon deflection angle is converted to incident momentum of muon (momentum resolution of spectrograph 17% to 38% for energy range 2.5 - 200 GeV) by the method described by Basak et al.(1). The density of muons of energies above a threshold value in EAS of measured parameters was determined as a function of muon radial distance from the shower core.

III-Results:

Some of the representative experimental data, with typical poissonian error on a few points only, in the form of muon lateral distribution for a fixed shower size at different threshold energies (fig.1), muon energy spectrum at a fixed radial distance for two different shower sizes (fig.2) and the variation of muon density with average shower size with threshold muon energy of 2.5 GeV at two different radial distances from the shower core (fig.3) are shown.

A comparision of the measured electron lateral distribution (fig.4), muon lateral distribution (threshold energy 2.5 GeV) (fig.5) and the ratio of muon and electron density for different shower sizes (fig.6) with data calculated by Monte Carlo simulation of Poirier et al. (4) utilising simulation codes SHOWERSIM (model WOO) and EGS for proton primaries is also given. The hadron-hadron interaction model WOO (details presented by Mikocki et al. (5)) has scaling behaviour below 1 TeV but at higher energies the

scaling is mildly violated in the fragmentation region and significantly violated in the central region. The hadron-air interaction cross section and the multiplicity of pions and kaons increase with energy but the inelasticity distribution (1/2 for nucleons and 2/3 for mesons) and the transverse momentum distribution (325 MeV/c for pions and 371 MeV/c for kaons) are independent of energy.

Discussion:

The present measurements of energy spectra and radial distributions of muons do not provide any evidence for heavy primaries (in the primary energy range 2.2 $X10^{14}$ - 4.8 $X10^{15}$ eV). The hadronic interaction characteristics assumed in the above mentioned model are found to be consistent with the measured data upto the fixed shower size of 10^5 particles. Using the same hadronic interaction characteristics the shape of the muon density distribution in primary iron initiated EAS is similar to that for proton initiated shower with the same primary energy but the magnitude of the distribution is higher for low energy muons in the vicinity of the EAS core (0 to 100 meter). The present experiment does not find such features in the observed muon data. The measured electron lateral distribution is in good agreement with the calculated distribution but the measured muon lateral distribution is much broader than the calculated. The same feature can be seen in the density ratio distribution (fig.6) which also shows that both the measured and calculated ratio exceeds unity beyond the distance of 100 meter from the core.

References:

1. Basak D.K. et al.
   Nucl. Inst. Methods Phys. Res., 227, (1984), 167.
2. Aliev N. et al.
   19th ICRC (La Jolla, 1985), 7, 191
3. Trzupek A. et al.
   23rd ICRC (Calgary, 1993), 4, 359
4. Poirier J., Gress J. and Mikocki S.
   21st ICRC (Adelaide, 1990), 9, 126
5. Mikocki S. et al., J. of Phys. G 13 (1987), L85

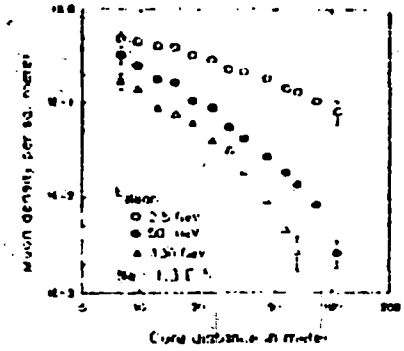

Fig. 1 Muon lateral distribution.

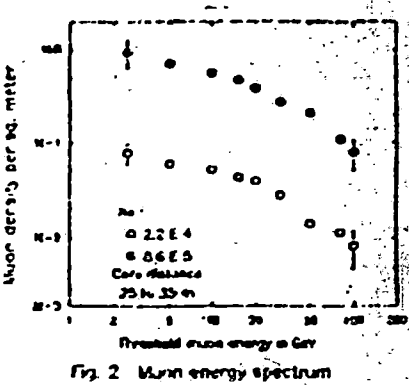

Fig. 2 Muon energy spectrum

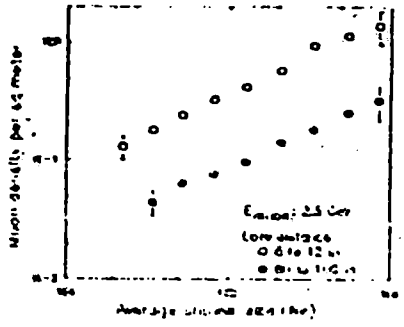

Fig. 3 Muon density and its distribution

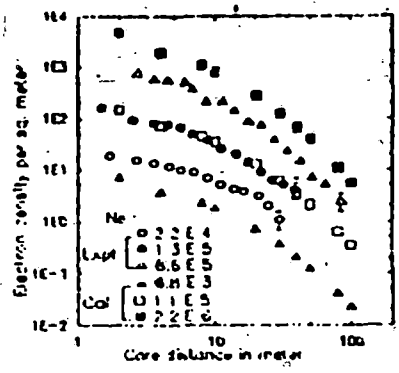

Fig. 4 Electron lateral distribution

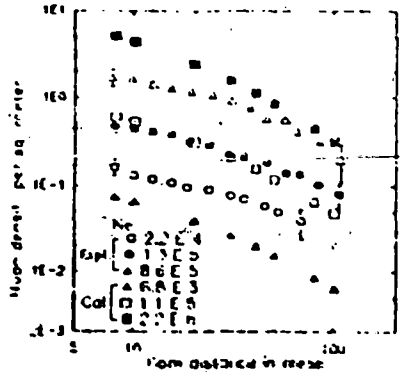

Fig. 5 Muon lateral distribution

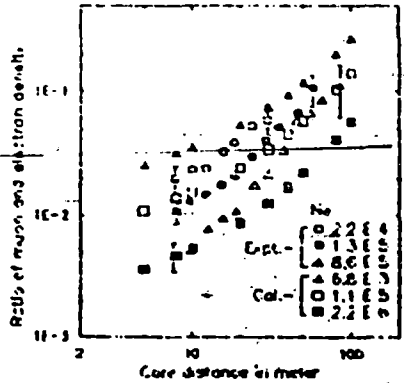

Fig. 6 Density ratio distribution

A SEARCH FOR ANISOTROPY IN THE ARRIVAL DIRECTION OF EAS BY COSMIC RAYS FROM DISCRETE SOURCES

C. Chakrabarti, D. Chanda, G. Saha, A. Mukherjee, A. Bhadra, S. Sanyal, R. Chettri, S. K. Sarkar, B. Ghosh and N. Chaudhuri

High Energy & Cosmic Ray Centre
North Bengal University (NBU)
Darjeeling 734430, INDIA

ABSTRACT

The NBU Cosmic Ray Telescope consisting of an EAS array of scintillation detectors and two magnet spectrographs has been operated in a search for any anisotropy in the directions of arrival of EAS events. The shower arrival directions are determined by fitting the measured shower particle arrival times. Initial results on distribution of events in declination and right ascension are given.

Introduction : A cosmic ray air shower telescope has been installed at a new location (latitude $26^{\circ}42'$ N, longitude $88^{\circ}21'$ E) to look for any anisotropy in the directional intensity of primary cosmic rays in the energy range 10^{14}-10^{16} eV. The set up consisting of plastic scintillation detectors for electrons, two shielded magnet spectrographs for muons and eight fast timing scintillation detectors for shower particles arrival time measurements has been in operation for some time now. Preliminary results from the measurements of shower arrival directions are presented in this report.

Method of analysis : Some 13 thousands EAS events have been registered by the EAS array so far. For each event the shower parameters : the shower size (N_e), the shower age (S) and the shower core location (X_o, Y_o) have been determined using a fitting function to fit the measured electron density data by an iterative procedure for minimizing chisquare using gradient search method. The analysis on a selected group of showers in the size range $10^{4.5}$-$10^{6.2}$ has led to

the following error estimates:
(i) core location error is within ± 1 m,
(ii) shower size error is ± 0.1 N_e,
(iii) age parameter error is within ± 0.06.

The arrival direction of the shower is determined fron the measured relative arrival time delay data by minimizing the quantity,

$$\chi^2 = W_i [lx_i + my_i + nz_i + c(t_i - t_o)]^2,$$

where t_i is the actual time measured by the ith detector, W_i is the statistical weight factor, c is the velocity of the EAS front which passes through the origin at t_o and l, m, n are the direction cosines of arrival.

From the best fitted values of direction cosines the direction of arrival of each EAS event has been determined in local coordinate system (zenith angle, azimuth angle). Finally the EAS arrival direction angles are transformed into right ascension (α) and declination (δ). The resolution of the EAS array has been determined by the divided array method using those events in which all the timing detectors yielded information about the arrival time of the EAS front. The systematic and statistical uncertainties in the measurement of arrival direction have been determined and taken into account in the analysis. The estimated resolutions are 1.1° in declination and 1.6° in right ascension.

Results :- Preliminary results from a small sample of shower arrival time data are given. The measured data on resolution of the EAS array are given in figures 1 and 2. The distribution of all the EAS events in declination (δ) is given in figure 3. The observed declination range is within -40° and $+88^\circ$ with a peak at 32°-34° bin. Similar declination distribution of Mitsuishi EAS data (Fujita et al., 1993) showed a peak within 30°-40°. The right ascension (α)-distribution is shown in figure 4. This distribution in right ascension has not been corrected for any effect arising out of occasional discontinuities in running time.

Reference :
Fujita K. et al, Proc. 23rd ICRC, Calgary, 1(1993)376

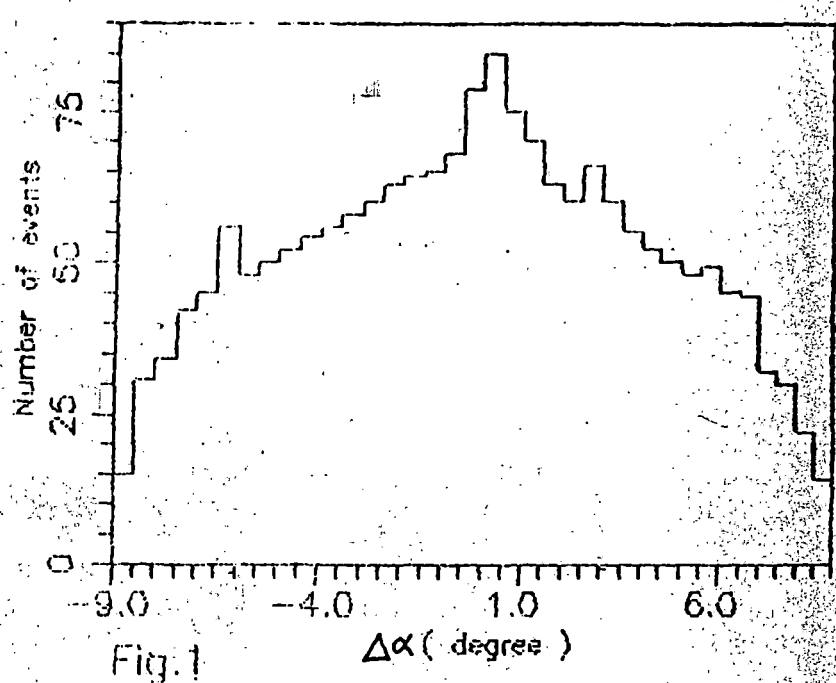
Number of events
0
25
50
75
-9.0
-4.0
1.0
6.0
Δα (degree)

Fig.1

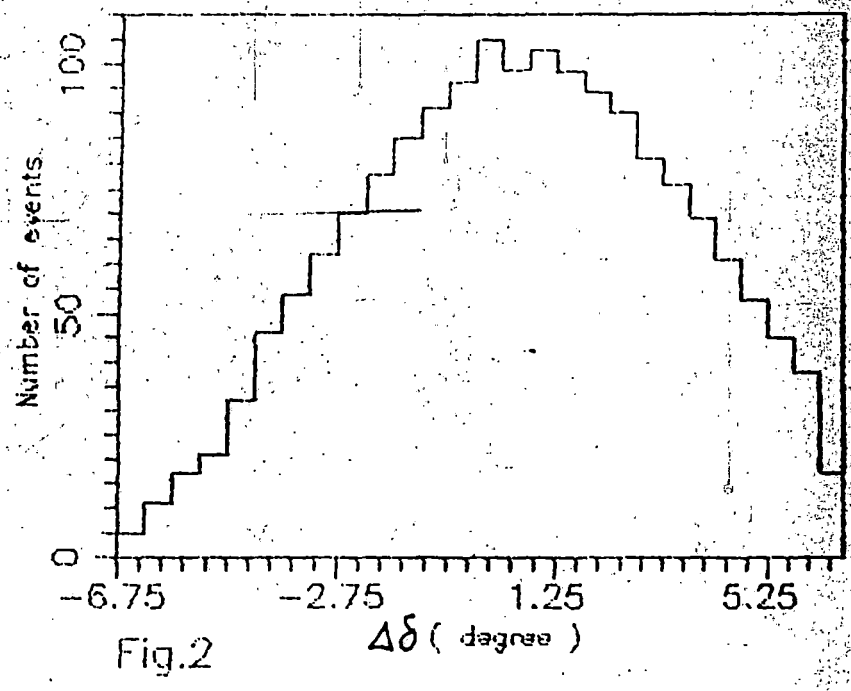
Number of events
0
50
100
-6.75
-2.75
1.25
5.25
Δδ (degree)

Fig.2

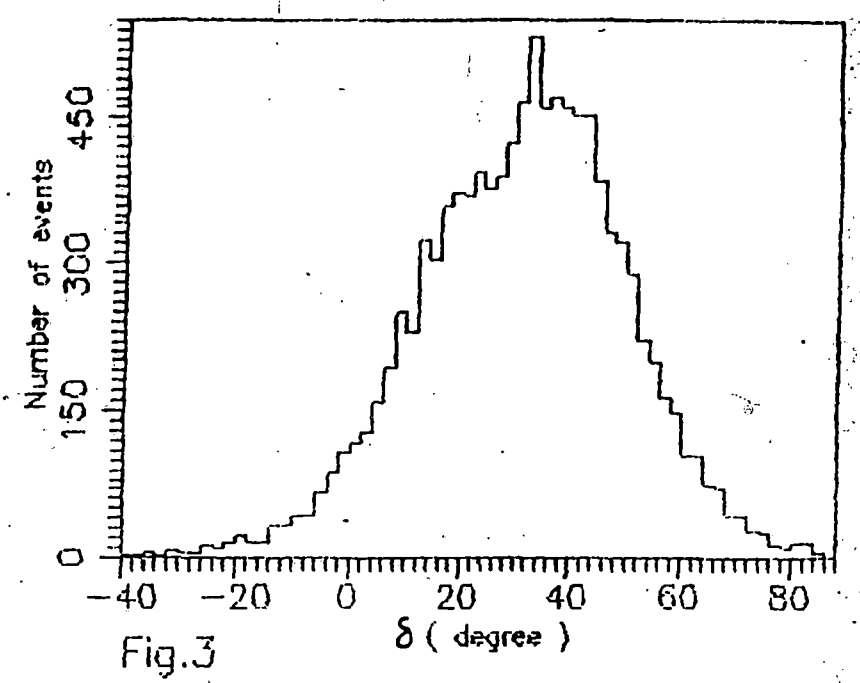
Number of events
0
150
300
450
−40
−20
0
20
40
60
80
δ (degree)

Fig.3

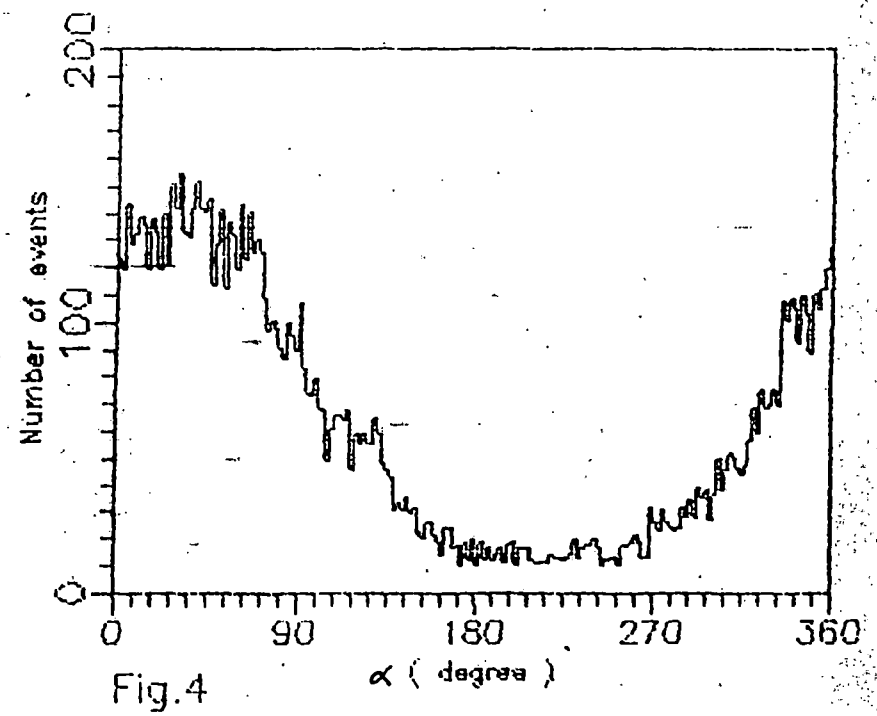
Number of events
0
100
200
0
90
180
270
360
α (degree)

Fig.4

An experimental study of Primary Cosmic Rays at the knee energy region by observation of Extensive Air Showers (EAS)

G. Saha , A. Bhadra , C. Chakrabarti , S.K. Sarkar and N. Chaudhuri

High Energy and Cosmic Ray Centre , North Bengal University , Darjeeling 734430 , India

Abstract

The simultaneous measurements have been made of the radial (lateral) electron density distribution and the radial muon density distribution at various measured muon energies in the range 2.5-100 GeV in vertically incident EAS in the size range 3.15×10^4-1.79×10^6 (primary energy range 2.4×10^{14} - 8.3×10^{15} eV) particles detected near sea-level. The characteristics of these radial distributions in terms of the measured shower parameters have been determined and used to draw conclusion about the average nuclear mass of the primaries of these EAS.

1. Introduction

It is well established that the Primary Cosmic Ray energy spectrum steepens in the energy range 10^{14} - 10^{16} eV known as the knee energy region .The spectrum steepening is thought to be due to mechanisms related to acceleration and propagation of Primary Cosmic Rays (PCR) .An Extensive Air Shower experiment at primary energy in the knee energy region in which the energy spectrum and lateral distribution of muons can be measured accurately over a wide range can indicate the trend of average behaviour of PCR mass at the knee region . In an EAS of size (N_e) 10^4 - 10^6 particles at sea - level total number of muons and muon lateral distribution ,if the primary is a heavy nucleus , will be different from those in a primary proton initiated shower and the difference can be detected from the data of a properly set-up experiment . In the present paper the results of an air shower experiment covering the knee energy region will be described . This experiment with the provision for differential measurement of both low and high energy muons simultaneously by two shielded magnet spectrographs has yielded both muon energy spectrum and radial density distributions at various muon energies. The properties of these distributions have been analysed to infer the trend of average PCR mass composition at the knee region.

2. North Bengal University (N.B.U) air shower experiment

The North Bengal University EAS array for observation of air showers has been developed in stages since 1980 (Basak et al [1]). The set-up has been designed to detect small and medium size air showers with a close -packed array (of spacing 8m) using an array of 35 scintillation detectors each of size 50 cm x 50 cm, two shielded muon magnet spectrographs (with a spacing of 4m, maximum

detectable momentum (MDM) 500 GeV c^{-1}, each of area 1m x 1m and cut off at an energy of 2.5 GeV) and a nuon flash tube (NFT) chamber as a low energy muon detector. Two spectrographs each with a lever arm of 6.3m were set up pointing to the zenith to collect muons above 2.5 GeV in incident vertical air showers. With such a close-packed array , the determination of shower size and other shower parameters has been more precise.

2·1. EAS detector array characteristics

The array of 35 close-packed plastic scintillation detectors (Fig.1) has been operating at a site of atmospheric depth ~ 1000 gcm^{-2} at the N.B.U campus. The response measured in terms of the relative light output of plastic scintillator (manufactured by Bhabha Atomic Research Centre, India) for incident EAS electrons is ~ 100% and the relative efficiency in terms of single particle pulse height is nearly uniform from centre to edge of each plastic scintillation detector. The pulses from all the 35 scintillation detectors are digitized by an analog to digital converter one after the other and connected to the memory unit for storing the digital information and subsequent transfer to the printer for printing on a paper tape. The printed outputs give the information about the particle densities on each detector in an individual shower.

The efficiency of detecting showers of different N_e and age(s) within the sensitive detecting area of ~1200 m^2 and the average triggering probability of the array for showers falling within 15^0 of the zenith are shown in figs. 2,3,4,5 and 6.

Two magnetic spectrographs and the NFT chamber were operated under an EAS trigger which was also used for the photographic recording of muon trajectories within a track location uncertainty of ± 0.14 cm.

The selection criteria for shower detection consists of the following steps:

(1) Shower is recorded by the detecting system if the registered electron density in any four adjacent detectors of the 8 central triggering detectors is greater than 4 particles/m^2 .

(2) The electron densities at 19 points are registered simultaneously with the phptographic recording of the trajectories of muons by the two spectrographs at four points in individual shower.

(3) For each recorded shower ,the core location , the shower size and the photon electron cascade age (s) of the EAS are determined by fitting the registered electron densities with the following formula for the electron density $\Delta(r)$

$$\Delta(r) = N_e/r_1^2[\, f(r/r_1,s)\,] \qquad \ldots\ldots\ldots\ldots\ldots\ldots \quad (1)$$

where $f(r/r_1, s) = c(s)\,(r/r_1)^{a1+a2(s-1)}\,(1+r/r_1)^{b1+b2(s-1)}$

c(s) is the normalisation constant , r_1= 24 m (Moliere unit of displacement at sea-level) and a1,a2,b1,b2 are constants . Some examples of average radial electron density distributions at N_e= 1.09×10^5 - 1.79×10^6 particles together with the graphs of fitting function are shown in Fig.7. The shower size recorded by the array is 3.15×10^4 - 1.79×10^6 particles .

3. Analysis and error estimation .

A standard χ^2 - minimization procedure based on the method of steepest descent has been used to determine the air shower parameters and to simulate the errors in the air shower parameters.

The errors in the determination of EAS parameters have been evaluated through the standard procedure of artificial shower analysis. A shower of known parameters is allowed to be incident at any point on the array selected at random and particle density in each detector is calculated according to the chosen lateral distribution function. To reproduce the experimental conditions, the statistical fluctuations in the number of particles in each detector and the systemetic errors in the conversion of pulse height into particle density are superposed on each density.For a set of densities for each shower,χ^2 - minimization procedure is applied to estimate the shower parameters . The estimated shower parameters give the deviations from the actual ones used for an artificial shower and lead to the following error estimates :

(1) ΔX = 2.40m
ΔY = 2.77m

(2) $\Delta N_e/N_e$ = 9.61%

(3) ΔS = .13

Some histograms for the deviations of the parameters are shown in Fig. 8.

4. Results on ' near vertical showers'

4·1. Determination of shower age (s) and energy of the shower.

Using all the registered electron densities in a shower event the best fitted value of the shower age(s) was determined by the method of least square. For each shower of fixed size and age (s)

the mean energy of the primary particle (proton) was obtained with a maximum error of 10% (which includes fluctuation in EAS development and the error in shower size measurement) from the energy scale established on the basis of hybrid Monte Carlo model (Trzupek et al [2]) for EAS at sea-level as given by

$$E_0\,(eV) = 3.03 \times 10^{10} \times N_e^{0.87} \quad \ldots\ldots (2)$$

4·2. Measurement of muon density

The average muon density in a shower as a function of the radial distance from the shower core was estimated for each of the various shower groups in the shower size range 3.15×10^4 - 1.79×10^6 particles using the average density defined as

$$\rho_\mu(\geq E_\mu, N_e(s), r) = N_\mu(\geq E_\mu, N_e(s), r) \,/\, N_f(N_e(s), r)\, A' \quad \ldots\ldots (3)$$

Where $N_\mu(\geq E_\mu, N_e(s), r)$ is the total number of muons recorded in a particular distance r for a particular shower size N_e in a certain period of time above a threshold energy ($\geq E_\mu$), $N_f(N_e(s), r)$ represents the total number of showers of size $N_e(s)$ at the same distance interval recorded at the same time and A' is the effective area of the muon detectors .

In a particular shower size group the muons are divided into groups on the basis of specified threshold energies (indicated as $\geq E_\mu$) and then each group is distributed into a number of bins in respect of radial distances from the shower core to determine the average muon density as a function of radial distance and threshold energy.

Some results on muon energy spectra and lateral distributions are given in Figs. 9 and 10 .

4·3. The dependence of muon density on shower size and radial distance

The variation of muon density at fixed radial distances has been studied as a function of shower size at various muon threshold energies by assuming a dependence of the form given by

$$\rho_\mu(\geq E_\mu, r) \sim N_e^{\beta(E_\mu, r)} \quad \ldots\ldots (4)$$

The fit to the observed data has yielded the results shown in Figs. 11,12 and 13.It is seen that at a fixed muon threshold energy β decreases slowly with radial distance for all shower sizes in the range 3.15×10^4 - 1.79×10^6 particles and the trend of variation of β with radial distance is similar for all muon threshold energies . All these results together seem to indicate that the muon distribution function does not change with primary energy .The values of the exponent (β) obtained by fitting the observed data are given in table 1.

Table 1. Values of the exponent β at different distance ranges for various muon energies

Muon Energy (GeV)	Value of β (for r=8-12m)	Value of β (for r=30-40m)
2.5	0.692±0.009	0.653±0.012
10	0.699±0.010	0.655±0.013
50	0.661±0.011	0.587±0.021

The measured lateral distribution of muons in showers of various sizes are fitted to a relation of the form

$$\rho_\mu (>E_\mu, r, N_e) \sim r^{-\alpha(>E\mu)} \quad \text{..... (5)}$$

A plot of this function for $N_e = 4.48 \times 10^5$ and $E_\mu \geq 2.5$ GeV is shown in fig. 14 as an example . The value of α derived from this plot is 0.647 . From fig.14. it is seen that except for the last radial bin (r=34.1m) the shower cores were inside the edges of the array where the efficiency of the array is large. For the last radial bin , which is also close to the array boundary , obviously the error of r and N_e are comparetively large but the overall effect of these errors on determination of α is small .The least - square fitted line obtained from the plot of log ρ_μ vs. log r at fixed N_e and E_μ gives the value of a . The mean values of α with r.m.s errors are given in table 2.

Values of α from the fit of the data for $E_\mu \geq 2.5$ GeV are shown as a function of N_e in Fig. 15. The trend of α vs E_o curve shows that α is a function of energy upto 4.6×10^{15} eV and becomes constant at higher energies. The lateral muon density distribution in a shower initiated by a heavy primary is flatter compared to the corresponding one initiated by a lighter primary at the same energy . In other wards for a lighter primary composition it is expected to have steeper muon lateral distribution and hence a large value of α .Therefore the variation of α with E_o as shown in fig.15 possibly indicates that the effective primary mass is decreasing with energy increasing from 4.3×10^{14} eV to around 4.6×10^{15}eV

Table 2. Values of the exponent α for various shower sizes at muon threshold energy ($\geq E_\mu$) 2.5 GeV

Shower size	$\alpha \pm d\alpha$
5.97×10^4	0.553±0.009
1.09×10^5	0.578±0.010
2.21×10^5	0.606±0.012
4.48×10^5	0.647±0.014
9.02×10^5	0.661±0.016
1.79×10^6	0.662±0.016

5. Discussion

The method used in the present analysis consists of examining the accurately measured muon densities as a function of shower size and the muon lateral distribution (for various muon threshold energies) as a function of shower size .The analysis also includes the results of an estimation of errors to the EAS parameters . The primary energy of an EAS event is not possible to be determined precisely from the observed particle density distribution due to the presence of fluctuations in an EAS development .However the mean primary energy range (2.4×10^{14}-8.3×10^{15} eV) concerned in the present experiment was determined by comparing the observed vertical shower size with the results of hybrid Monte Carlo model for proton primary at sea-level covering this primary energy range. Some representative examples of measured muon energy spectra and radial distributions are presented in Figs. 9 and 10 to show that these provide a firm experimental base for comparing with different models of EAS. An analysis of these results given in section 4.3 leads to the following conclusion :

The radial muon density distribution at low and high muon energies does not change with the primary energy

For low energy muons radial muon density distribution steepens in the primary energy range 4.3×10^{14} - 4.6×10^{15} eV with radial distance (r) indicating that the effective primary mass decreasing between 4.3×10^{14} - 4.6×10^{15} eV.

Y.Kawamura et al [3] and M.Ichimura et al [4] have derived similar conclusion about primary mass in the knee energy region from direct observations from their new emulsion chamber experiments . From an analysis of low energy EAS muons Blake et al [5] reported similar trend for average primary mass in the primary energy region 6.0×10^{14} , - 5×10^{15} eV.

This work is being continued to improve statistics on this aspect of study using muon lateral distributions at different energies of muons in EAS. The existing array is being expanded to operate at larger shower sizes so that the present method of analysis can be applied under better accuracies on the determination of EAS parameters.

Reference

(1) Basak, D.K.,Chakraborti N.,Ghosh B.,Goswami G.C. and Chaudhuri N. (1984). Nucl.Instrum.Methods 227,167

(2) Trzupek A.,Lu Y. and Poirier J. (1993), 23rd ICRC , Calgary , Vol.4, p. 359

(3) Kawamura Y. et al (1989) . Phy.Rev. D40,729

(4) Ichimura M. et al (1992) , ICRR Report 287, 92-95

(5) Blake P.R and Tummey S.P. (1993), 23rd ICRC ,Calgary,Vol.4, p.363

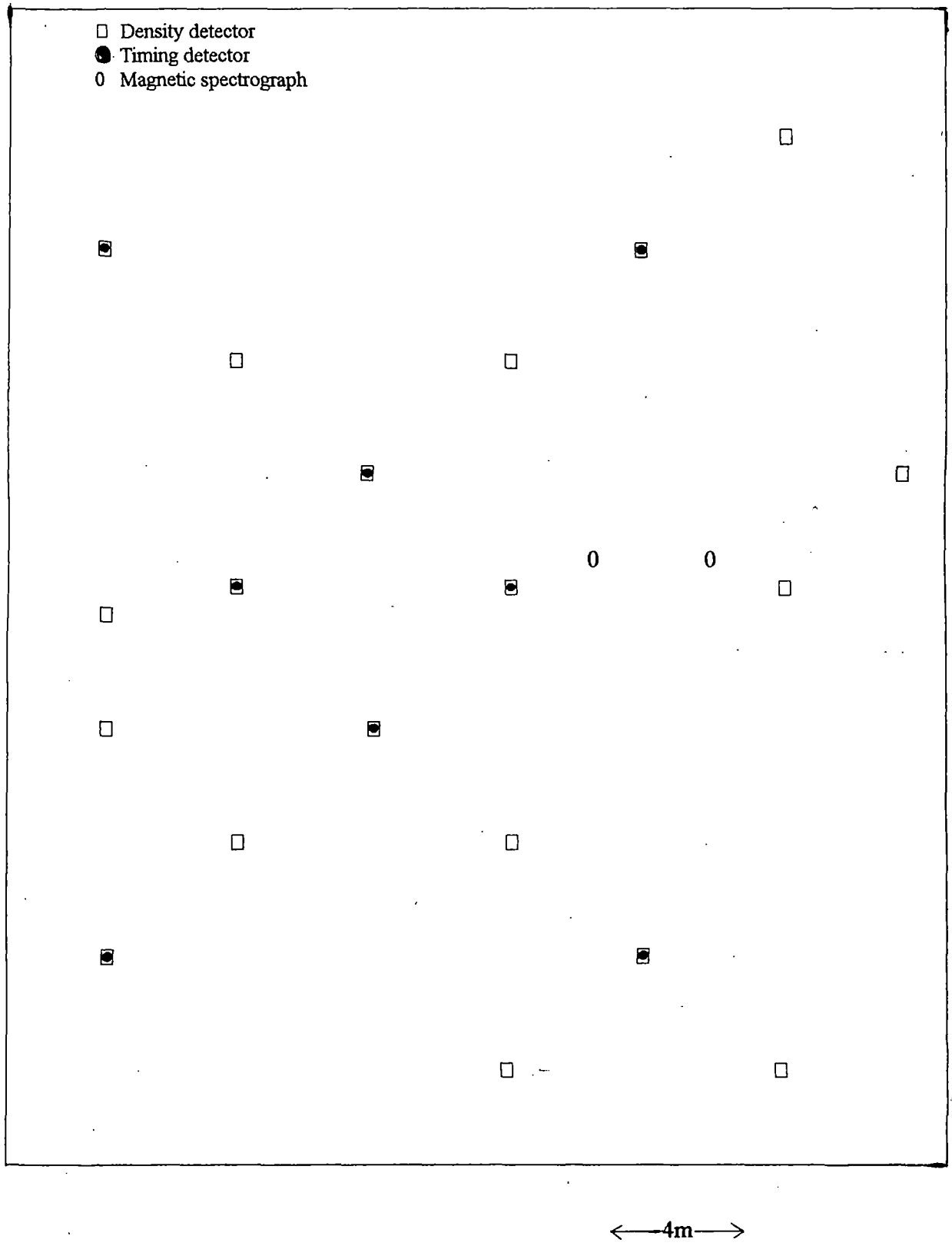

Fig. 1. The NBU EAS array

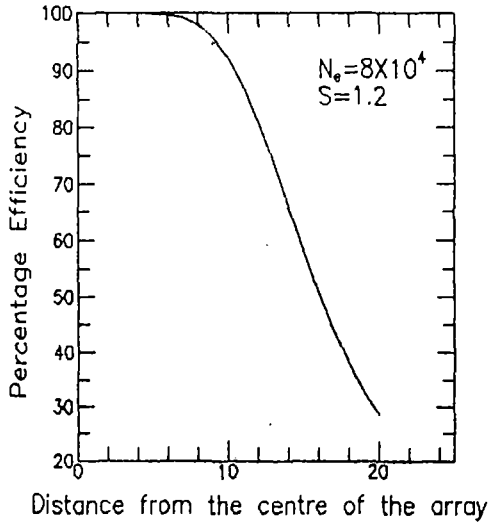

Fig.2

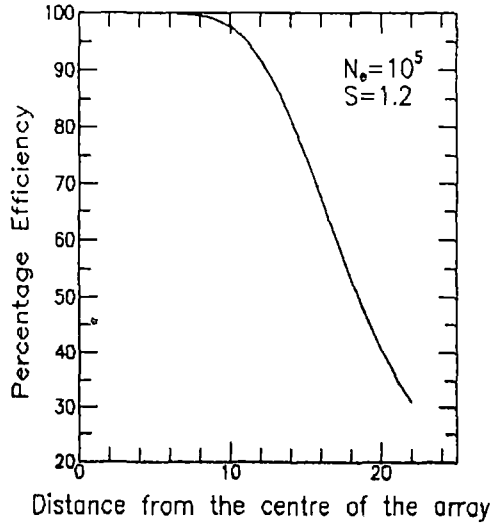

Fig.3

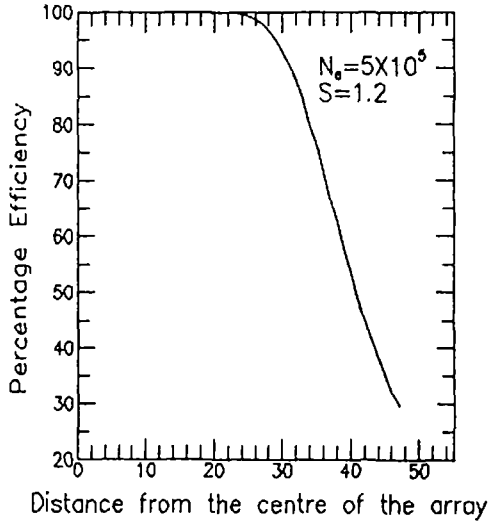

Fig.4

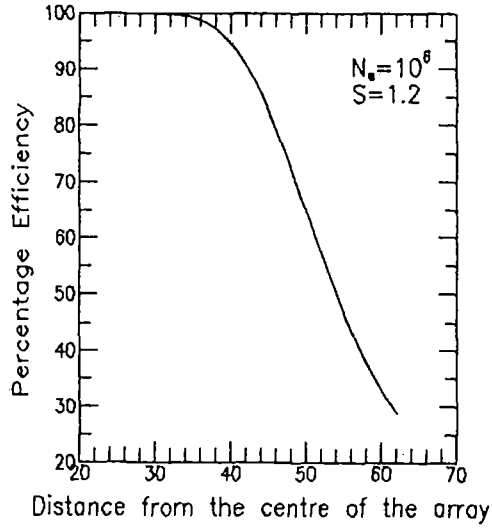

Fig.5

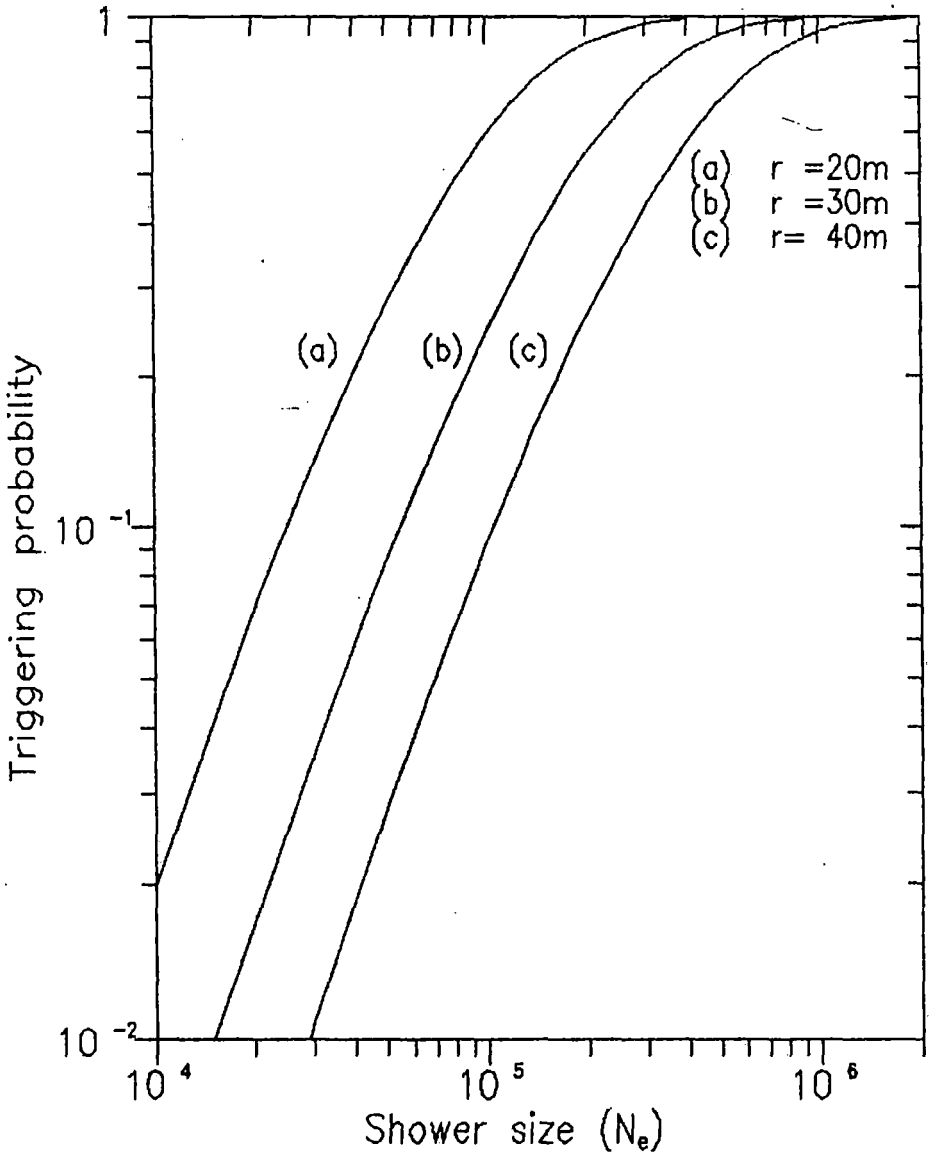
1
10^{-1}
10^{-2}
Triggering probability
10^{4}
10^{5}
10^{6}
Shower size (N_e)
(a) r =20m
(b) r =30m
(c) r= 40m
(a)
(b)
(c)

Fig.6

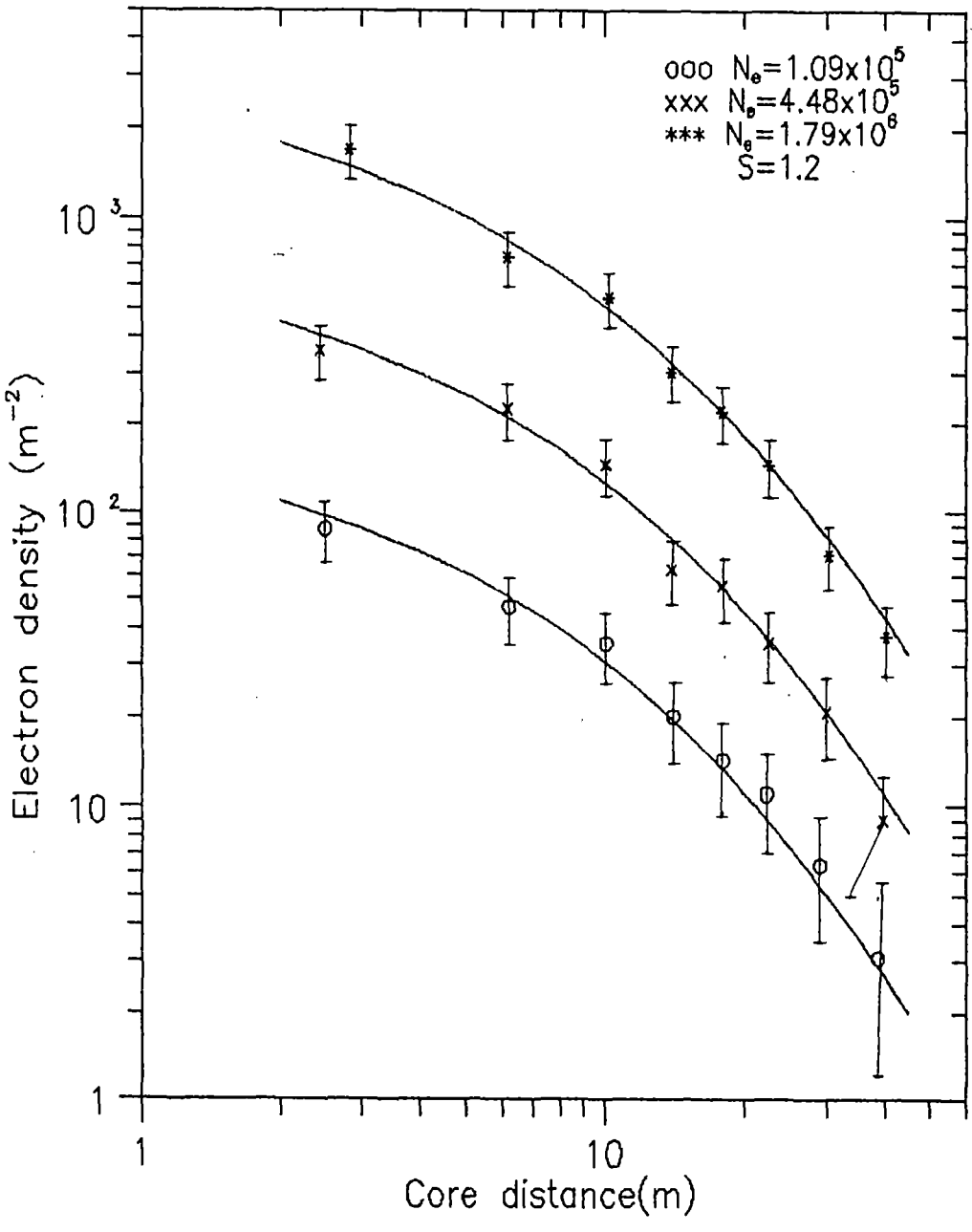
ooo N_e=1.09x10^5
xxx N_e=4.48x10^5
*** N_e=1.79x10^6
S=1.2
Electron density (m^{-2})
10^3
10^2
10
1
1
10
Core distance(m)

Fig.7

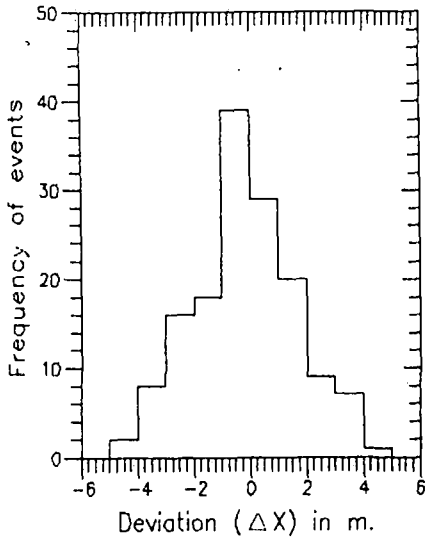
Frequency of events
Deviation (△X) in m.

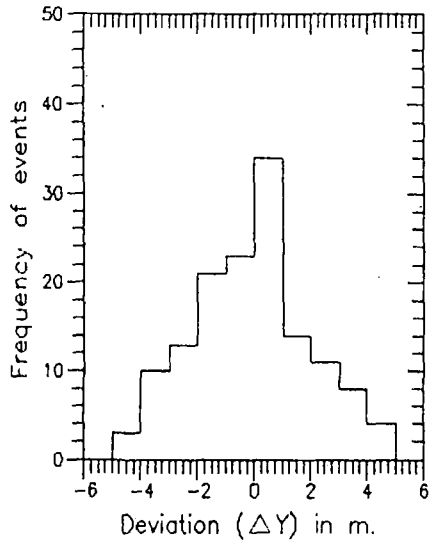
Frequency of events
Deviation (△Y) in m.

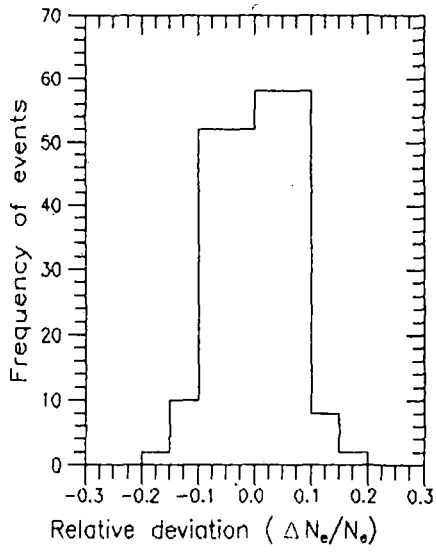
Frequency of events
Relative deviation (△Ne/Ne)

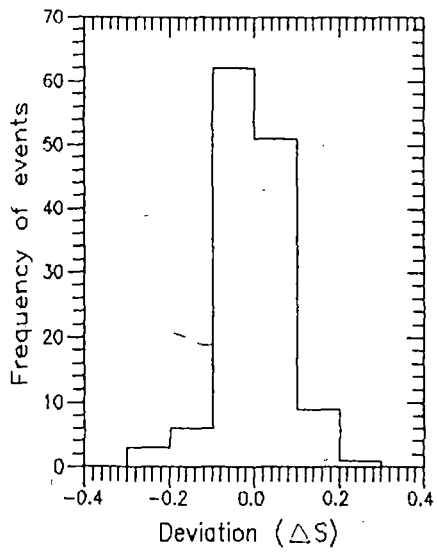
Frequency of events
Deviation (△S)

Fig.8

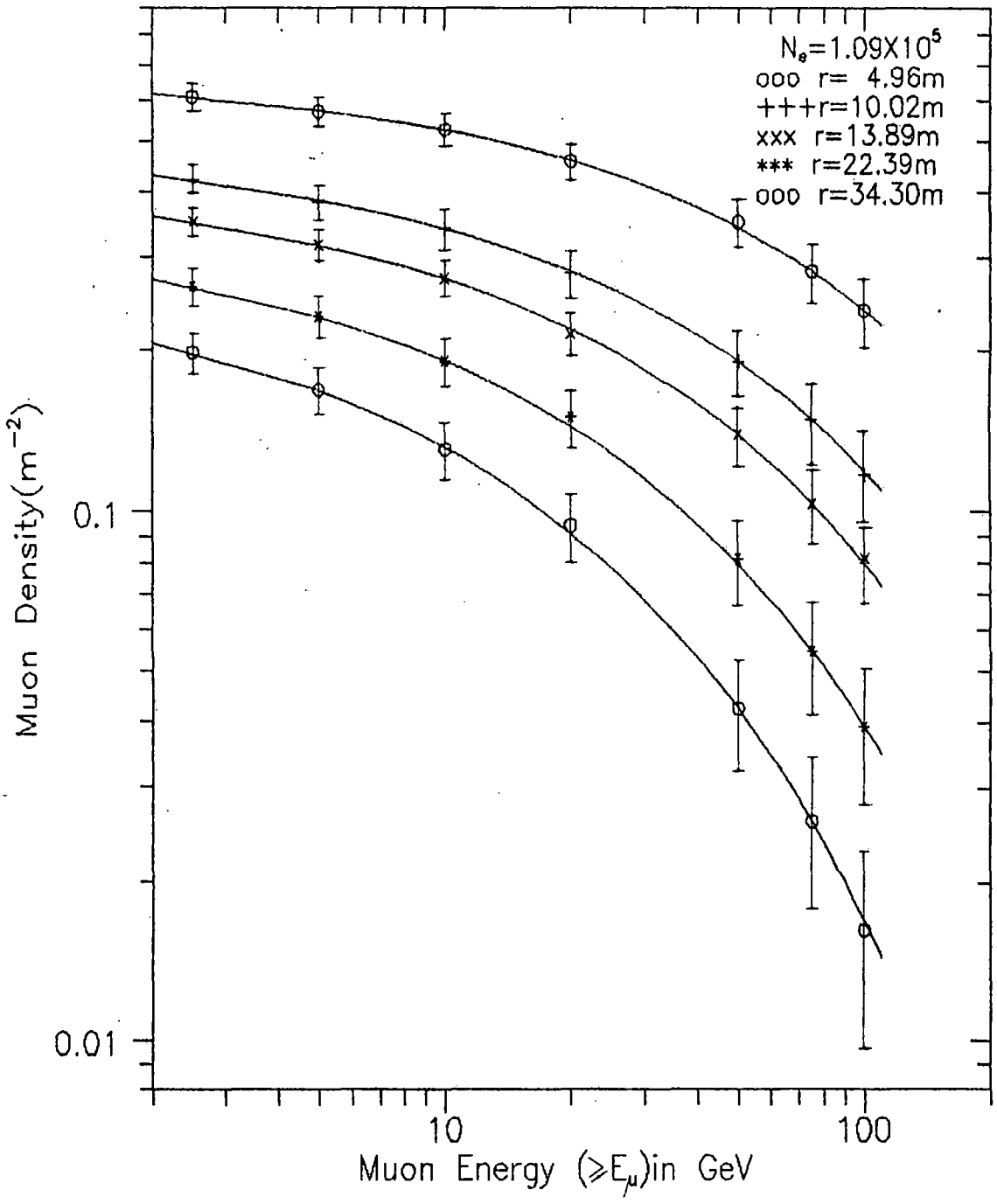
N_e=1.09X10^5
ooo r= 4.96m
+++r=10.02m
xxx r=13.89m
*** r=22.39m
ooo r=34.30m
Muon Density(m^{-2})
0.1
0.01
10
100
Muon Energy ($\geq E_\mu$)in GeV

Fig.9

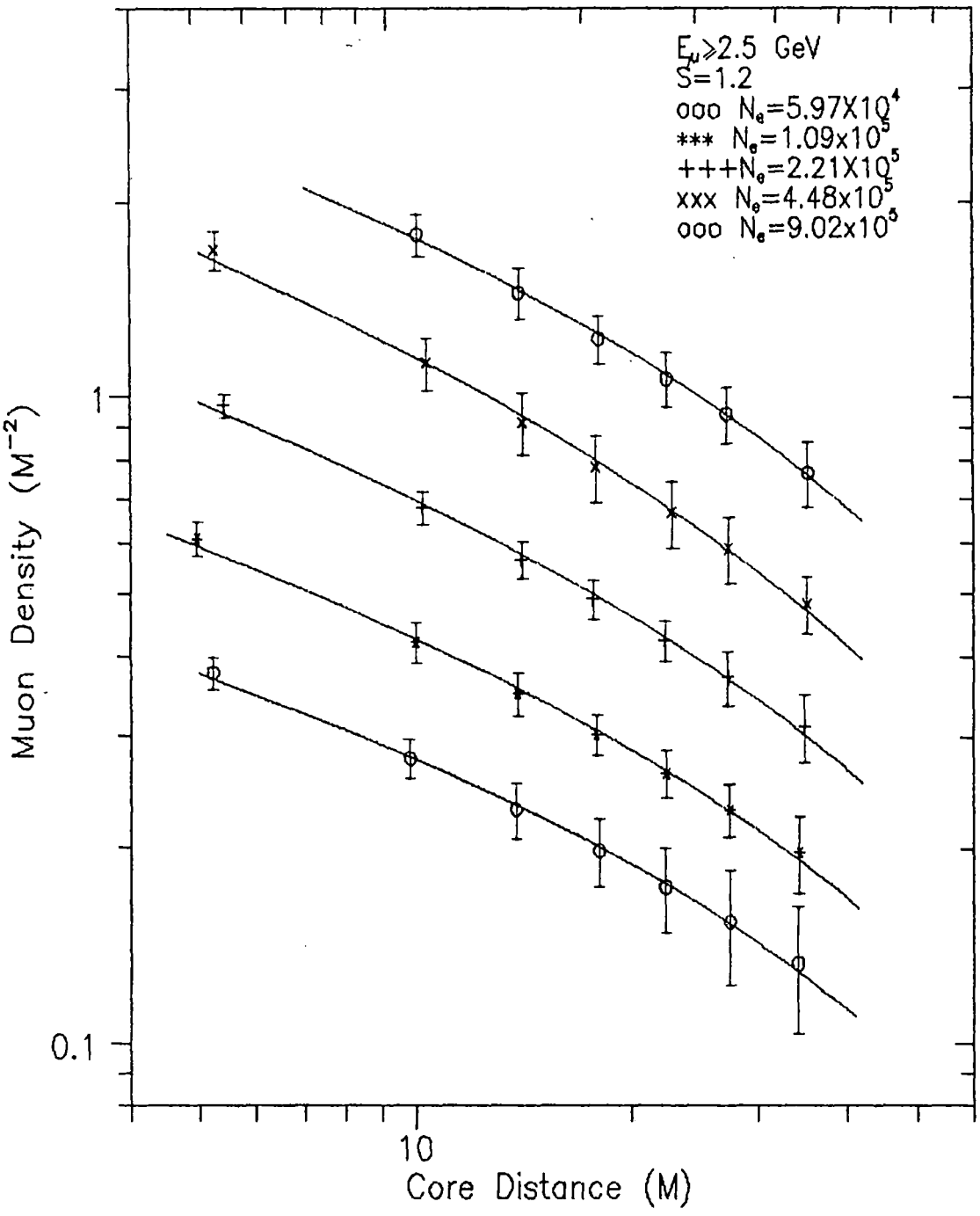
$E_\mu \geq 2.5$ GeV
S=1.2
ooo N_e=5.97X10^4
*** N_e=1.09x10^5
+++N_e=2.21X10^5
xxx N_e=4.48x10^5
ooo N_e=9.02x10^5
Muon Density (M^{-2})
1
0.1
10
Core Distance (M)

Fig.10

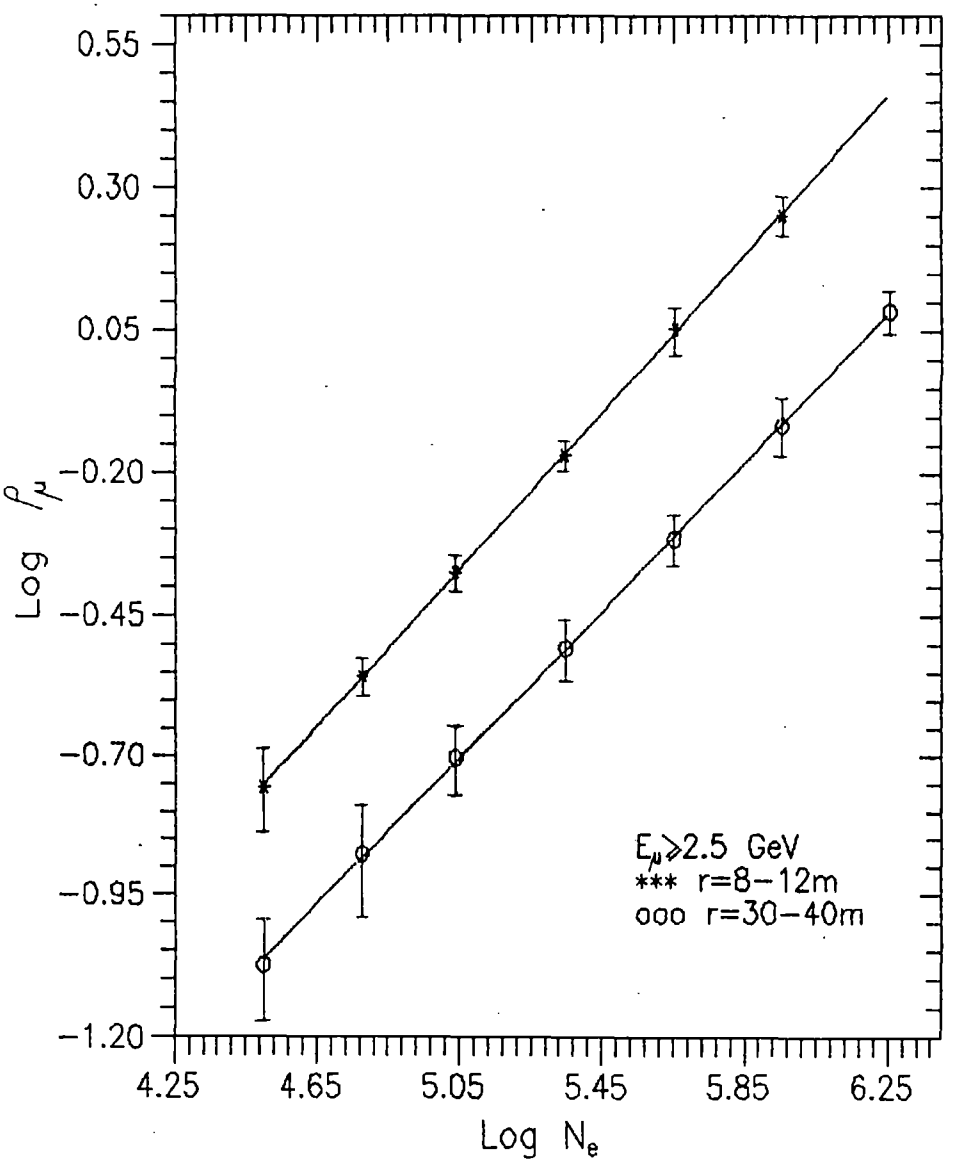
0.55
0.30
0.05
−0.20
−0.45
−0.70
−0.95
−1.20
Log ρ_μ
4.25
4.65
5.05
5.45
5.85
6.25
Log N_e
$E_\mu \geq 2.5$ GeV
*** r=8−12m
ooo r=30−40m

Fig.11

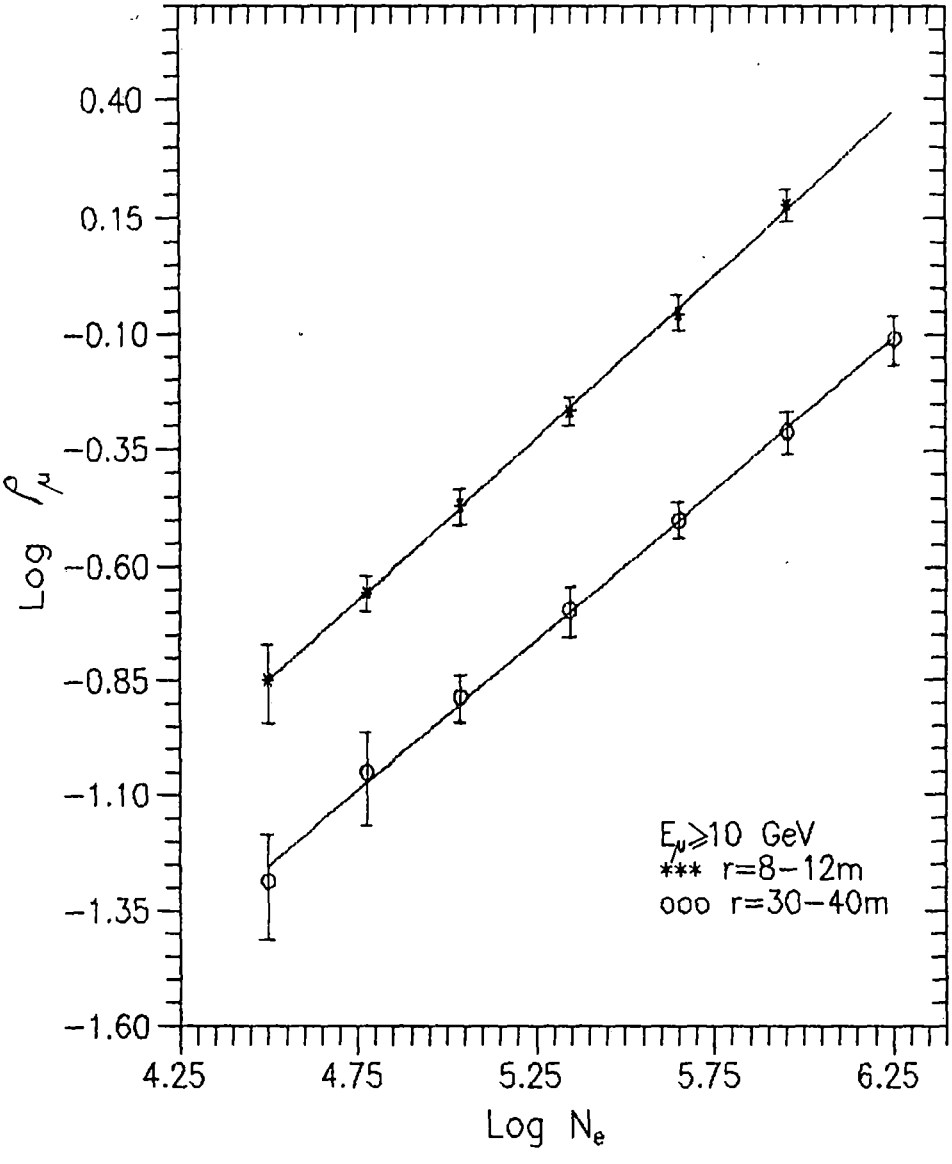
0.40
0.15
−0.10
−0.35
−0.60
−0.85
−1.10
−1.35
−1.60
Log ρ_μ
4.25
4.75
5.25
5.75
6.25
Log N_e
$E_\mu \geq 10$ GeV
*** r=8−12m
ooo r=30−40m

Fig.12

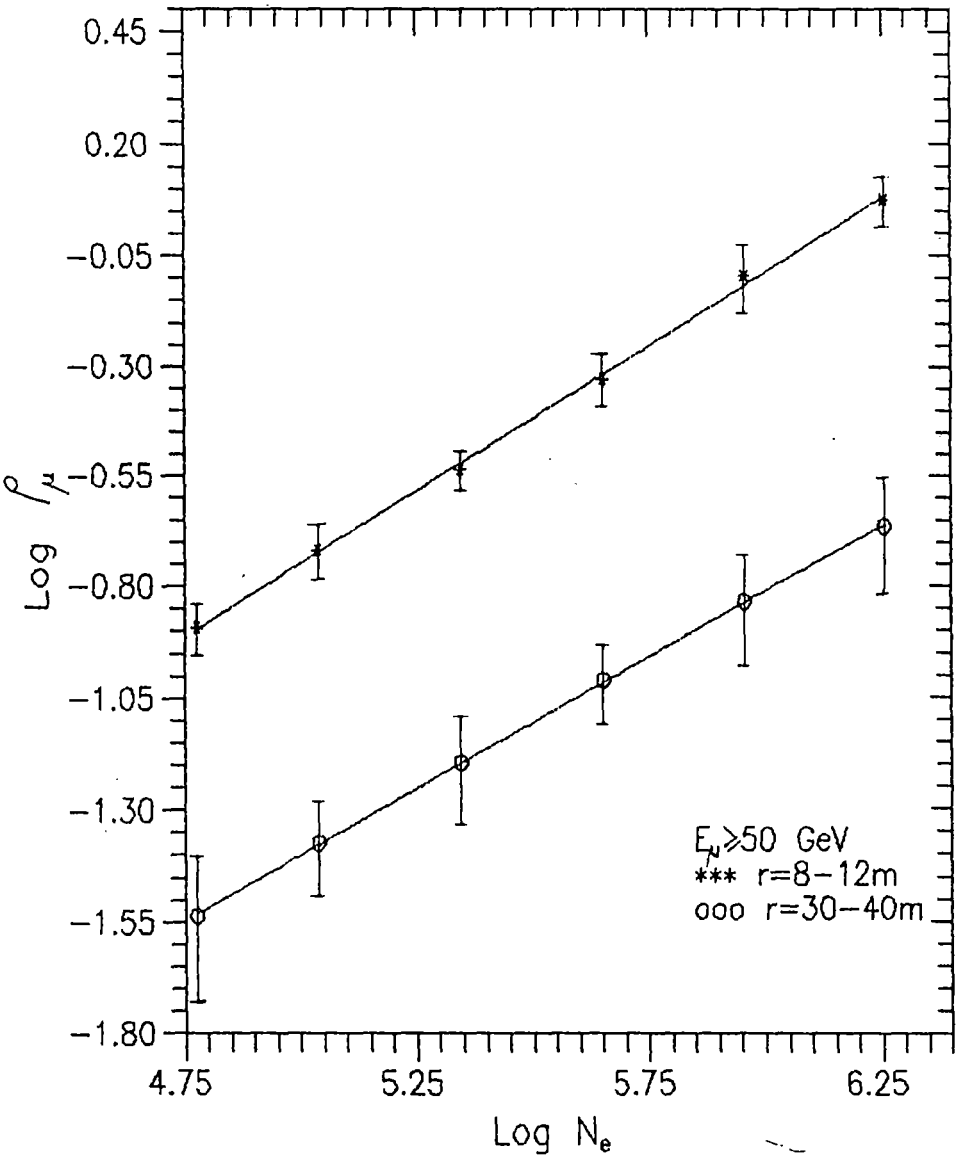
0.45
0.20
−0.05
−0.30
−0.55
−0.80
−1.05
−1.30
−1.55
−1.80
Log ρ_μ
4.75
5.25
5.75
6.25
Log N_e
$E_\mu \geqslant 50$ GeV
*** r=8−12m
ooo r=30−40m

Fig.13

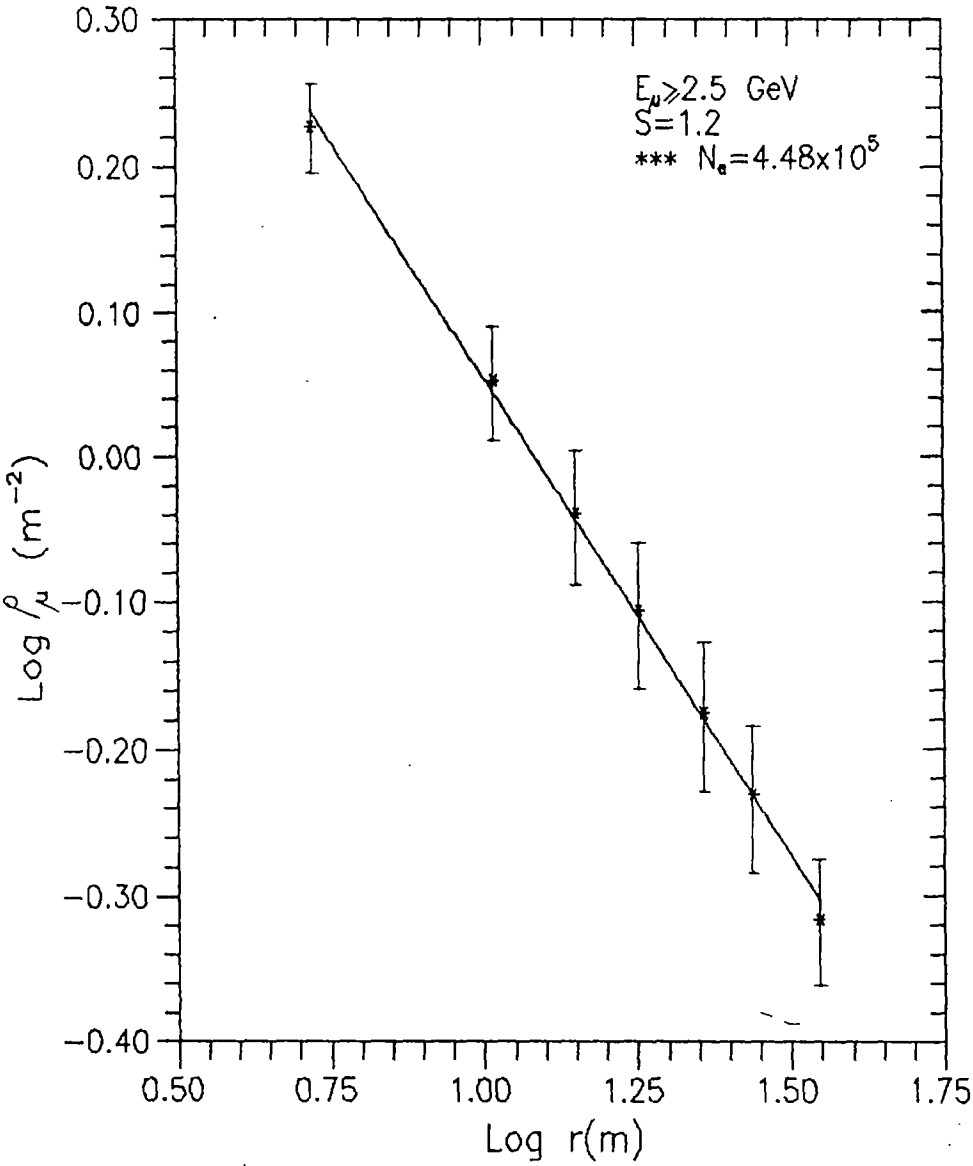
$E_\mu \geq 2.5$ GeV
S=1.2
*** $N_e = 4.48 \times 10^5$
0.30
0.20
0.10
0.00
−0.10
−0.20
−0.30
−0.40
Log ρ_μ (m^{-2})
0.50
0.75
1.00
1.25
1.50
1.75
Log r(m)

Fig.14

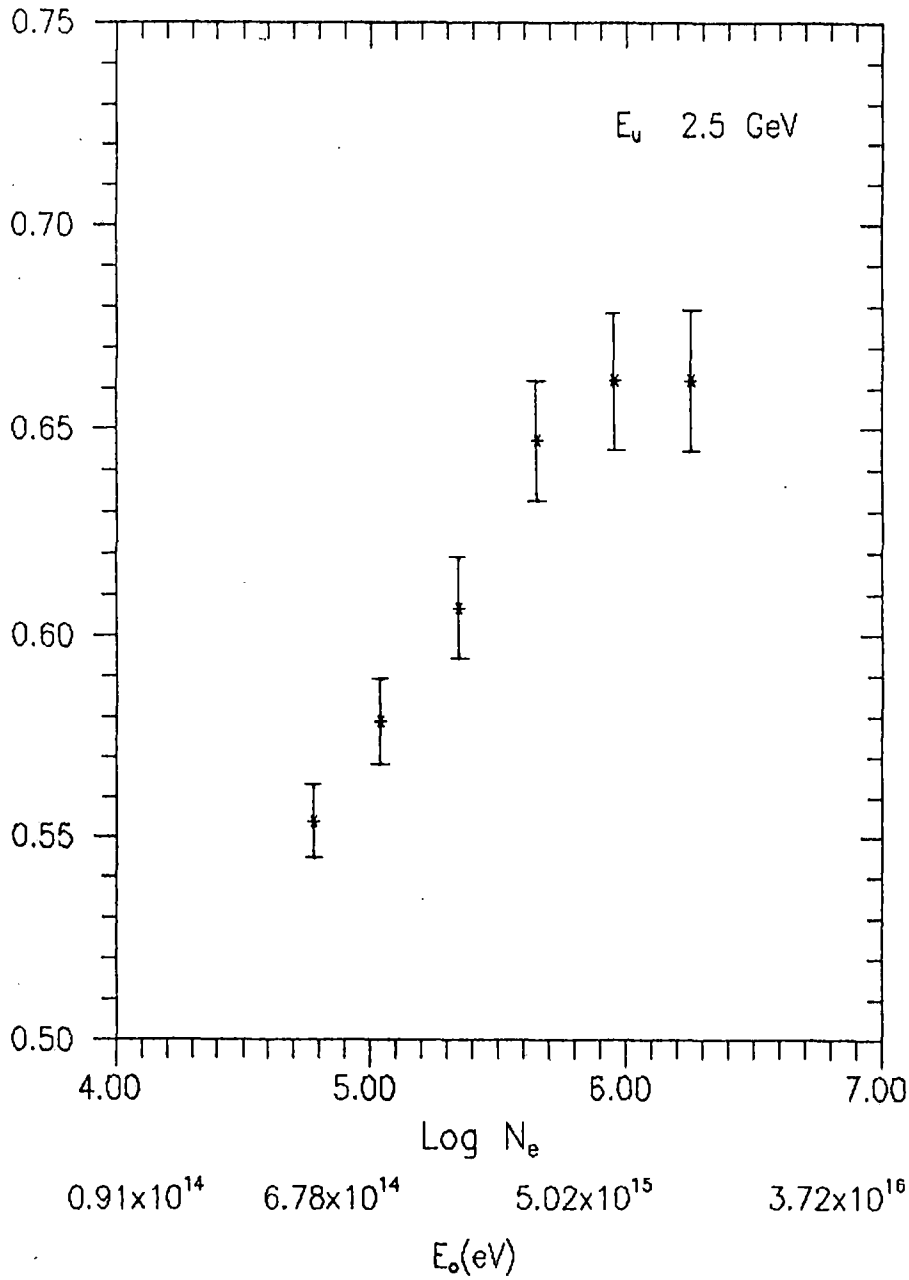
0.75
0.70
0.65
0.60
0.55
0.50
E_u 2.5 GeV
4.00
5.00
6.00
7.00
Log N_e
0.91×10^{14}
6.78×10^{14}
5.02×10^{15}
3.72×10^{16}
E_o(eV)

Fig.15.

Figure captions

Fig.1. A diagram of N.B.U air shower array set-up

Fig.2. The efficiency of detection of the array as a function of distance from the centre of the array for s= 1.2 and $N_e = 8x10^4$

Fig.3. Same as in Fig.2 but for $N_e = 10^5$

Fig.4. Same as in Fig.2 but for $N_e = 5x10^5$

Fig.5. Same as in Fig.2 but for $N_e = 10^6$

Fig.6. The average triggering probability for the array of detectors as a function of shower size for core distances at 20m,30m and 40m

Fig.7. Plots of lateral electron density distribution at shower size $1.09x10^5$-$1.79x10^6$ with shower age (s) = 1.2

Fig.8. Error distribution in core location ,shower size and age parameter.

Fig.9. Variation of muon density with muon energy at various radial distances.

Fig.10. Lateral muon density distribution at the threshold energy of 2.5 GeV for showers of size range $5.97x10^4$ - $9.02x10^5$ of s =1.2

Fig.11. Variation of muon density at radial distance ranges 8-12m and 30-40m with shower size at muon threshold ($\geq E_\mu$) energy 2.5 GeV

Fig.12. Same as in Fig.11 but for muon threshold ($\geq E_\mu$) energy 10 GeV

Fig.13. Same as in Fig.11 but for muon threshold ($\geq E_\mu$) energy 50 Gev

Fig.14. Variation of muon density with radial distance for $N_e=4.48x10^5$

Fig.15. Variation of α with shower size (N_e) at the muon threshold ($\geq E_\mu$) energy 2.5 GeV